DEVELOPMENT OF AN INTRAOPERATIVE IMAGING TOOL FOR THYROID AND PARATHYROID SURGICAL GUIDANCE

By

Emmanuel Amissah Mannoh

Dissertation

Submitted to the Faculty of the

Graduate School of Vanderbilt University

in partial fulfillment of the requirements

for the degree of

DOCTOR OF PHILOSOPHY

in

Biomedical Engineering

May 31, 2021

Nashville, Tennessee

Approved:

Anita Mahadevan-Jansen, Ph.D.

Andrew K. Dunn, Ph.D.

Benoit Dawant, Ph.D.

Carmen C. Solórzano, M.D.

Justin S. Baba, Ph.D.

Yuankai (Kenny) Tao, Ph.D

To my family

For their unwavering love and support

throughout my graduate career

ACKNOWLEDGEMENTS

I would like to thank all the members of my Ph.D. committee for the time and guidance they provided throughout the course of my graduate career. I especially want to thank my advisor, Dr. Anita Mahadevan-Jansen, for her mentorship which has helped me become an independent researcher. She taught me the need to find the appropriate tool to address clinical problems. I am grateful for the enormous trust she placed in me by giving me the freedom to explore different avenues and not losing patience even when progress was slow, especially at the start. I would like to thank Dr. Carmen Solórzano, without whom a lot of this work would not have been possible. She opened the doors of her operating room to me and was extremely generous with her time in providing feedback for constant improvement. I want to thank Dr. Andrew Dunn for welcoming me to his lab at the University of Texas at Austin to learn about laser speckle contrast imaging. Thank you to Dr. Benoit Dawant for much needed instruction on image processing techniques, as well as to Dr. Kenny Tao for extremely helpful instruction on optical design. I also want to thank Dr. Justin Baba for multiple thought-provoking discussions helping to shape my research strategy, in addition to occasional banter over soccer teams. I am sorry that Liverpool will not get to have a real Premier League celebration, but who knows, maybe in another 30 years.

Besides Dr. Solórzano, I also want to thank Dr. Naira Baregamian, another endocrine surgeon who welcomed me into her operating room and without whom a lot of this work would not have been possible. Additionally I would like to thank all the surgical residents, scrub nurses, circulator nurses and anesthesiologists at the Vanderbilt University Medical Center who were involved in this work, for generously accommodating my intrusion into their workspace. I also want to thank all the patients who consented to be involved in this research.

Thank you to all the members of the Vanderbilt Biophotonics Center, for providing a sense of community, and for frequent feedback that improved the quality of my work. I am fortunate to have made many friends among you and across the Vanderbilt University campus. Thank you Dr. Giju Thomas for your ever-present advice throughout my Ph.D. career. I am grateful that I could always come to you with questions and leave with a better understanding of the clinical landscape. Thank you also, together with Graham, for many much needed destressing conversations. Thank you to Logan for helpful discussions on career paths and for (unwisely?) trusting me with your car so I could get a driver's license. And of course, thank you to Kuniko and Arlo. Covid-19 lockdowns would have been a lot tougher without your friendship.

Finally, I would like to thank my family for their constant support throughout this process. To my aunt Sue, thank you immensely for being my home away from home. Thank you for believing in me and encouraging me to explore my talents. To my sisters, Ida and Ivy, thank you for your love and support, and for constantly pushing me to improve in all aspects. Most importantly, thank you to my parents, Gloria and Emmanuel, for your unwavering love, support and investment in my education over the years. I will forever be grateful that you gave me the freedom to pursue the career path I was most passionate about.

This work was made possible by the financial support of grants from the National Institutes of Health, and the Constantine A. Paras BME Graduate Memorial Fellowship from the Dean Paras Foundation.

TABLE OF CONTENTS

Page

LIST OF TABLES

Table Page

LIST OF FIGURES

Figure Page

Figure Page

CHAPTER 1

INTRODUCTION

1.1 Motivation

Diseases of the thyroid and parathyroid glands often require surgery as treatment, with an average of over 10,000 parathyroidectomies[1] and over 92,000 thyroidectomies[2] performed annually in the United States alone. Trends show increasing numbers of thyroid procedures performed, and an estimated 169,000 were conducted in 2016[3]. Surgery in the neck puts healthy parathyroid glands at risk for damage as a result of their small size[4] and visual similarity to other tissues such as lymph nodes[5]. Furthermore, the nature of the parathyroid blood supply, likened to the stem of a cherry[6], makes the glands highly susceptible to blood flow loss during surgery. Hypoparathyroidism, which is an inability to produce sufficient amounts of parathyroid hormone (PTH), often results from damage to the parathyroid glands. The action of PTH serves to increase blood calcium concentration when it is low, and the parathyroid glands are primarily responsible for calcium regulation[7]. Consequently, hypoparathyroidism leads to hypocalcemia which requires therapeutic management in order to avoid the associated harmful effects like cardiac arrhythmias and seizures[7,8]. Hypocalcemia is reported to occur after as much as 47% of thyroidectomies[9] and is a major cause for malpractice litigation after endocrine neck surgery[10].

To help reduce the incidence of hypocalcemia after endocrine neck surgery, better intraoperative guidance is required. While there is a wealth of preoperative information available to the surgeon, there are not many tools available to guide surgery intraoperatively, therefore surgeons are often left to rely on their experience[11]. The two challenges faced in surgery are accurate identification of the parathyroid glands, and assessment of their blood supply. Over the past decade, work from our lab has established near-infrared autofluorescence (NIRAF) detection as a reliable label-free method for intraoperative parathyroid identification[12–17]. The technique has been adopted by other researchers and there are now two FDA cleared clinical devices for intraoperative parathyroid identification using NIRAF detection[18]. This dissertation focuses on developing a solution to the second problem: objectively and accurately assessing parathyroid vascularity. There is currently no gold standard for making this assessment, hence surgeons often rely on visual inspection. An ideal solution would be real-time, label-free and compatible with NIRAF detection. The overall goal of this work is to provide a tool for complete assessment of the parathyroid gland to better guide endocrine neck surgeries.

1.2 Goal

An ideal technique for assessing parathyroid vascularity should be able to provide objective information in real-time, while doing so without significant additional risk to the patient and without the need for exogenous contrast agents. It should also be capable of being readily integrated with NIRAF detection, which has proven to be highly successful in identifying parathyroid glands intraoperatively. Laser speckle contrast imaging (LSCI) is a promising solution in this regard. This technique relies solely on computational analysis of the interference pattern produced by coherent light incident on a tissue surface to provide contrast related to the flow of blood cells. It is also a relatively simple optical imaging technique, thus making combination with autofluorescence imaging feasible. ***The underlying hypothesis of this work is that intraoperative LSCI can provide an objective and accurate assessment of the state of vascularity of a parathyroid gland and therefore its viability***. This would be the first reported application of LSCI towards this problem, and the technique has the potential to become the objective gold standard in an area where one is lacking.

The primary goal of this project is to develop a device based on LSCI for intraoperative real-time assessment of parathyroid gland vascularity, and to demonstrate the potential of the technique for helping improve patient outcomes after thyroidectomy. The success of this work will potentially minimize the incidence of post-surgical hypocalcemia by assisting surgeons in determining which, if any, parathyroid glands should be autotransplanted during surgery. Combination with NIRAF imaging will provide endocrine surgeons with a tool to help both identify parathyroid glands and assess their vascularity during surgery. To achieve this, the following specific aims are proposed.

1.3 Specific Aims

Specific Aim 1: Assess the efficacy of laser speckle contrast imaging in distinguishing between vascularized and compromised parathyroid glands intraoperatively.

An LSCI system was developed for *in vivo* imaging of parathyroid glands in the operating room. The ability of the device to distinguish between well-perfused or vascularized parathyroid glands and those

that had suffered vascular compromise was evaluated in patients undergoing thyroidectomy at Vanderbilt University Medical Center (VUMC). Given the lack of an objective gold standard for assessing parathyroid vascularity, a surgeon with multiple years of experience served as the gold standard. Validation of the technique was performed in patients undergoing parathyroidectomy, where ligation of the blood supply to the diseased gland prior to excision is part of standard procedure. Success of this work demonstrates the sensitivity of LSCI to parathyroid gland vascularity and its potential for use during endocrine neck surgeries.

Specific Aim 2: Evaluate the potential for impact of intraoperative laser speckle contrast imaging on improving patient outcomes.

Parathyroid hormone levels within the first 24 hours after surgery are indicative of whether or not a patient will develop hypocalcemia[19]. Therefore, to evaluate the potential benefit of LSCI, intraoperative measurements using the device developed under Aim 1 were compared against postoperative day 1 PTH and blood calcium levels in patients undergoing thyroidectomy at VUMC. The surgeons involved in this work were blinded from intraoperative LSCI data and therefore patient care was not influenced by any measurements made. Full accomplishment of this work establishes a quantitative value for classifying a parathyroid gland as adequately vascularized for normal postoperative function, as determined by the outcomes of patients in the study. It also determines the minimum number of vascularized parathyroid glands needed for normal PTH levels post-surgery. This will provide surgeons with added guidance to help make intraoperative decisions on whether parathyroid autotransplantation is necessary in order to minimize the likelihood of post-surgical hypocalcemia. Finally, it could help with the planning of post-surgical care for a patient, as the surgeon would know early on those most likely to have trouble regulating calcium.

Specific Aim 3: Develop clinical imaging device combining near-infrared autofluorescence imaging with laser speckle contrast imaging.

Work under this aim involved design and development of an imaging device combining LSCI with NIRAF imaging for complete assessment of the parathyroid gland. In the previous two aims, manual segmentation of images was required in order to extract LSCI data on the parathyroid glands. This could

be a barrier to clinical translation. Therefore, under this aim, an algorithm was also developed to use the fluorescence images to localize the parathyroid in order to automate the extraction of the related LSCI data. Finally, using this device, LSCI was compared with indocyanine green (ICG) angiography, a fluorescent-dye-based technique gaining interest for use in assessing parathyroid vascularity. The two techniques were used to image parathyroid glands in patients undergoing thyroidectomy or parathyroidectomy at VUMC and the results revealed similarity between the two methods. The success of this work now provides surgeons with a single tool for real-time label-free identification of parathyroid glands and assessment of vascularity during surgery.

1.4 Summary of Chapters

Chapter 1 provides an introduction to the problem motivating the work presented in this dissertation and states the underlying hypothesis. The goal of the project is laid out and the specific aims designed to achieve this goal are defined. The outcomes of each aim are briefly summarized.

Chapter 2 provides relevant background material on the clinical challenge of preserving healthy parathyroid function during endocrine neck surgeries. Information on the anatomy and physiology of the thyroid and parathyroid glands is presented, as well as a discussion of various methods that have been employed for intraoperative parathyroid identification and vascularity assessment. Finally, LSCI is discussed as a potential method to evaluate parathyroid blood flow, and the significance and innovation of the work in this dissertation are summarized.

Chapter 3 presents the first reported study demonstrating the use of LSCI to assess parathyroid vascularity. Results show that the technique is highly accurate in detecting differences in parathyroid vascularity, and is also capable of detecting loss of blood flow to a parathyroid gland before it becomes visually apparent to the surgeon.

Chapter 4 describes a surgeon-blinded prognostic study in which the relationship between intraoperative LSCI measurements and postoperative outcomes of thyroidectomy patients was evaluated. A threshold for adequate parathyroid vascularity based on LSCI data was established, and the minimum number of vascularized parathyroid glands needed for normal postoperative function was identified.

Chapter 5 details the design, development and characterization of an imaging device combining LSCI with NIRAF imaging. The chapter also presents an automated segmentation algorithm developed for the purpose of simplifying the delivery of LSCI data to the surgeon, and thereby reducing a barrier to clinical translation of the technique. Representative intraoperative images from a few cases are presented.

Chapter 6 compares LSCI with a dye-based method for assessing parathyroid vascularity, ICG angiography. Using the device developed in Chapter 5, both sets of imaging data were acquired for the same parathyroid glands. Results show similarity between the two techniques.

Chapter 7 summarizes the work presented in this dissertation and proposes directions for future work on the project. It also summarizes the potential broader impact of this work on endocrine surgery, biophotonics, and the larger society.

Appendix A briefly presents an alternative approach to automated parathyroid segmentation than that in Chapter 5. This method is based on convolutional neural networks and has the potential to overcome limitations identified in Chapter 5. The method is proposed as the basis for future work.

1.5 References

1. Kim, S. M., Shu, A. D., Long, J., Montez-Rath, M. E., Leonard, M. B., Norton, J. A. & Chertow, G. M. Declining Rates of Inpatient Parathyroidectomy for Primary Hyperparathyroidism in the US. *PLoS One* **11**, e0161192 (2016).
2. Sun, G. H., DeMonner, S. & Davis, M. M. Epidemiological and Economic Trends in Inpatient and Outpatient Thyroidectomy in the United States, 1996–2006. *Thyroid* **23**, 727–733 (2013).
3. Sosa, J. A., Hanna, J. W., Robinson, K. A. & Lanman, R. B. Increases in thyroid nodule fine-needle aspirations, operations, and diagnoses of thyroid cancer in the United States. *Surgery* **154**, 1420–1427 (2013).
4. Mohebati, A. & Shaha, A. R. Anatomy of thyroid and parathyroid glands and neurovascular relations. *Clin. Anat.* **25**, 19–31 (2012).
5. Johnson, N. A., Tublin, M. E. & Ogilvie, J. B. Parathyroid Imaging: Technique and Role in the Preoperative Evaluation of Primary Hyperparathyroidism. *Am. J. Roentgenol.* **188**, 1706–1715 (2007).
6. Halsted, W. S. & Evans, H. M. The parathyroid glandules. Their blood supply, and their preservation in operation upon the thyroid gland. *Ann. Surg.* **XLVI**, 489–506 (1907).

7. Naveh-Many, T. Development of Parathyroid Glands. in *Molecular Biology of the Parathyroid* 1–2 (Landes Bioscience / Eurekah.com, 2005).

8. Mannstadt, M., Bilezikian, J. P., Thakker, R. V., Hannan, F. M., Clarke, B. L., Reijnmark, L., Mitchell, D. M., Vokes, T. J., Winer, K. K. & Shoback, D. M. Hypoparathyroidism. *Nat. Rev. Dis. Prim.* **3**, 1–21 (2017).

9. McHenry, C. R., Speroff, T., Wentworth, D. & Murphy, T. Risk factors for postthyroidectomy hypocalcemia. *Surgery* **116**, 641–7; discussion 647-8 (1994).

10. Pattou, F., Combemale, F., Fabre, S., Carnaille, B., Decoulx, M., Wemeau, J.-L., Racadot, A. & Proye, C. Hypocalcemia following Thyroid Surgery: Incidence and Prediction of Outcome. *World J. Surg* **22**, 718–724 (1998).

11. Meltzer, C., Hull, M., Sundang, A. & Adams, J. L. Association between Annual Surgeon Total Thyroidectomy Volume and Transient and Permanent Complications. *JAMA Otolaryngol. - Head Neck Surg.* **145**, 830–837 (2019).

12. Paras, C., Keller, M., White, L., Phay, J. & Mahadevan-Jansen, A. Near-infrared autofluorescence for the detection of parathyroid glands. *J. Biomed. Opt.* **16**, 067012 (2011).

13. McWade, M. A., Paras, C., White, L. M., Phay, J. E., Mahadevan-Jansen, A. & Broome, J. T. A novel optical approach to intraoperative detection of parathyroid glands. *Surgery* **154**, 1371–7; discussion 1377 (2013).

14. McWade, M. A., Paras, C., White, L. M., Phay, J. E., Solórzano, C. C., Broome, J. T. & Mahadevan-Jansen, A. Label-free Intraoperative Parathyroid Localization With Near-Infrared Autofluorescence Imaging. *J. Clin. Endocrinol. Metab.* **99**, 4574–4580 (2014).

15. McWade, M. A., Sanders, M. E., Broome, J. T., Solórzano, C. C. & Mahadevan-Jansen, A. Establishing the clinical utility of autofluorescence spectroscopy for parathyroid detection. *Surgery* **159**, 193–202 (2016).

16. Thomas, G., McWade, M. A., Paras, C., Mannoh, E. A., Sanders, M. E., White, L. M., Broome, J. T., Phay, J. E., Baregamian, N., Solórzano, C. C. & Mahadevan-Jansen, A. Developing a Clinical Prototype to Guide Surgeons for Intraoperative Label-Free Identification of Parathyroid Glands in Real Time. *Thyroid* **28**, 1517–1531 (2018).

17. Thomas, G., McWade, M. A., Nguyen, J. Q., Sanders, M. E., Broome, J. T., Baregamian, N., Solórzano, C. C. & Mahadevan-Jansen, A. Innovative surgical guidance for label-free real-time parathyroid identification. *Surgery* **165**, 114–123 (2019).

18. FDA. FDA permits marketing of two devices that detect parathyroid tissue in real-time during surgery | FDA. https://www.fda.gov/news-events/press-announcements/fda-permits-marketing-two-devices-detect-parathyroid-tissue-real-time-during-surgery.

19. Julián, M. T., Balibrea, J. M., Granada, M. L., Moreno, P., Alastrué, A., Puig-Domingo, M. & Lucas, A. Intact parathyroid hormone measurement at 24 hours after thyroid surgery as predictor of parathyroid function at long term. *Am. J. Surg.* **206**, 783–789 (2013).

CHAPTER 2

BACKGROUND

2.1 Anatomy and Physiology of the Thyroid and Parathyroid Glands

2.1.1 Anatomy and physiology of the thyroid gland

The thyroid gland is one of the largest endocrine glands in the human body[1]. It is situated within the neck and sits on the ventral surface of the trachea, beneath the larynx as indicated in Figure 2.1. The name thyroid arises from the Greek word thyreoeidos, which is indicative of its resemblance to a shield covering the trachea[2]. The thyroid develops from the pharynx during gestation and consists of two lateral lobes joined together by the isthmus anterior to the trachea. In a normal thyroid gland, each lobe measures about 40 mm, superiorly to inferiorly, about 15-20 mm in width, and is about 20-39 mm thick[2]. The blood supply to the thyroid is primarily provided by the superior and inferior thyroid arteries, which are branches off the carotid and subclavian arteries respectively[2].

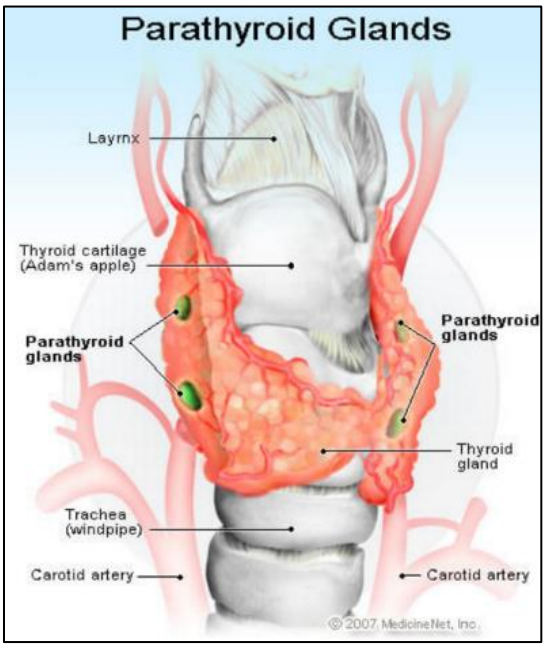

Figure 2.1. Anatomy of the thyroid and parathyroid glands[3].

The thyroid gland is involved in regulating a large number of the body's physiological processes. Broadly speaking, it regulates how the body burns energy and makes proteins, and also dictates how responsive the body should be to the effects of other hormones[1]. It does this through the hormones it secretes, primarily thyroxine and triiodothyronine. Thyroid hormones are especially important during neonatal development where they are responsible for stimulating gene transcription for cells across the entire body. Because they are so crucial for proper cell differentiation and development, a deficiency in thyroid hormone during this period results in abnormal development of all organ systems. This is particularly pronounced in the nervous system leading to severe mental retardation, a syndrome termed cretinism[1]. In adults, thyroid hormones are also important for proper cognitive functioning and it has been reported that abnormal levels in the plasma is a significant risk factor for dementia[1]. The thyroid also secretes the hormone calcitonin which is important for calcium homeostasis. When the body senses increased levels of calcium in the blood, the thyroid secretes calcitonin which suppresses osteoclast activity on bone, thereby reducing the amount of calcium that enters the bloodstream from the resorbed bone[4].

2.1.2 Anatomy and physiology of the parathyroid glands

The parathyroid glands also develop from the pharynx and lie in close proximity to the thyroid (see Figure 2.1), hence their name. A normal parathyroid gland is usually ovoid in shape and about 3-8 mm in length, giving it the resemblance of a grain of rice, and its color can vary from yellow to reddish-brown[2,5]. The parathyroid glands are classified as either superior or inferior, depending on their origin and location. The superior parathyroid glands originate from the fourth pharyngeal pouch and attach to the posterior surface of the thyroid as it migrates outward during neonatal development[2]. This makes them comparatively easier to find during surgery – one autopsy study of 503 cadavers found that 80% of superior parathyroid glands were found within a 2 cm diameter circumscribed area on the posterior surface of the thyroid[2,6]. The inferior parathyroid glands originate from the third pharyngeal pouch, which is the same location that gives rise to the thymus. As the thymus migrates outward and downward to its final position in the mediastinum, the inferior parathyroid glands are pulled along with it. Consequently the inferior parathyroid glands can be found anywhere in this large region bordered at its base by the pericardium[2]. A study of 645 parathyroid glands from 160 subjects found 42% of the inferior glands to reside on the anterior or postero-lateral surface of the lower poles of the thyroid, while 39% were located

in the lower neck close to the thymus. Additionally, 15% were lateral to the thyroid and 2% were found within the thymus[2,7]. On rare occasions, a parathyroid gland (either superior or inferior) could be located within the thyroid gland, which can lead to collateral damage if surgery on either of these glands is warranted[2]. There are typically four parathyroid glands: two superior and two inferior. However, it is possible for an individual to have fewer or more than four glands. In a reported autopsy study, 13% of cases had more than four glands, 84% had four glands, and 3% had three[2,6]. It is widely accepted that the parathyroid glands receive their blood supply from branches of the inferior thyroid artery[2], however studies have shown that they can also be supplied by the superior thyroid artery[8]. Regardless of which scenario exists for each individual, it is important to note that the parathyroid glands are always supplied with blood by the same vessels that supply the thyroid. It is also important to note that the arterial blood vessel directly connected to the parathyroid is very delicate, being likened to the stem of a cherry[9].

The parathyroid glands are the body's main organs for combatting hypocalcemia. This is a very important function since calcium is vital for muscle contraction, neuronal excitability, blood coagulation and bone mineralization. Insufficient serum calcium can therefore lead to muscle spasms, cardiac arrhythmias, tetany and, if unchecked, eventually death[10]. When calcium-sensing receptors residing within the parathyroid glands detect low levels of serum calcium, the parathyroid glands immediately secrete parathyroid hormone (PTH) in response. Together with Vitamin D, PTH increases extracellular calcium levels by acting on bone, the kidneys and the intestines. In bone it promotes resorption, in the kidneys it acts to prevent calcium elimination in the urine, and in the intestines it favors absorption of calcium through the intestinal wall[10]. The action of PTH is opposite to that of calcitonin.

2.2 Diseases of the Thyroid and Parathyroid Glands

2.2.1 Diseases of the thyroid gland

Diseases of the thyroid affect roughly 200 million people throughout the world, the majority of these being women[11]. Most of these diseases manifest as either an overactive or underactive thyroid, conditions

termed hyperthyroidism and hypothyroidism respectively. Many thyroid diseases result in enlargement of the gland.

Hypothyroidism is the more common of the two and is marked by insufficient production of the thyroid hormones thyroxine and triiodothyronine. Clinical symptoms are nonspecific and include fatigue, mental depression, intolerance to cold, weight gain, dry skin and hair, and constipation. Therefore it is often diagnosed by blood tests[11]. It is most often caused by Hashimoto's disease, an autoimmune condition in which the immune system attacks the thyroid gland and impairs its function[12]. Hypothyroidism can be classified as primary, secondary or tertiary, depending on where in the production line of thyroid hormone (TH) the problem originates. Under normal conditions, the pituitary gland secretes thyroid-stimulating hormone (TSH) which directs the thyroid to produce TH. The action of the pituitary gland is in turn controlled by the hypothalamus which secretes thyroid-releasing hormone. In primary hypothyroidism, the dysfunction is at the level of the thyroid gland, while in secondary and tertiary hypothyroidism, the dysfunction is at the level of the pituitary gland and hypothalamus respectively. Secondary and tertiary hypothyroidism are however rare[11]. Given that thyroxine and triiodothyronine are made from iodine – which can only be obtained by dietary intake – another cause of hypothyroidism is insufficient amounts of iodine in one's diet. This is typically accompanied by a goiter (an enlargement of the thyroid). The enlargement occurs because the body senses the reduced levels of TH, causing the pituitary gland to secrete TSH in an attempt to stimulate TH production. However, since iodine concentrations are sub-optimal, the thyroid cannot produce TH. This results in a feedback loop where the thyroid is constantly stimulated with TSH, eventually leading to hypertrophy of the gland[11].

Hyperthyroidism, like the name implies, leads to excessive production of TH. Clinical symptoms include insomnia, increased bowel movements, fatigue, palpitations, tremors, weight loss, nervousness and heat intolerance. It is diagnosed by physical examination of the enlarged gland and by measuring TH levels in the blood. It is most often caused by Graves' disease, an inheritable disease in which the body's immune system attacks the thyroid gland and causes it to become enlarged and overactive[13].

Cancer is also another disease that affects the thyroid. In 80% of cases, this takes the form of papillary carcinomas or adenocarinomas which only affect one lobe of the thyroid[14].

2.2.2 Diseases of the parathyroid glands

Similar to diseases of the thyroid, diseases of the parathyroid glands result in either hyperactivity or underactivity of the glands, termed hyperparathyroidism and hypoparathyroidism respectively. There are two main forms of hyperparathyroidism, primary and secondary. Primary hyperparathyroidism is known to occur in 1% of the adult population in Western countries[15]. In primary hyperparathyroidism, the problem arises from the gland itself. This is typically an adenoma or benign growth that enlarges the parathyroid, causing it to be more active than a normal gland, however it can sometimes be a malignant cancer[16]. Primary hyperparathyroidism can affect one or more of the parathyroid glands. Secondary hyperparathyroidism results from a chronic abnormal stimulus for the production of PTH, and is often due to renal failure. When the kidneys fail, Vitamin D synthesis is impaired. Since the action of PTH to increase blood calcium levels requires the aid of Vitamin D, there is constant stimulation of the glands in response to perpetually low calcium levels, leading to hypertrophy. Kidney failure also means increased levels of phosphates in the blood and reduced levels of calcium, both of which contribute toward the chronic stimulation of the parathyroid glands (hyperphosphatemia is known to directly stimulate PTH synthesis)[16]. In secondary hyperparathyroidism all the parathyroid glands are enlarged. Patients with highly overactive parathyroid glands typically suffer from bone disease and kidney stones due to the resulting excessive bone resorption[17].

Hypoparathyroidism, on the other hand, is mostly caused by damage to the parathyroid glands during neck surgeries, although it has been reported that rare genetic defects can also lead to an inability to produce PTH[18]. Another form of the disorder, termed pseudo-hypoparathyroidism, was discovered in individuals who produce normal PTH but have an insensitivity to the effects of the hormone[17]. Both types of hypoparathyroidism result in abnormally low levels of serum calcium, leading to tetany and eventually death if the patient falls below 50% of normal calcium levels.

2.3 Hypoparathyroidism after Neck Surgery

For many of these conditions, especially when it comes to hypertrophied glands, surgical intervention is necessary. In the United States, about 10,000 and 92,000 patients each year require parathyroidectomies[19] and thyroidectomies[20] respectively to remove benign or malignant glands. During

these surgeries, it is possible for healthy parathyroid glands to be damaged or accidentally excised, due to their small size and visually similar appearance to other tissues. Furthermore, it is possible for the blood supply to the healthy parathyroid glands to be damaged, rendering the glands nonfunctional. This is more critical during thyroid surgeries. Because the parathyroid glands receive their blood supply from the same vessels supplying the thyroid, it can be challenging to resect the thyroid while leaving the parathyroid blood supply intact. The close proximity of the parathyroid glands to the thyroid (they are sometimes loosely attached to the surface of the thyroid, and on rare occasions can be embedded within the thyroid) also adds to this challenge. It has been reported that between 9-50% of thyroidectomies result in post-surgical hypoparathyroidism, either due to inadvertent damaging of the blood supply to one or more parathyroid glands or accidental excision of the glands[21–25]. This surgery-induced hypoparathyroidism can be temporary or permanent, and there is a wide range of reported rates on this problem due to differences in surgeon experience[26] and the lack of a standardized definition[27]. The condition is mostly temporary, however it is reported that 1.5-4% of cases result in permanent hypoparathyroidism[21,24]. Given regular calcium and Vitamin D supplements, most patients are able to maintain normal serum calcium levels. However, especially for those patients in which the condition is permanent, this results in an unnecessary economic burden[28].

2.4 The Two-part Challenge to Preserve Healthy Parathyroid Function in Surgery

2.4.1 Intraoperative parathyroid gland identification

The first challenge in preserving healthy parathyroid gland function during surgery is being able to accurately identify the glands intraoperatively. Due to their small size and visual similarity to other tissues such as lymph nodes and fat, this can be difficult. Advances in preoperative imaging techniques such as ultrasonography, computed tomography, magnetic resonance imaging, and sestamibi scan to localize the glands have helped reduce collateral damage involved with the procedures[15], however they do not provide guidance during the surgery. Previously, techniques for intraoperative guidance were proposed including the application of contrast agents[29–31], optical coherence tomography (OCT)[32–34], elastic scattering and diffuse reflectance imaging[35], however they had limited success. It was not until Paras *et al.* discovered

the phenomenon of parathyroid autofluorescence that there was a viable real-time and label-free technique to identify parathyroid glands intraoperatively[36]. When illuminated with near-infrared light, parathyroid glands emit autofluorescence with a peak at about 820 nm. This near-infrared autofluorescence (NIRAF) is absent or diminished in other tissues within the neck, providing contrast between the parathyroid glands and the rest of the surgical field. Further work showed that the ratio of the parathyroid NIRAF to that of the thyroid ranges from 1.2 to above 20[37,38]. These findings led to the development of a clinical device employing a fiber-optic probe for intraoperative parathyroid detection[39–41]. The parathyroid NIRAF can also be detected through imaging, typically employing a long-pass filter in front of a camera to visualize the fluorescence[42–47]. On one hand, the probe-based approach provides spectral information and allows quantifying fluorescence intensity in real-time. Additionally, due to its similarity to nerve-monitoring devices used routinely in thyroid surgeries, it is easier for surgeons to adopt. In contrast, the imaging approach provides useful spatial information for parathyroid localization. Studies have also suggested that the imaging approach is able to detect parathyroid glands obscured by fat or connective tissue[48]. Both approaches have demonstrated the consistency of parathyroid autofluorescence and its utility in helping identify parathyroid glands during surgery, regardless of their disease state, as well as helping reduce inadvertent excision of healthy parathyroid glands.

2.4.2 Parathyroid vascularity assessment

Accurate assessment of parathyroid blood flow or vascularity is the second challenge in preserving healthy parathyroid function post-surgery. This is important because a parathyroid gland that has lost its blood supply, or has been devascularized, will no longer function. If identified during the course of the surgery, the devascularized gland is typically autotransplanted. Autotransplantation is a process whereby the devascularized parathyroid gland is excised, minced into tiny fragments, and reinserted into a pouch made usually in the sternocleidomastoid muscle in the side of the neck[49]. With time, the transplanted gland is integrated into the muscle and functions like a normal parathyroid gland. This is likely aided by the wound-healing process which results in recruitment of neutrophils and angiogenesis at the site of the wound (in this case the pouch), reestablishing the connection between the minced gland and the circulatory system. A similar process has been reported in the transplantation of pancreatic islets into striated muscle[50]. Autotransplantation of parathyroid glands to the muscles of the forearm has also been shown to preserve parathyroid function[49,51]. Autotransplantation of parathyroid glands in humans was first

described in 1926, and since then it has been shown to be a more reliable solution than leaving a potentially devascularized parathyroid gland in situ. Consequently, some surgeons prefer to always transplant one parathyroid gland during total thyroidectomies[49].

As beneficial as autotransplantation is, in that it restores function to a parathyroid gland that would have otherwise been lost, there is a non-trivial failure rate involved in the reintegration process. Reports indicate that about 14-17% of these transplantations fail to revive normal parathyroid function[52,53]. It follows that correctly assessing the state of vascularity of a parathyroid gland before deciding on whether or not to transplant is crucial. There is currently no objective gold standard for making this determination, and surgeons largely rely on their subjective visual assessment and experience.

2.5 Techniques to Assess Parathyroid Vascularity

There is currently no real-time objective diagnostic tool for assessing parathyroid gland vascularity during surgery. The most common approach taken by surgeons is to visually assess the color and turgor of the gland. According to one surgeon (personal conversation), a devascularized parathyroid gland turns dark and shrivels with time. This is likely due to the gland pooling with deoxygenated blood. What this description also implies is that if vascular compromise does not result in blood pooling in the gland, it can easily be missed by surgeons. It is believed that a more reliable technique of assessing parathyroid gland vascularity is the demonstration of continuous bright red bleeding after needle prick or cutting off tiny fragments. However, this is also problematic as bleeding may be sluggish simply due to the effects of anesthesia[23], while also putting the patient at additional risk for harm.

2.5.1 Topical application of lidocaine

One approach that was introduced to assess parathyroid vascularity involved the application of a 2% lidocaine solution to the surface of parathyroid glands. Rather than transplant every parathyroid gland that was suspected of being devascularized during thyroidectomies, the authors first bathed the gland with 2-3 mL of a 2% lidocaine solution for 1 to 2 minutes. Lidocaine acts as a vasodilator and can therefore restore adequate blood flow to a partially devascularized parathyroid gland. If color and turgidity returned

to the gland after use of lidocaine, and continuous bright red bleeding upon needle prick was confirmed, the gland was deemed viable and left in place. Otherwise, it was excised and transplanted. This study reported 40 parathyroid glands from 100 patients requiring autotransplantation after application of the lidocaine solution. It does not however report how many partially devascularized glands were subsequently declared viable after the application of lidocaine. An important consideration with this technique is that lidocaine also acts as an ion channel blocker. Therefore, care needs to be taken to avoid contact with the recurrent laryngeal nerve, which is exposed during the surgery, as this could result in vocal cord paresis/paralysis[23].

2.5.2 Intraoperative parathyroid hormone measurement

Intraoperative measurement of serum PTH levels is performed routinely during parathyroidectomies to confirm removal of the hyperactive parathyroid glands. The half-life of PTH in the blood is just a few minutes, and therefore removal of a parathyroid gland (especially an overactive one) leads to noticeable decreases in serum PTH within a relatively short amount of time[22]. Though not widely used for that purpose, this technique can also be applied during thyroidectomies to check for accidental devascularization of parathyroid glands. The baseline serum PTH is recorded before the procedure and compared against the value after removal of the thyroid. In one study where this was performed, a blood sample was taken 10 minutes after complete removal of the thyroid gland to assess PTH levels. The test itself took on average another 18 minutes, meaning altogether the surgeon had to wait about half an hour to find out if serum PTH levels had dropped. Further complicating matters is the fact that this test does not give any indication as to which parathyroid gland may have been damaged. The only remedy is to check the excised thyroid specimen to see if it contains any accidentally excised parathyroid tissue. If it does, this tissue is autotransplanted[22].

2.5.3 Laser Doppler flowmetry

A technique that can non-invasively measure the flow of blood is laser Doppler flowmetry (LDF). It relies on the phenomenon of the Doppler Effect. Simply put, the frequency of detected light waves changes as the light source and target (blood cells) move relative to each other. This method relies on point-based measurements and so can be slower, if spatial information is desired, or suboptimal, in that only a small

portion of the tissue of interest is evaluated. In 1994, a study was performed on 53 patients undergoing thyroidectomies and parathyroidectomies to identify the major blood supply vessels to the parathyroid glands using LDF. The investigators constricted the inferior and superior thyroid arteries in turn and then simultaneously, while recording the reduction in blood flow using a commercial LDF system. Measurements made by the system are from deeper layers (~5 mm on average) of the tissue and so in cases where the parathyroid gland was lying against a major vessel or thyroid tissue, a physical barrier had to be placed between the two to prevent false readings. The main outcome of this study was to demonstrate that the blood supply to parathyroid glands may not be as greatly dependent on the inferior thyroid artery as was thought[54], however it also gave some hope for using LDF to assess parathyroid vascularity. This group went on to perform another study on patients undergoing thyroidectomies in which they used LDF to assess changes in parathyroid gland perfusion after removal of thyroid tissue. Their results showed that these measurements were uncorrelated with the macroscopic visual assessment made by the surgeon[55]. This negative result was likely influenced by the fact that this method makes point-based measurements rather than assessing the parathyroid gland as a whole. It could also have been negatively affected by the measurement depth of the probe which may have collected data from tissues beneath the parathyroid glands.

2.5.4 Confocal endomicroscopy with fluorescein

Confocal endomicroscopy using the dye fluorescein has been applied to image blood flow in parathyroid glands[56]. In a preliminary study on 10 patients, the data obtained was compared with the assessments of two experienced high-volume endocrine surgeons. While results showed 74% and 96% sensitivity and specificity respectively in differentiating between viable and non-viable parathyroid glands, work remains to validate this technique. Additionally, it requires administration of a fluorescent dye, raising concerns about toxicity and allergic reactions[57].

2.5.5 Indocyanine green angiography

More recently, a group reported on the use of indocyanine green (ICG) fluorescence for angiography of parathyroid glands[58]. ICG is a water-soluble dye that remains almost entirely bound to proteins when injected into the bloodstream and so does not diffuse through blood vessel walls, making it an excellent

contrast agent for highlighting vasculature. It is eventually broken down in the liver and excreted into bile. Because of its characteristics, ICG is often used as a means to confirm perfusion of vessels. In another study, none of the patients in whom at least one well-vascularized parathyroid gland was identified by ICG angiography experienced transient or permanent hypoparathyroidism. Of the six patients in whom no vascularized gland could be identified by ICG angiography, two developed transient hypoparathyroidism[59]. The determination of vascularity was made by qualitative visual assessment of the ICG fluorescence images and assigning scores according to a 3-level scoring system. This makes it difficult to standardize observations as one surgeon may assign a different score compared to another surgeon for the same parathyroid gland. Furthermore, the technique does require administration of an exogenous contrast agent (ICG), which could put the patient at additional risk for harm. A small percentage of patients can experience severe allergic reactions to the dye[60]. Additionally, it is limited in how frequently it can be performed during surgery, to avoid toxicity[59]. Finally, the technique is limited in its ability to be combined with NIRAF detection for parathyroid identification. The fluorescence of ICG has a peak around 830 nm[61], and therefore overlaps spectrally with the parathyroid autofluorescence. Once ICG is administered, it perfuses any tissue with an intact blood supply and so there is no longer a fluorescence contrast between the parathyroid glands and other tissues. Use of ICG angiography together with NIRAF detection in neck surgeries would require that all parathyroid glands first be identified with NIRAF detection, before the administration of ICG to evaluate perfusion. However, this is not always practical.

2.6 Potential Optical Imaging Alternatives to Current Techniques

There remains a critical need for a real-time, label-free and objective method for assessing the vascularity of parathyroid glands intraoperatively. When evaluating the glands, surgeons often use color as the first indication as to whether or not they have been devascularized. Based on this fact, diffuse reflectance spectroscopy/imaging (DRS/I) could potentially be employed in a device for assessing parathyroid vascularity. The technique involves illuminating an object with light of known wavelengths and capturing the light that gets scattered back. It can be done with a “white light” source (a continuum of wavelengths within the visible spectrum) or a single wavelength source, with data recorded either as a function of wavelength (DRS) or in an image (DRI)[62]. A pulse oximeter relies on a form of diffuse

reflectance. It illuminates the finger with light of two different wavelengths (660 nm and 940 nm) and measures the amount of light that is transmitted through to the detector on the other side of the tissue, per wavelength. Oxy- and deoxyhemoglobin absorb these wavelengths of light differently, with deoxyhemoglobin absorbing more than oxyhemoglobin at 660 nm and vice versa at 940 nm. Based on the intensity of light detected at both wavelengths, the relative concentrations of oxy- and deoxyhemoglobin can be calculated and used to determine the oxygen saturation of the tissue[63].

A similar technique could be used to objectively assess parathyroid gland vascularity. Since a devascularized parathyroid gland will stop receiving oxygenated blood, it might begin to pool with deoxygenated blood. However, similar to visual assessment, DRS/I will be limited by how quickly the gland pools with deoxygenated blood. Additionally, it could be susceptible to false positives since bruising could cause a darkening of the gland even though it may not be completely devascularized. A better solution to this problem would be a method that detects the flow of blood, rather than its mere presence. Laser speckle contrast imaging is such a technique.

2.7 Laser Speckle Contrast Imaging

Laser speckle contrast imaging (LSCI) is an optical imaging technique that is similar in principle to LDF. However, rather than relying on point-based measurements, it is a wide-field imaging technique. It was first introduced in the early 1980's in the form of single-exposure speckle photography[64], which was a two-step process that required first taking a photograph of laser light illuminating the target tissue, developing the film, and then performing an optical high-pass spatial filtering to highlight regions of increased blood flow. With the advancement of digital technology, it was later developed into a digital technique which made its application more streamlined[65]. The technique works by analyzing the interference pattern produced when an object is illuminated with coherent light. There are minute differences in path lengths traveled by light waves scattering from the surface of the object, on the order of the wavelength of the light source. This results in bright and dark spots of constructive and destructive interference on a sensor imaging the object, and is known as a speckle pattern. Movement of particles within a few hundred microns of the surface causes this speckle pattern to fluctuate. Therefore, when an image of a speckle pattern is acquired over a finite exposure time, the pattern in regions where flow of

particles is occurring will be blurred in a manner dependent on the velocity of flow and on the exposure time of the imaging sensor. Quantitatively, it has been shown that the spatial variance of the speckle pattern is related to temporal quantities by:

$$\sigma_s^2 = \frac{2}{T}\int_0^T \left(1 - \frac{\tau}{T}\right) C_t(\tau) d\tau \tag{2.1}$$

T is the exposure time and $C_t(\tau)$ is the autocovariance of the intensity fluctuations of a single speckle[66]. As Equation 2.1 shows, the spatial variation in the speckle pattern reduces with longer integration times (the image gets more blurry). This also happens under conditions of faster flow which causes the speckle pattern to quickly decorrelate (small $C_t(\tau)$). This blurring can be difficult to detect visually, and so the goal of single-exposure speckle photography was to enhance the contrast between blurry and less-blurry regions of the speckle pattern. To do this, a photograph of the speckle pattern would be acquired and developed on a transparency in the first step. In the second step, the transparency would be placed in an imaging setup and illuminated with collimated light. High-pass spatial filtering would then be performed (by physically blocking low spatial frequencies in the center of the Fourier plane of the imaging setup) to attenuate light from the lower frequency components of the image, corresponding to the blurred regions. This enhanced contrast and enabled much easier visual identification of regions of flow. This technique was difficult and time-consuming to implement however, due to the need to first develop the image on a transparency and then perform spatial filtering. With further advances in technology, it developed into a technique that could be performed without the need to develop photographs, which made real-time applications possible[65]. Currently, to enhance spatial contrast in digital images of speckle patterns, a quantity termed the spatial speckle contrast is computed. At each location in the image, this quantity is given by the ratio of the standard deviation of pixel intensities within a region centered on that pixel, divided by the mean intensity within that region (Equation 2.2).

$$K_s = \frac{\sigma_s}{\langle I \rangle} \tag{2.2}$$

Choosing the size of the window within which to calculate speckle contrast is important as it leads to a trade-off between spatial resolution and accuracy of the of the speckle contrast map. With a smaller window size, there are fewer pixels to estimate the speckle contrast from, leading to a greater chance for inaccuracy. Conversely, with a larger window size, the spatial resolution of the speckle contrast map is reduced as each pixel includes information from a lot more neighboring pixels. A window size of 5 x 5 or 7 x 7 pixels is generally considered to be a good compromise[67].

This technique has been employed in a wide range of biomedical applications for measuring blood flow, where the vessels of interest are generally superficial, such as the retina, skin and brain[68]. Many of its applications have been in laboratory settings for investigating phenomena such as skin blood flow dynamics in response to external stimuli[69,70], and cerebral blood flow in animal models of stroke[71]. Clinically, LSCI and similar techniques have been applied to monitoring Port Wine Stain laser therapy[72], correlating microvascular blood flow with healing time in burn wounds[73], and measuring cerebral blood flow in patients undergoing brain tumor resection[74]. However, there are no published reports on the application of LSCI for assessing parathyroid gland vascularity during endocrine surgery. Laser speckle contrast imaging appears to be a promising approach to meet the need for a real-time, label-free and objective method of assessing parathyroid gland vascularity. Firstly, it directly assesses the flow of blood rather than an accumulation of deoxygenated blood like visual inspection or diffuse reflectance. Secondly, it is a wide-field imaging technique and can be performed much faster than point-based measurements such as LDF. Additionally, the equipment needed to perform LSCI need not be very complicated – all that is required is a coherent light source and a camera to detect the speckle pattern.

2.8 Significance and Innovation

The work presented in this dissertation addresses an unmet need for an accurate, real-time, label-free and objective approach to assess parathyroid gland vascularity during endocrine neck surgeries. It also proposes a single label-free solution for complete assessment of the parathyroid gland to improve surgical guidance. The innovation of this work includes the following:

1. This work contains the first report on the use of LSCI to assess parathyroid gland vascularity. Additionally, while a large number of studies employing LSCI for different problems image at a high

enough resolution to highlight blood vessels and quantify differences in blood flow rates, this work does not require resolving the microvasculature of the parathyroid. This makes it possible to image at a lower resolution, simplifying the construction of devices for intraoperative use.

2. This work also establishes first set of parameters for evaluating parathyroid vascularity with LSCI. One barrier to the clinical adoption of LSCI for parathyroid preservation is that there are no established parameters based on patient outcome data to provide guidance during surgery. The work presented in this dissertation fills this gap.
3. There is technical innovation in the development of a combined LSCI and NIRAF imaging device. Furthermore, this work reports an innovative approach to automating the extraction of parathyroid speckle contrast by exploiting the combination of the two techniques. This reduces a barrier to clinical translation, making it easier for surgeons to adopt the technique.

2.9 References

1. Kuehn, Francis, S., Lozada & Mauris, P. *Thyroid Hormones*. (Nova, 2009).
2. Mohebati, A. & Shaha, A. R. Anatomy of thyroid and parathyroid glands and neurovascular relations. *Clin. Anat.* **25**, 19–31 (2012).
3. MedicineNet. Medical Definition of Parathyroid gland. http://www.medicinenet.com/script/main/art.asp?articlekey=4773 (2007).
4. Felsenfeld, A. J. & Levine, B. S. Calcitonin, the forgotten hormone: does it deserve to be forgotten? *Clin. Kidney J.* **8**, 180–7 (2015).
5. Fancy, T., Gallagher, D. & Hornig, J. D. Surgical anatomy of the thyroid and parathyroid glands. *Otolaryngol. Clin. North Am.* **43**, 221–7, vii (2010).
6. Akerström, G., Malmaeus, J. & Bergström, R. Surgical anatomy of human parathyroid glands. *Surgery* **95**, 14–21 (1984).
7. Wang, C. The anatomic basis of parathyroid surgery. *Ann. Surg.* **183**, 271–5 (1976).
8. Nobori, M., Saiki, S., Tanaka, N., Harihara, Y., Shindo, S. & Fujimoto, Y. Blood supply of the parathyroid gland from the superior thyroid artery. *Surgery* **115**, 417–23 (1994).
9. Halsted, W. S. & Evans, H. M. The parathyroid glandules. Their blood supply, and their preservation in operation upon the thyroid gland. *Ann. Surg.* **XLVI**, 489–506 (1907).
10. Naveh-Many, T. *Molecular Biology of the Parathyroid*. (Kluwer Academic / Plenum Publishers, 2005).

11. Gowda, C. & Nandi, D. Thyroid Diseases. in *Encyclopedia of Global Health* (SAGE Publications, Inc.). doi:10.4135/9781412963855.n1167.

12. American Thyroid Association. Hashimoto's Thyroiditis | American Thyroid Association. https://www.thyroid.org/hashimotos-thyroiditis/ (2021).

13. American Thyroid Association. Graves' Disease. https://www.thyroid.org/graves-disease/ (2021).

14. The American Cancer Society. What Is Thyroid Cancer? https://www.cancer.org/cancer/thyroid-cancer/about/what-is-thyroid-cancer.html (2016).

15. Mohebati, A. & Shaha, A. R. Imaging techniques in parathyroid surgery for primary hyperparathyroidism. *Am. J. Otolaryngol.* **33**, 457–468 (2012).

16. Kim, L. Hyperparathyroidism: Primary Hyperparathyroidism. http://emedicine.medscape.com/article/127351-overview?pa=4AxcIjxHxMV6bNDVEa8zaqz%2FOFFtZL4SYrtNSy1E6e6sim3UAgfd7PjK5RizEedlsYVXQ5wnaSWTq%2FJND3YZdPEiL5fM42L%2B9xlMlua7G1g%3D#a3 (2016).

17. Potts, J. T. Parathyroid hormone: past and present. *J. Endocrinol.* **187**, 311–25 (2005).

18. Clarke, B. L. Epidemiology of hypoparathyroidism. in *Hypoparathyroidism* 139–154 (Springer-Verlag Milan, 2015). doi:10.1007/978-88-470-5376-2_14.

19. Kim, S. M., Shu, A. D., Long, J., Montez-Rath, M. E., Leonard, M. B., Norton, J. A. & Chertow, G. M. Declining Rates of Inpatient Parathyroidectomy for Primary Hyperparathyroidism in the US. *PLoS One* **11**, e0161192 (2016).

20. Sun, G. H., DeMonner, S. & Davis, M. M. Epidemiological and Economic Trends in Inpatient and Outpatient Thyroidectomy in the United States, 1996–2006. *Thyroid* **23**, 727–733 (2013).

21. McHenry, C. R., Speroff, T., Wentworth, D. & Murphy, T. Risk factors for postthyroidectomy hypocalcemia. *Surgery* **116**, 641–7; discussion 647-8 (1994).

22. Ezzat, W., Fathey, H., Fawaz, S., El-Ashri, A., Youssef, T. & Othman, H. Intraoperative parathyroid hormone as an indicator for parathyroid gland preservation in thyroid surgery. *Swiss Med. Wkly.* (2011) doi:10.4414/smw.2011.13299.

23. Kuriloff, D. B. & Kizhner, V. Parathyroid gland preservation and selective autotransplantation utilizing topical lidocaine in total thyroidectomy. *Laryngoscope* **120**, 1342–1344 (2010).

24. Rajinikanth, J., Paul, M. J., Abraham, D. T., Ben Selvan, C. K. & Nair, A. Surgical audit of inadvertent parathyroidectomy during total thyroidectomy: incidence, risk factors, and outcome. *Medscape J. Med.* **11**, 29 (2009).

25. Lin, D. T., Patel, S. G., Shaha, A. R., Singh, B. & Shah, J. P. Incidence of Inadvertent Parathyroid Removal During Thyroidectomy. *Laryngoscope* **112**, 608–611 (2002).

26. American College of Surgeons. Total Thyroidectomy Complication Rates and Costs Are Lower if Surgeon Performs 25 or More Cases Yearly. https://www.facs.org/media/press-releases/2015/sosa (2015).

27. Edafe, O. & Balasubramanian, S. P. Incidence, prevalence and risk factors for post-surgical

hypocalcaemia and hypoparathyroidism. *Gland Surgery* vol. 6 S59–S68 (2017).

28. Zahedi Niaki, N., Singh, H., Moubayed, S. P., Leboeuf, R., Tabet, J.-C., Christopoulos, A., Ayad, T., Olivier, M.-J., Guertin, L. & Bissada, E. The Cost of Prolonged Hospitalization due to Postthyroidectomy Hypocalcemia: A Case-Control Study. *Adv. Endocrinol.* **2014**, 1–4 (2014).

29. Hyun, H., Park, M. H., Owens, E. A., Wada, H., Henary, M., Handgraaf, H. J. M., Vahrmeijer, A. L., Frangioni, J. V. & Choi, H. S. Structure-inherent targeting of near-infrared fluorophores for parathyroid and thyroid gland imaging. *Nat. Med.* **21**, 192–197 (2015).

30. Antakia, R., Gayet, P., Stephanie, G., Stephenson, T. J., Brown, N. J., Harrison, B. J. & Balasubramanian, S. P. Near infrared fluorescence imaging of rabbit thyroid and parathyroid glands. *J. Surg. Res.* **192**, 480–486 (2014).

31. Tummers, Q. R. J. G., Schepers, A., Hamming, J. F., Kievit, J., Frangioni, J. V., Van De Velde, C. J. H. & Vahrmeijer, A. L. Intraoperative guidance in parathyroid surgery using near-infrared fluorescence imaging and low-dose Methylene Blue. *Surg. (United States)* **158**, 1323–1330 (2015).

32. Conti De Freitas, L. C., Phelan, E., Liu, L., Gardecki, J., Namati, E., Warger, W. C., Tearney, G. J. & Randolph, G. W. Optical coherence tomography imaging during thyroid and parathyroid surgery: A novel system of tissue identification and differentiation to obviate tissue resection and frozen section. *Head Neck* **36**, 1329–1334 (2014).

33. Ladurner, R., Hallfeldt, K. K. J., Al Arabi, N., Stepp, H., Mueller, S. & Gallwas, J. K. S. Optical coherence tomography as a method to identify parathyroid glands. *Lasers Surg. Med.* **45**, 654–659 (2013).

34. Sommerey, S., Al Arabi, N., Ladurner, R., Chiapponi, C., Stepp, H., Hallfeldt, K. K. J. & Gallwas, J. K. S. Intraoperative optical coherence tomography imaging to identify parathyroid glands. *Surg. Endosc.* **29**, 2698–2704 (2015).

35. Schols, R. M., Bouvy, N. D., Wieringa, F. P., Alić, L. & Stassen, L. P. S. Diffuse optical reflectance spectrometry in thyroid and parathyroid surgery | Request PDF. in *21st International Congress of the European Association of Endoscopic Surgery* (2012).

36. Paras, C., Keller, M., White, L., Phay, J. & Mahadevan-Jansen, A. Near-infrared autofluorescence for the detection of parathyroid glands. *J. Biomed. Opt.* **16**, 067012 (2011).

37. McWade, M. A., Paras, C., White, L. M., Phay, J. E., Mahadevan-Jansen, A. & Broome, J. T. A novel optical approach to intraoperative detection of parathyroid glands. *Surgery* **154**, 1371–7; discussion 1377 (2013).

38. McWade, M. A., Sanders, M. E., Broome, J. T., Solórzano, C. C. & Mahadevan-Jansen, A. Establishing the clinical utility of autofluorescence spectroscopy for parathyroid detection. *Surgery* **159**, 193–202 (2016).

39. Thomas, G., McWade, M. A., Paras, C., Mannoh, E. A., Sanders, M. E., White, L. M., Broome, J. T., Phay, J. E., Baregamian, N., Solórzano, C. C. & Mahadevan-Jansen, A. Developing a Clinical Prototype to Guide Surgeons for Intraoperative Label-Free Identification of Parathyroid Glands in Real Time. *Thyroid* **28**, 1517–1531 (2018).

40. Thomas, G., Squires, M. H., Metcalf, T., Mahadevan-Jansen, A. & Phay, J. E. Imaging or Fiber Probe-Based Approach? Assessing Different Methods to Detect Near Infrared Autofluorescence for Intraoperative Parathyroid Identification. *J. Am. Coll. Surg.* **229**, 596-608.e3 (2019).

41. Thomas, G., McWade, M. A., Nguyen, J. Q., Sanders, M. E., Broome, J. T., Baregamian, N., Solórzano, C. C. & Mahadevan-Jansen, A. Innovative surgical guidance for label-free real-time parathyroid identification. *Surg. (United States)* **165**, 114–123 (2019).

42. McWade, M. A., Paras, C., White, L. M., Phay, J. E., Solórzano, C. C., Broome, J. T. & Mahadevan-Jansen, A. Label-free Intraoperative Parathyroid Localization With Near-Infrared Autofluorescence Imaging. *J. Clin. Endocrinol. Metab.* **99**, 4574–4580 (2014).

43. Ladurner, R., Sommerey, S., Arabi, N. Al, Hallfeldt, K. K. J., Stepp, H. & Gallwas, J. K. S. Intraoperative near-infrared autofluorescence imaging of parathyroid glands. *Surg. Endosc.* **31**, 3140–3145 (2017).

44. Dip, F., Falco, J., Verna, S., Prunello, M., Loccisano, M., Quadri, P., White, K. & Rosenthal, R. Randomized Controlled Trial Comparing White Light with Near-Infrared Autofluorescence for Parathyroid Gland Identification During Total Thyroidectomy. *J. Am. Coll. Surg.* **228**, 744–751 (2019).

45. Kose, E., Kahramangil, B., Aydin, H., Donmez, M. & Berber, E. Heterogeneous and low-intensity parathyroid autofluorescence: Patterns suggesting hyperfunction at parathyroid exploration. *Surgery* **165**, 431–437 (2019).

46. De Leeuw, F., Breuskin, I., Abbaci, M., Casiraghi, O., Mirghani, H., Ben Lakhdar, A., Laplace-Builhé, C. & Hartl, D. Intraoperative Near-infrared Imaging for Parathyroid Gland Identification by Auto-fluorescence: A Feasibility Study. *World J. Surg.* **40**, 2131–2138 (2016).

47. Kahramangil, B., Dip, F., Benmiloud, F., Falco, J., de La Fuente, M., Verna, S., Rosenthal, R. & Berber, E. Detection of Parathyroid Autofluorescence Using Near-Infrared Imaging: A Multicenter Analysis of Concordance Between Different Surgeons. *Ann. Surg. Oncol.* **25**, 957–962 (2018).

48. Kim, S. W., Song, S. H., Lee, H. S., Noh, W. J., Oak, C., Ahn, Y.-C. & Lee, K. D. Intraoperative Real-Time Localization of Normal Parathyroid Glands With Autofluorescence Imaging. *J. Clin. Endocrinol. Metab.* **101**, 4646–4652 (2016).

49. Ahmed, N., Aurangzeb, M., Muslim, M. & Zarin, M. Routine parathyroid autotransplantation during total thyroidectomy: A procedure with predictable outcome. *J. Pakistan Med. Assoc.* **63**, 190–3 (2013).

50. Christoffersson, G., Henriksnäs, J., Johansson, L., Rolny, C., Ahlström, H., Caballero-Corbalan, J., Segersvärd, R., Permert, J., Korsgren, O., Carlsson, P.-O. & Phillipson, M. Clinical and Experimental Pancreatic Islet Transplantation to Striated Muscle. *Diabetes* **59**, (2010).

51. El-Sharaky, M. I., Kahalil, M. R., Sharaky, O., Sakr, M. F., Fadaly, G. A., El-Hammadi, H. A. & Moussa, M. M. Assessment of parathyroid autotransplantation for preservation of parathyroid function after total thyroidectomy. *Head Neck* **25**, 799–807 (2003).

52. Sierra, M., Herrera, M. F., Herrero, B., Jiménez, F., Sepúlveda, J., Lozano, R. R., Gamino, R., González, O. & Correa-Rotter, R. Prospective biochemical and scintigraphic evaluation of

autografted normal parathyroid glands in patients undergoing thyroid operations. *Surgery* **124**, 1005–10 (1998).

53. Lo, C. Y. & Tam, S. C. Parathyroid autotransplantation during thyroidectomy: Documentation of graft function. *Arch. Surg.* **136**, 1381–1385 (2001).

54. Johansson, K., Ander, S., Lennquist, S. & Smeds, S. Human parathyroid blood supply determined by laser-Doppler flowmetry. *World J. Surg.* **18**, 417–420 (1994).

55. Ander, S., Johansson, K. & Smeds, S. In situ preservation of the parathyroid glands during operations on the Thyroid. *Eur. J. Surg.* **163**, 33–7 (1997).

56. Chang, T.-P., Palazzo, F., Tolley, N., Constantinides, V., Yang, G.-Z. & Darzi, A. Vascularity assessment of parathyroid glands using confocal endomicroscopy: Towards an intraoperative imaging tool for real-time in situ viability assessment. *Eur. J. Surg. Oncol.* **40**, S3 (2014).

57. Alford, R., Simpson, H. M., Duberman, J., Hill, G. C., Ogawa, M., Regino, C., Kobayashi, H. & Choyke, P. L. Toxicity of Organic Fluorophores Used in Molecular Imaging: Literature Review. *Mol. Imaging* **8**, 7290.2009.00031 (2009).

58. Vidal Fortuny, J., Karenovics, W., Triponez, F. & Sadowski, S. M. Intra-Operative Indocyanine Green Angiography of the Parathyroid Gland. *World J. Surg.* **40**, 2378–2381 (2016).

59. Fortuny, J. V., Belfontali, V., Sadowski, S. M., Karenovics, W., Guigard, S. & Triponez, F. Parathyroid gland angiography with indocyanine green fluorescence to predict parathyroid function after thyroid surgery. *Br. J. Surg.* **103**, 537–543 (2016).

60. Chu, W., Chennamsetty, A., Toroussian, R. & Lau, C. Anaphylactic Shock After Intravenous Administration of Indocyanine Green During Robotic Partial Nephrectomy. *Urol. Case Reports* **12**, 37–38 (2017).

61. Yuan, B., Chen, N. & Zhu, Q. Emission and absorption properties of indocyanine green in Intralipid solution. *J. Biomed. Opt.* **9**, 497 (2004).

62. Moy, A. J. & Tunnell, J. W. Diffuse Reflectance Spectroscopy and Imaging. in *Imaging in Dermatology* 203–215 (Elsevier Inc., 2016). doi:10.1016/B978-0-12-802838-4.00017-0.

63. Ortega, R., Hansen, C. J., Elterman, K. & Woo, A. Pulse Oximetry. *N. Engl. J. Med.* **364**, (2011).

64. Fercher, A. F. & Briers, J. D. Flow Visualization By Means Of Single-Exposure Speckle Photography. *Opt. Commun.* **37**, (1981).

65. Briers, J. D. & Webster, S. Laser Speckle Contrast Analysis (LASCA): A Nonscanning, Full-Field Technique for Monitoring Capillary Blood Flow. *J. Biomed. Opt.* **1**, 174–179 (1996).

66. Duncan, D. D. & Kirkpatrick, S. J. Can laser speckle flowmetry be made a quantitative tool? *J. Opt. Soc. Am. A. Opt. Image Sci. Vis.* **25**, 2088–94 (2008).

67. Briers, D., Duncan, D. D., Hirst, E., Kirkpatrick, S. J., Larsson, M., Steenbergen, W., Stromberg, T. & Thompson, O. B. Laser speckle contrast imaging: theoretical and practical limitations. *J. Biomed. Opt.* **18**, 066018 (2013).

68. Boas, D. A. & Dunn, A. K. Laser speckle contrast imaging in biomedical optics. *J. Biomed. Opt.*

15, 011109 (2010).

69. Choi, B., Kang, N. M. & Nelson, J. S. Laser speckle imaging for monitoring blood flow dynamics in the in vivo rodent dorsal skin fold model. *Microvasc. Res.* **68**, 143–6 (2004).

70. Iredahl, F., Löfberg, A., Sjöberg, F., Farnebo, S. & Tesselaar, E. Non-Invasive Measurement of Skin Microvascular Response during Pharmacological and Physiological Provocations. *PLoS One* **10**, e0133760 (2015).

71. Dunn, A. K., Bolay, H., Moskowitz, M. A. & Boas, D. A. Dynamic imaging of cerebral blood flow using laser speckle. *J. Cereb. Blood Flow Metab.* **21**, 195–201 (2001).

72. Huang, Y.-C., Ringold, T. L., Nelson, J. S. & Choi, B. Noninvasive blood flow imaging for real-time feedback during laser therapy of port wine stain birthmarks. *Lasers Surg. Med.* **40**, 167–173 (2008).

73. Mirdell, R., Iredahl, F., Sjöberg, F., Farnebo, S. & Tesselaar, E. Microvascular blood flow in scalds in children and its relation to duration of wound healing: A study using laser speckle contrast imaging. *Burns* **42**, 648–654 (2016).

74. Richards, L. M., Kazmi, S. S., Olin, K. E., Waldron, J. S., Fox, D. J. & Dunn, A. K. Intraoperative multi-exposure speckle imaging of cerebral blood flow. *J. Cereb. Blood Flow Metab.* 0271678X1668698 (2017) doi:10.1177/0271678X16686987.

CHAPTER 3

INTRAOPERATIVE ASSESSMENT OF PARATHYROID VIABILITY USING LASER SPECKLE CONTRAST IMAGING

Emmanuel. A. Mannoh[1], Giju Thomas[1], Carmen C. Solorzano[2], Anita Mahadevan-Jansen[1]

[1] Department of Biomedical Engineering, Vanderbilt University, Nashville, TN 37235

[2] Division of Surgical Oncology and Endocrine Surgery, Vanderbilt University Medical Center, Nashville, TN 37232

This chapter was adapted with permission from:

"Intraoperative Assessment of Parathyroid Viability using Laser Speckle Contrast Imaging"

Scientific Reports. 2017

3.1 Abstract

Post-surgical hypoparathyroidism and hypocalcemia are known to occur after nearly 50% of all thyroid surgeries as a result of accidental disruption of blood supply to healthy parathyroid glands, which are responsible for regulating calcium. However, there are currently no clinical methods for accurately identifying compromised glands and the surgeon relies on visual assessment alone to determine if any gland(s) should be excised and auto-transplanted. Here, we present Laser Speckle Contrast Imaging (LSCI) for real-time assessment of parathyroid viability. Taking an experienced surgeon's visual assessment as the gold standard, LSCI can be used to distinguish between well vascularized (n = 32) and compromised (n = 27) parathyroid glands during thyroid surgery with an accuracy of 91.5%. Ability to detect vascular compromise with LSCI was validated in parathyroidectomies. Results showed that this technique is able to detect parathyroid gland devascularization before it is visually apparent to the surgeon. Measurements can be performed in real-time and without the need to turn off operating room lights. LSCI shows promise as a real-time, label-free, objective method for helping reduce hypoparathyroidism after thyroid surgery.

3.2 Introduction

Approximately 8 million Americans are diagnosed annually with some form of thyroid disease[1], over 92,000 of whom undergo partial or total thyroidectomy as definitive treatment[2]. An estimated 3% of these procedures result in the patient being permanently unable to produce sufficient levels of parathyroid hormone for normal serum calcium regulation[3,4]. Additionally, a significant proportion of patients suffer from a transient form of this post-surgical hypoparathyroidism and consequent hypocalcemia[5–8], with some studies reporting incidences as high as 47%[8]. Hypocalcemia can lead to cardiac arrhythmias, muscle spasms, tetany and eventually death, and is a huge economic burden for these patients who may require extended hospital stays or have to take regular calcium supplements for the rest of their lives to prevent these effects[9]. It is also one of the main causes for malpractice lawsuits after endocrine surgery[7]. Post-surgical hypoparathyroidism results from accidental disruption of the blood supply to, or accidental removal of, otherwise healthy parathyroid glands, organs responsible for regulating calcium. There are typically four parathyroid glands, which contain calcium-sensing receptors and secrete parathyroid hormone (PTH) in response to low serum calcium. Parathyroid hormone acts on bone to promote resorption, on the kidneys to reduce calcium elimination in urine, and on the intestines to promote calcium absorption through the intestinal wall, all of which help to increase serum calcium[10]. Vascular compromise of parathyroid glands may occur after thyroidectomy because of the close proximity of the parathyroid glands to the thyroid. In many cases, the parathyroid glands derive their blood supply from the same blood vessels that feed the thyroid[11]. Fortunately, devascularized parathyroid glands can be salvaged by autotransplantation – a procedure by which the gland is excised and transplanted typically into the sternocleidomastoid muscle[12]. However, identifying these glands is challenging and currently depends on subjective visual assessment and surgeon experience. Additionally, failure to revive parathyroid function after autotransplantation has been reported to occur in 14-17% of cases[12,13]. As a result, a surgeon needs to be certain that a parathyroid gland is devascularized, and therefore not viable if left in place, before committing to this procedure.

A number of techniques have been employed to assess parathyroid viability, intraoperatively. A common approach is to look for bright red bleeding after pricking the parathyroid gland with a needle or cutting off tiny fragments[14], however care needs to be taken not to irreversibly damage the gland. Topical application of a dilute lidocaine solution has been employed to cause vasodilation in vascularized parathyroid glands. Any gland that does not swell after application of lidocaine is considered not viable

and is therefore autotransplanted. This procedure is risky, since lidocaine can cause paralysis of the vocal cords if it comes into contact with the exposed laryngeal nerve[14]. Intraoperative measurement of PTH is performed routinely in parathyroidectomies to confirm removal of the hyperactive gland. Since the half-life of PTH in the blood is 3-5 minutes, removal of a parathyroid gland leads to noticeable decrease in serum PTH within a relatively short amount of time. Based on this concept, intraoperative measurement of PTH has also been employed in thyroidectomies[15], however this approach gives no indication of which parathyroid gland might be compromised. Another approach is to use indocyanine green (ICG) angiography to identify devascularized parathyroid glands. One study reported that hypoparathyroidism did not occur after surgery in thyroidectomy patients where at least one parathyroid gland was determined (by qualitative assessment of ICG fluorescence) to be well vascularized[16]. This method requires administration of an exogenous contrast agent and is limited by how frequently it can be performed. There is therefore a critical need for a real-time, contrast-free and objective method for assessing the viability of parathyroid glands intraoperatively.

Here, we present the first report on the application of Laser Speckle Contrast Imaging (LSCI) to meet this need. This technique was first introduced in the 1980's as a photographic method for obtaining spatial maps of the velocity distribution in a field[17]. With the advancement of digital technology, it was later developed into a digital technique which made its application more streamlined[18]. The technique analyzes the interference pattern produced when coherent light is incident on a surface. Minute differences in path length created by the light waves scattering from different regions produce bright and dark spots of constructive and destructive interference respectively, termed as a speckle pattern. This speckle pattern fluctuates depending on how fast particles are moving within a few hundred microns of the surface. Blurring of the speckle pattern occurs when the motion is fast relative to the integration time of the detector. Analyzing this spatial blurring provides contrast between regions of faster versus slower motion and forms the basis of LSCI[19]. Quantitatively, the speckle contrast is defined as the ratio of the standard deviation of pixel values to the mean (Equation 3.1), calculated within a given region.

$$K_s = \frac{\sigma_s}{\langle I \rangle} \tag{3.1}$$

This technique is sensitive to microvascular blood flow and has been employed in a variety of tissues where the vessels of interest are generally superficial, such as the retina, skin and brain[19]. Many of its applications have been in laboratory settings for investigating phenomena such as skin blood flow dynamics in response to external stimuli[20,21], and cerebral blood flow in animal models of stroke[22]. Clinically, LSCI and similar techniques have been applied to monitoring Port Wine Stain laser therapy[23], correlating microvascular blood flow with healing time in burn wounds[24], and measuring cerebral blood flow in patients undergoing brain tumor resection[25]. However, there are no published reports on the application of LSCI or any other label-free optical method for assessing parathyroid gland viability during endocrine surgery. Parathyroid glands are densely packed with blood vessels, given that they secrete PTH to the entire body. Furthermore, their small size (3-8 mm[11]) makes many of these vessels superficial, making these glands suitable targets for assessment using LSCI.

The goal of this study is to evaluate the capability of LSCI to distinguish between vascularized and compromised parathyroid glands as determined by an experienced surgeon, in real-time during endocrine surgery. This pilot study was performed in patients undergoing thyroidectomies and parathyroidectomies by measuring the speckle contrast of parathyroid glands *in vivo.* Performance of LSCI was evaluated in thyroidectomies, by grouping speckle contrast from normal functioning and compromised parathyroid glands according to the surgeon's classification. Validation was performed in parathyroidectomies, where the state of vascularity of the parathyroid gland was controlled in glands planned for excision. Results demonstrate the effectiveness of LSCI for parathyroid gland assessment.

3.3 Materials and Methods

3.3.1 LSCI system design

The LSCI system developed for this study is shown in Figure 3.1. It is mounted on an articulated arm attached to a mobile cart. A 785 nm diode laser (Innovative Photonics Solutions, Monmouth Junction, NJ) is coupled through a 400 µm fiber optic patch cord (Thorlabs, Newton, NJ) to a lens tube containing a 75 mm focal length biconvex lens (Thorlabs, Newton, NJ). This lens diverges the laser light to a ~8 cm

diameter spot at a distance of about 45 cm from the edge of the lens. The irradiance at the surface was measured to be ~0.6 mW/cm^2. A near-infrared optimized camera (acA1300-60gmNIR, Basler AG, Ahrensburg, Germany) captures the images, which are focused onto the camera sensor by an imaging lens system (Navitar 50 mm F/2.8, Navitar, Woburn, MA). The camera is aligned vertically, and the angle between the illumination beam and the line of sight of the camera is fixed at approximately 9° and was designed to reduce specular reflection. Attached to the front end of the lens system is a focus tunable lens (EL-16-40-TC-VIS-5D-M27, Optotune, Dietikon, Switzerland). This allows the images to be focused during each procedure from outside the sterile field as the height of the operating table may be slightly adjusted during surgery. The field of view of the camera was measured to be about 5 cm x 6 cm. A 5 mW 660 nm laser pointer (DigiKey, Thief River Falls, MN) is attached such that its beam is co-localized with the center of the camera's field of view at a distance of 45 cm. The purpose of this laser pointer is to guide the surgeon in positioning the system above a parathyroid gland so that it is approximately in the center of the field of view. Images recorded by the camera are sent to a laptop computer for processing and display.

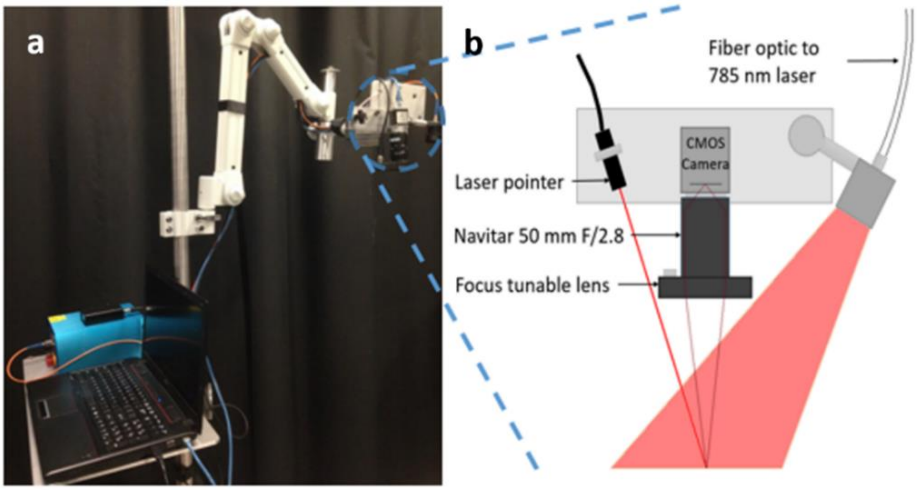

Figure 3.1. Clinical LSCI system. Picture of device (a), schematic of imaging end (b).

3.3.2 Ensuring adequate sampling of speckle pattern

An important consideration when performing LSCI is that the speckle pattern be adequately sampled. The smallest speckle should be at least twice the size of the sensor pixel in order to meet the Nyquist sampling criterion and avoid underestimating speckle contrast[26]. To test whether the developed LSCI system met this criterion, an optical tissue phantom made of polydimethylsiloxane (PDMS) with titanium dioxide to simulate tissue scattering (reduced scattering coefficient of 8 cm^{-1}) was illuminated and imaged with the device using different aperture sizes. The power spectrum was analyzed to ensure there was no aliasing. The iris size was set close to f/16 and locked in this position for the entire study. A well-defined energy band centered at the origin of the power spectrum confirmed no aliasing. Although larger apertures also had no aliasing, this aperture size was chosen because it also resulted in very little background from ambient lighting.

3.3.3 Patient recruitment and imaging protocol

This study was conducted in accordance with the Declaration of Helsinki and its amendments. The study was approved by the Vanderbilt University Medical Center (VUMC) Institutional Review Board (IRB). Patients undergoing partial or total thyroidectomy at the Vanderbilt University Medical Center were recruited and written informed consent was obtained from each patient (n = 20) prior to participation.

Images of parathyroid glands were recorded during the course of surgery at the discretion of the surgeon. The surgeon first determined the state of vascularity of the gland based on visual inspection, and then positioned the device above the surgical field so that the laser pointer beam was on the parathyroid gland. With the camera integration time set to about 50 ms to allow imaging with the room lights on, white light images were initially acquired to identify the location of the parathyroid gland. The laser pointer was turned off and the integration time was then set to 5 ms for the rest of the image acquisitions. All speckle contrast images were generated with an integration time of 5 ms. This integration time is within the range typically used for LSCI[19], and results in the room lights contributing very little signal to the image while effectively detecting the 785 nm speckle pattern. Next, the 785 nm laser was turned on and images were acquired and sent to the computer for real-time processing of speckle contrast images. Roughly fifteen seconds of acquisition was allowed for each gland to ensure that a sufficient number of images was obtained. The surgeon was blinded to all images during the surgery.

3.3.4 Validation of technique

Eight patients undergoing parathyroidectomy at the VUMC were recruited and written informed consent obtained prior to participation following IRB approval. As part of standard procedure, the surgeon ligated blood supply to the diseased parathyroid gland prior to excision. Speckle contrast images were acquired before and less than one minute after the surgeon ligated the blood supply to the gland, in preparation for removal. To confirm removal of the hyperactive parathyroid gland, intraoperative measurement of PTH was performed before and 10 minutes after excision of the gland. Changes in speckle contrast between the vascularized and ligated state were assessed.

3.3.5 Speckle contrast calculation

The number of pixels over which spatial speckle contrast is calculated is important, with too few pixels resulting in inaccuracy in contrast estimation while too many pixels sacrificing spatial resolution. Calculating speckle contrast over a 5 x 5 or 7 x 7 pixel region is generally considered a good compromise[27]. In this work, a 5 x 5 pixel window was used in calculating speckle contrast. The window is moved across the image of the acquired speckle pattern and at each location, the speckle contrast is calculated as the standard deviation of pixel intensity values within the window divided by the mean (Equation 3.1). The resultant speckle contrast image has values that theoretically range from 0 to 1, with values closer to 0 representing regions of greater vascular flow and values closer 1 representing regions of less vascular flow. It has been demonstrated that the quantity measured by LSCI is related to a product of speed and diameter of the vessel[28]. In this application, the microvasculature cannot be resolved due to the relatively large field of view required, and the measured speckle contrast is taken to be an ensemble measurement of the microvessels on the surface of the gland. Image acquisition and display is performed through a custom LabVIEW program, while a custom dynamic link library file enables processing and display at about 10 frames per second.

3.3.6 Data analysis

Data was analyzed using MATLAB R2015a (The MathWorks Inc., Natick, MA). Speckle contrast images displayed in this manuscript are each an average of 20 consecutively generated maps. This was

done to improve the spatial resolution of the final image. For any case where a sudden movement or a headlamp accidentally turned towards the surgical field caused a global sharp decrease in speckle contrast, these frames were excluded from averaged images. To correct for slight movement of the surgical field during recordings, an image registration algorithm was employed before averaging. The parathyroid gland was then demarcated using the "roipoly" function, avoiding bright spots caused by specular reflection, and the average speckle contrast within this region was calculated. In future iterations of the device, polarizers could be used to reduce specular reflection. The data was then grouped into vascularized and compromised according to the surgeon's assessment of the gland. Compromised parathyroid glands were also further grouped into those that the surgeon decided to transplant and those that were left in place. Tests for statistical significance were performed using a two-sided two sample Student's t-test and p-values less than 0.01 were considered statistically significant.

3.3.7 Measuring the effect of ambient lighting on speckle contrast images

A microfluidic flow phantom made of PDMS and titanium dioxide to achieve a reduced scattering coefficient of 8 cm^{-1} was used to evaluate the effect of ambient lighting on speckle contrast images in the laboratory. The device had a 400 μm channel through which a solution of 0.4 g of milk powder diluted in 50 mL of water was flowed. Images were acquired with the room lights on and then off, and 20 speckle contrast images were averaged for each condition.

For one patient undergoing parathyroidectomy, two sets of measurements on one parathyroid gland were obtained to determine the effect of the operating room (OR) lights on speckle contrast images. The surgeon first positioned the device so the parathyroid gland was in the field of view. Images were recorded with the operating room lights on, but with the surgical lights above the operating table pointing away from the surgical field. Then, without moving the device, all operating room lights were turned off and another set of images were obtained. For each condition, 20 speckle contrast images were averaged and the same region of interest was used to calculate average parathyroid gland speckle contrast.

3.4 Results

3.4.1 Effect of ambient lighting on speckle contrast images

Performing measurements without the need to turn off the OR lights is essential so that any disruption to the surgical workflow is minimized. The effect of ambient lights on speckle contrast was evaluated in the laboratory on a microfluidic flow phantom with a milk powder solution flowing through its 400 µm channel (Figure 3.2a,b). Speckle contrast is displayed as false-color images throughout this manuscript to distinguish them from white light images which are in grayscale. A rectangular region of interest crossing the channel was selected and line profiles perpendicular to the channel within this region were averaged for both conditions, lights on and lights off. The average speckle contrast across the surface of the phantom dropped by 0.01 when the lights were turned on, however remained about the same within the channel.

To determine how room lights would affect LSCI data acquired in the operating room, the system was tested *in vivo* on a patient undergoing parathyroidectomy. One set of images was acquired with the room lights on and the surgical lights above the operating table pointed away from the surgical field. (The lights above the operating table had to be turned away due to their much higher intensity which saturated the camera and did not permit acquisition of useful LSCI data). Another set of images was then acquired with all lights off. For each condition, 20 speckle contrast images were averaged after acquisition and the same region of interest was used to calculate average parathyroid gland speckle contrast. There was a 1.7% decrease in the average speckle contrast value of the parathyroid gland when the OR lights were left on, compared to when they were off (Figure 2c-f). These decreases in speckle contrast are to be expected since room/OR lights have a broad frequency spectrum[29] and therefore do not produce a speckle pattern. The uniform lighting fills in dark spots in the speckle pattern generated by the laser, thereby reducing the contrast. However, the magnitude of this decrease in the case of the *in vivo* parathyroid gland measurement (~0.002) was miniscule compared to the possible range of speckle contrast values (0 to 1). Additionally, this value is less than 2% of the range of average parathyroid gland speckle contrast obtained in this study. These results indicated that the performance of LSCI is negligibly affected by ambient light and validates its application in the operating room with the OR lights on but pointed away from the patient during image acquisition.

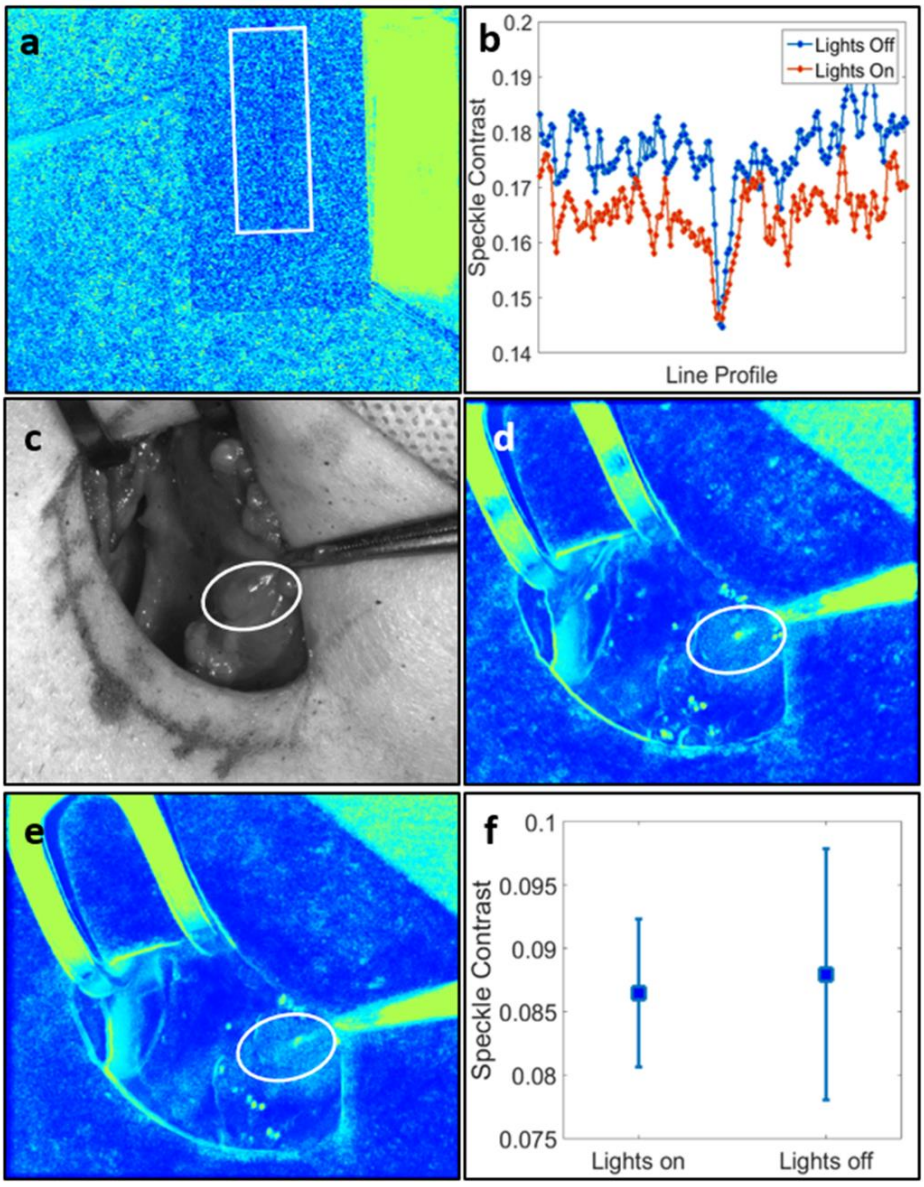

Figure 3.2. Overhead lights have minimal effect on LSCI system. Figure shows speckle contrast image of microfluidic flow phantom (a) and average line profile perpendicular to flow channel for both lighting conditions (b); white light image of surgical field with OR lights on (c); speckle contrast image with OR lights on (d); speckle contrast image with OR lights off (e); mean and standard deviation of speckle contrast within parathyroid for both cases (f). Parathyroid glands are indicated with white ellipses and the flow phantom region of interest is indicated with a white rectangle.

3.4.2 Vascularized vs. compromised parathyroid glands

The LSCI system was tested in twenty patients undergoing thyroidectomy at Vanderbilt University Medical Center. Speckle contrast images of parathyroid glands were acquired during the course of surgery and at the discretion of the participating surgeon. The surgeon's visual assessment of the gland's viability (without input from speckle contrast images) was recorded at the time of image acquisition for each gland. Figure 3.3 shows examples of parathyroid glands considered vascularized and compromised. The left column shows white light images of the surgical field, and the right column shows the corresponding speckle contrast image (average of 20 images). Parathyroid glands are indicated with a white ellipse. As these images show, parathyroid glands considered vascularized by the surgeon have lower speckle contrast than those considered to be compromised.

The average speckle contrast within each parathyroid gland was calculated, avoiding bright spots of specular reflection. This data was then grouped according to the surgeon's visual assessment of vascularity, which served as the gold standard. Using a two-sample two-sided Student's t-test, a statistically significant difference ($p < 0.0001$) was observed in the speckle contrast between glands considered vascularized versus compromised as determined by the surgeon (Figure 3.4a). Within the compromised group, there were 5 glands that were transplanted, and 22 others that the surgeon decided could be left in place without significant adverse effects to the patient. While the mean speckle contrast was higher in the transplanted group, this difference was not found to be significant using a two-sample t-test. These results are shown in Figure 3.4b.

Using speckle contrast as a classifier to distinguish between the vascularized and compromised parathyroid glands, a receiver operating characteristic (ROC) curve was generated with an area under the curve of 0.935 (Figure 3.4c). The optimum threshold for distinguishing between the two groups was found to be 0.09, which resulted in a sensitivity of 92.6% (25/27 compromised glands correctly identified) and a specificity of 90.6% (29/32 vascularized glands correctly identified). From this, the overall accuracy was calculated to be 91.5%.

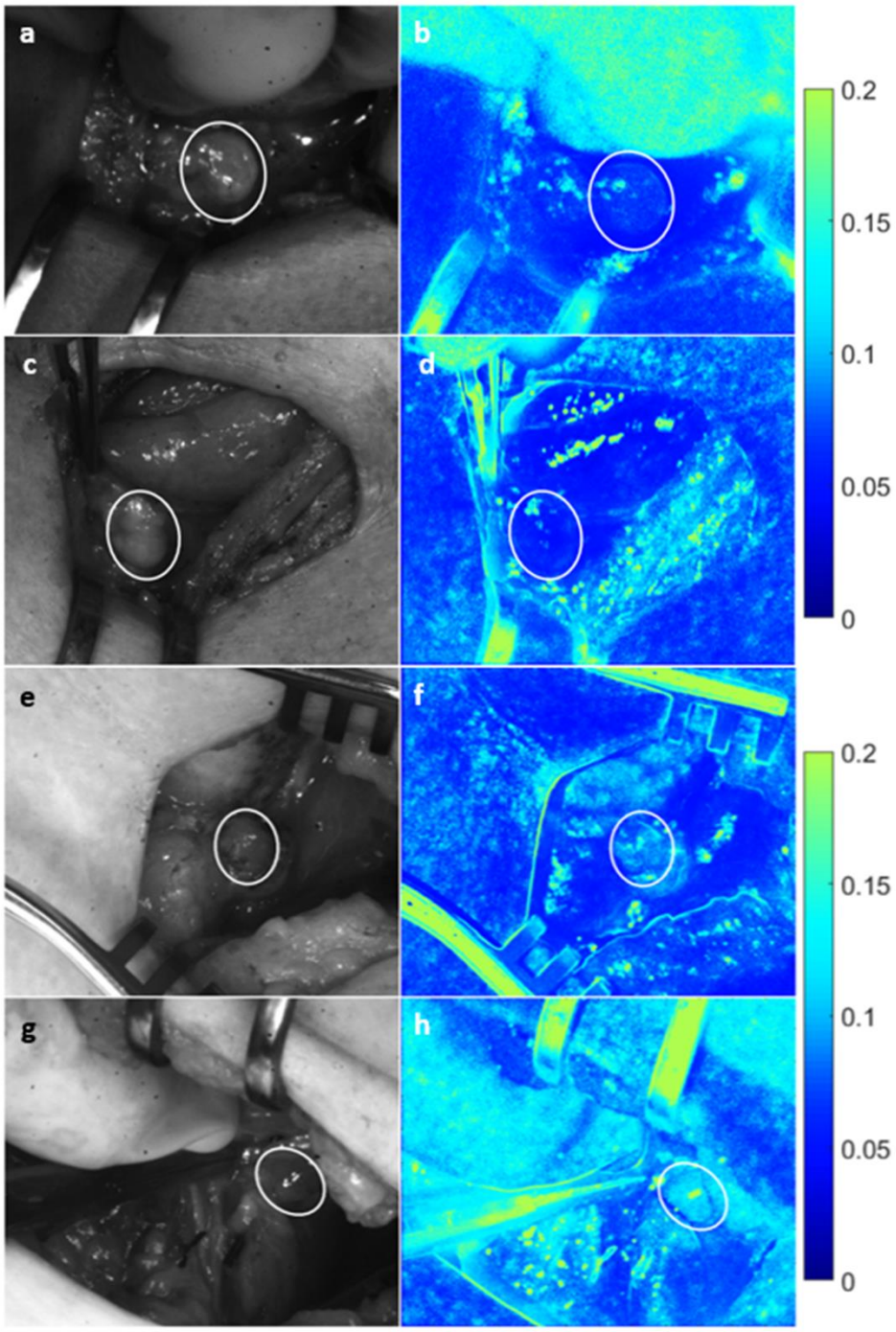

Figure 3.3. Speckle contrast is lower for well vascularized parathyroid glands. Images are shown for two examples each of vascularized (a-d) and compromised (e-h) parathyroid glands. Left column (a,c,e,g) shows white light images, with the corresponding speckle contrast images (b,d,f,h) in the right column. Parathyroid glands are indicated with white ellipses.

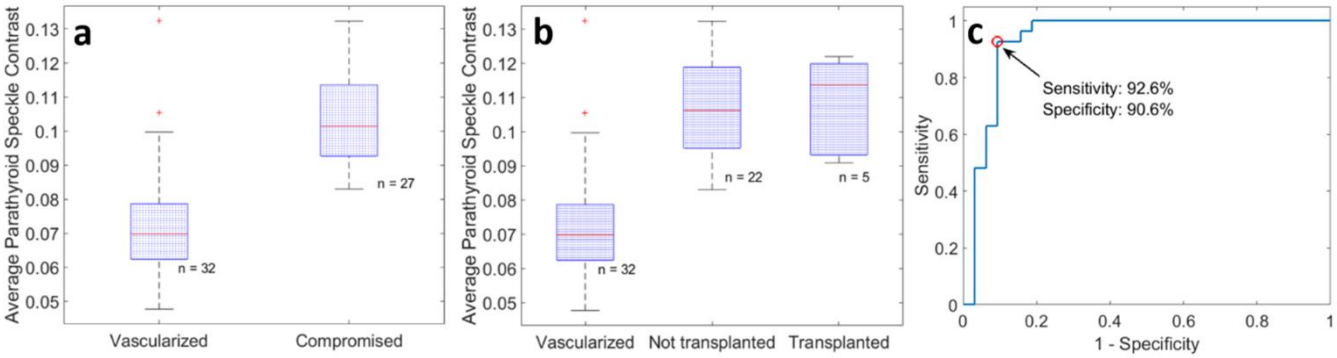

Figure 3.4. Average parathyroid gland speckle contrast grouped according to surgeon's assessment. Speckle contrast is significantly lower ($p < 0.0001$) for vascularized glands (a). Of the compromised glands only 5 required transplantation, however no significant difference was observed between this sub-group and the compromised glands that were left in place (b). Classifying parathyroid glands based on average speckle contrast generated an ROC curve with an area under the curve of 0.935, and an optimum point with sensitivity and specificity of 92.6% and 90.6% respectively (c).

3.4.3 Validation of technique

Given that assessment of parathyroid gland viability currently relies on a surgeon's subjectivity, and these normal functioning glands cannot be excised for histological validation without compromising patient care, validation of LSCI for this application was performed on eight patients undergoing parathyroidectomy, where a diseased parathyroid gland is planned for removal. As part of standard procedure, the surgeon ties off all blood supply to the gland prior to excision. This provides a controllable scenario for evaluating the capability of the device to detect when a parathyroid gland is compromised as well as to determine the detection limit (or time) of the system. To confirm removal of the hyperactive parathyroid gland, intraoperative measurement of PTH is routinely performed before and 10 minutes after excision of the gland.

An example of a hypercellular diseased parathyroid gland marked for removal is shown in Figure 3.5. Again, the left column shows white light images while the corresponding speckle contrast images are in the right column. Images on the top row are of the gland before the surgeon tied off the blood supply. Images on the bottom row were taken on average 30 seconds after the surgeon tied off the blood supply to the gland. According to the surgeon and as seen in the white light image, this gland did not appear visually different from its initial state. However, there is a noticeable change in the speckle contrast

images. In all cases, speckle contrast increased by a minimum of 18% after the surgeon tied off the blood supply (data shown in Table 3.1; mean increase of 0.043). Further, post-excision intraoperative PTH was also lower than pre-excision PTH, confirming removal of the diseased gland.

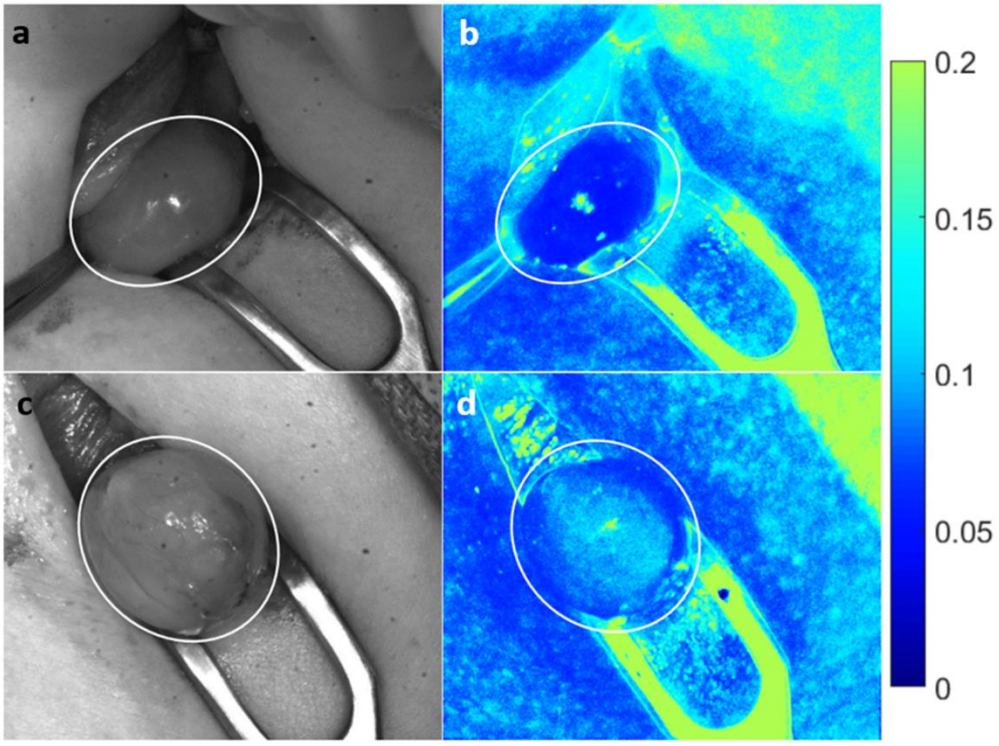

Figure 3.5. Change in speckle contrast occurs seconds after blood supply ligation. A noticeable change in speckle contrast (b,d) was observed in the same parathyroid gland seconds after tying off blood supply to the gland, however no such change was observed in white light images (a,c). Images (a) and (b) were taken before, while images (c) and (d) were taken about 30 seconds after ligation of the blood supply. Parathyroid gland is indicated with a white ellipse.

Table 3.1. Summary of data from excised diseased parathyroid glands. In all cases there was a large increase in speckle contrast seconds after ligation of the blood supply to the gland. There was also a decrease in PTH related to the number of diseased glands removed. In patient 5, LSCI data was obtained from 3 glands that were excised, however PTH measurement was not performed after removal of glands 2 and 3.

Patient #	**Pre-ligation speckle contrast**	**Post-ligation speckle contrast**	**Pre-excision [PTH] (pg/mL)**	**Post-excision [PTH] (pg/mL)**
1	0.076	0.126	86	26
2	0.057	0.094	142	34
3	0.062	0.131	172	32
4	0.074	0.130	119	115
4	0.069	0.119	115	45
5	0.064	0.093	151	53
5	0.048	0.085	53	N/A
5	0.084	0.113	N/A	N/A
6	0.063	0.092	130	31
7	0.067	0.115	76	26

3.5 Discussion

This work demonstrates the capability of LSCI to intraoperatively distinguish between vascularized and compromised parathyroid glands. These measurements can be performed in real-time and with the operating room lights on, minimizing disruption to the surgical workflow. The average speckle contrast value of vascularized parathyroid glands was significantly lower than that of the compromised parathyroid glands, consistent with the understanding that reduced blood flow causes less blurring of the speckle pattern and therefore a higher speckle contrast[19]. Using the ROC curve in Figure 3.4c, a speckle contrast value of ~0.09 was found to be optimal in distinguishing between the two groups with 91.5% accuracy. The ability of LSCI to accurately detect compromised vascularity in the parathyroid gland was validated in the parathyroidectomy cases. These images further show that this device is able to detect changes in speckle contrast within seconds of devascularization. This is much earlier than a surgeon would be able to identify based on visual inspection alone which relies on the gland turning dark with deoxygenated blood and losing turgor, a process which can take several minutes and is often missed. Unlike other techniques that have been used to assess parathyroid gland viability, LSCI can be performed non-invasively, with no risk of damage to the parathyroid gland by physical trauma, nor damage to any nearby tissues. It does not require administration of an exogenous contrast agent, which can take 1-2 minutes to achieve optimum circulation[16]. Additionally, multiple measurements can be made on the same gland

without risk of toxicity. The device enables real-time assessment by processing and displaying speckle contrast images at 10 frames per second. The images shown in this manuscript were created after acquisition by averaging individual frames in order to improve spatial resolution. However, quantitative information on a region of interest can also be displayed in real-time if desired as this information is generated concurrently with imaging. This technique can be performed with the room lights on, only requiring that the lights above the operating table be pointed away from the surgical field.

The biggest challenge facing this study is the fact that the current gold standard for assessing parathyroid gland viability intraoperatively relies on the surgeon's experience which is highly subjective. The surgeon that participated in this study has multiple years of experience in this field and is therefore more likely than not to provide accurate assessments. However, thyroidectomies are routinely performed by general surgeons and residents who may perform less than 25 of these cases in a year. According to the American College of Surgeons this is likely to result in a higher error rate[30], indicating the need for objective assessment of parathyroid viability. These results demonstrate that LSCI has the potential to become the gold standard in this field.

In the absence of an objective gold standard to validate the performance of this device, paired measurements were made in parathyroidectomy cases where the state of vascularity was controlled. It should be noted that the PTH measurements made after excision of the glands are not meant to directly correlate with speckle contrast values but are simply to confirm that the excised tissues are diseased parathyroid glands. A more robust validation method would be to measure PTH after tying off the gland but before excision. However, this was not feasible as it takes about 5-10 minutes for PTH levels to stabilize to a new value and such a procedure would extend OR time and lead to added risk for the patient.

While this device performed with high accuracy in distinguishing between vascularized and compromised parathyroid glands in thyroidectomies, there were 5 instances of disagreement with the surgeon. One case shed light on a possible reason for this disagreement. This particular parathyroid gland was evaluated by the surgeon to be initially well vascularized, however its speckle contrast value suggested otherwise as observed in Figure 3.6b. After 15 minutes, the surgeon re-evaluated this gland as devascularized and transplanted it, with speckle contrast images agreeing with this assessment (Figure 3.6d). This case further demonstrates the ability of LSCI to detect vascular compromise before it is visually apparent to the surgeon.

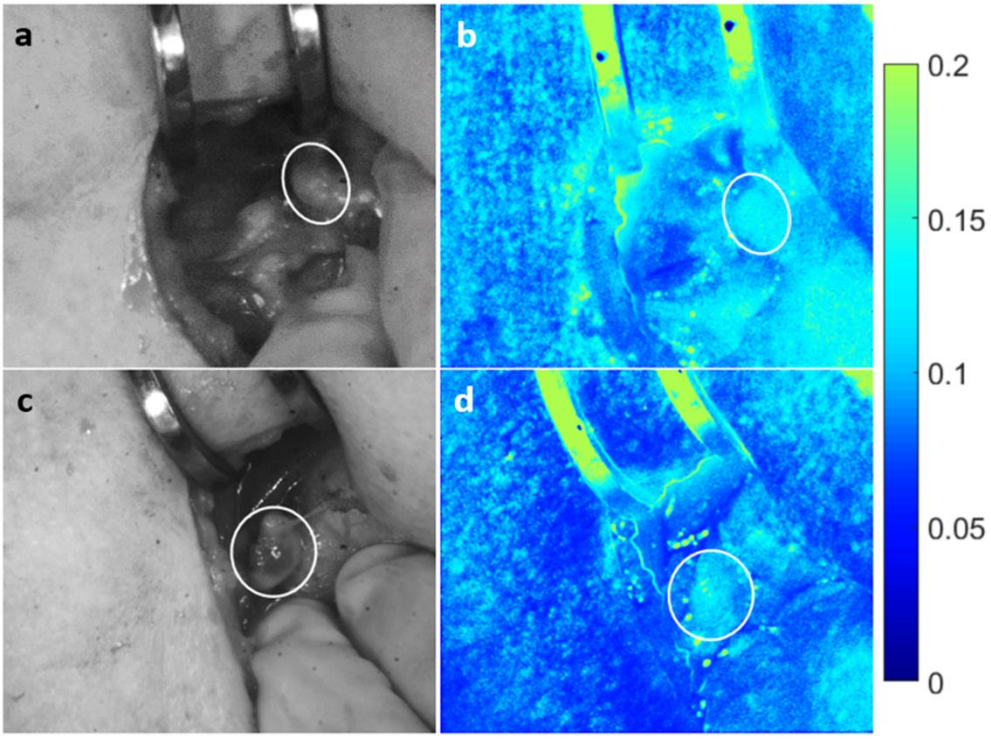

Figure 3.6. LSCI detects vascular compromise in healthy parathyroid gland before it is visually apparent. White light image of a parathyroid gland initially thought well vascularized (a) did not agree with speckle contrast image (b). After 15 minutes, this gland was re-evaluated as devascularized (c) and transplanted. Speckle contrast image (d) supported this assessment. Parathyroid gland is indicated with a white ellipse.

An interesting observation was that of the 27 glands the surgeon considered to have suffered vascular compromise, only 5 were autotransplanted. The rest were considered capable of recovery. However, no significant differences in speckle contrast were observed between these two groups (though the small sample size for the transplanted group will make any differences difficult to identify). This warrants further investigation with a larger study to identify what is truly viable. Future studies will additionally acquire pre- and post-surgery PTH measurements in patients with autotransplanted and intact parathyroid glands so that patient outcome may be correlated with speckle contrast images. This will enable answering questions such as: “Should all glands with speckle contrast above a given threshold be autotransplanted in order to avoid hypoparathyroidism?”, and/or, “Is it safe to leave suspicious-looking glands in place if at least one parathyroid has speckle contrast below this threshold?”

It should be noted that LSCI senses motion, therefore these measurements are highly susceptible to random movement of the surgical field caused by the patient's breathing and movement of the hands holding retractors to expose the surgical field. Image registration was used to align images prior to averaging, however this does not avoid the artificial decrease in speckle contrast introduced to a single frame by such motion. For reference, the average speckle contrast of an excised parathyroid gland placed on a stable surface in the same operating room was measured to be 0.2, whereas the highest value obtained *in vivo* was about 0.13. In spite of this unavoidable source of error, very distinct differences in speckle contrast were obtained as demonstrated by the parathyroidectomy data (Table 3.1). To improve the accuracy of the final image, any image with jerky motion or a headlamp accidentally turned towards the surgical field (visually identified as a global sharp decrease in speckle contrast) was excluded from the averaging. This was done manually due to the rarity of the event. Only a few data points (<5) in the boxplots in Figure 3.4 and none of the displayed images suffered from this problem. However, in each case, sufficient data was acquired so that 20 images could still be averaged. In the future, should it be required, an algorithm could be employed to automate this process and reject speckle contrast images with values a specified percentage below the mean. Another point to consider is that while speckle contrast values theoretically range between 0 and 1, in practice this is difficult to achieve. A layer of stationary scatterers above the moving scatterers of interest (for example, epithelial cells making up the walls of blood vessels) introduce a static component to the speckle pattern that makes the minimum obtainable speckle contrast greater than 0. Additionally, spatial averaging of light across individual pixels in the instrument causes the maximum obtainable speckle contrast to be less than 1. This can be corrected for with a linear factor[31], which could be implemented in future to further improve the present system. Regardless of these limitations, this study was able to demonstrate the applicability of LSCI as a real-time, contrast-free and objective guidance tool for assessing parathyroid gland viability intraoperatively. It will be of particular benefit to less experienced surgeons and residents, and could reduce hospitalization and long-term medication costs associated with post-surgical hypoparathyroidism. This device could also have applicability for other clinical procedures where there is the need to non-invasively investigate the presence of tissue blood flow.

3.6 Conclusion

We present LSCI as a potential real-time, non-invasive, contrast-free and objective tool for guiding surgeons during thyroid surgeries to assess the viability of parathyroid glands. The device developed in this study can provide this information to surgeons with minimal disruption to the surgical workflow, and can detect vascular compromise in its early stages before it becomes evident to the surgeon's eye. This tool can therefore significantly minimize post-surgical hypoparathyroidism and its consequent morbidities and costs.

3.7 Acknowledgements

The authors acknowledge the financial support of the National Institutes of Health Award #R42CA192243. We would like to thank Dr. Andrew Dunn and Dr. Lisa Richards for their advice on setting up an LSCI system, as well as providing instructions on making microfluidic flow phantoms. We would also like to thank Christine O'brien and Oscar Ayala for their valuable feedback in preparing this manuscript.

3.8 References

1. American Thyroid Association. General Information/Press Room. http://www.thyroid.org/media-main/about-hypothyroidism/ (2017).
2. Sun, G. H., DeMonner, S. & Davis, M. M. Epidemiological and Economic Trends in Inpatient and Outpatient Thyroidectomy in the United States, 1996–2006. *Thyroid* **23**, 727–733 (2013).
3. Rafferty, M. A., Goldstein, D. P., Rotstein, L., Asa, S. L., Panzarella, T., Gullane, P., Gilbert, R. W., Brown, D. H. & Irish, J. C. Completion Thyroidectomy Versus Total Thyroidectomy: Is There a Difference in Complication Rates? An Analysis of 350 Patients. *J. Am. Coll. Surg.* **205**, 602–607 (2007).
4. Schwartz, A. E. & Friedman, E. W. Preservation of the parathyroid glands in total thyroidectomy. *Surg. Gynecol. Obstet.* **165**, 327–32 (1987).
5. Ritter, K., Elfenbein, D., Schneider, D. F., Chen, H. & Sippel, R. S. Hypoparathyroidism after total thyroidectomy: incidence and resolution. *J. Surg. Res.* **197**, 348–53 (2015).

6. Demeester-Mirkine, N., Hooghe, L., Van Geertruyden, J. & De Maertelaer, V. Hypocalcemia after thyroidectomy. *Arch. Surg.* **127**, 854–8 (1992).

7. Pattou, F., Combemale, F., Fabre, S., Carnaille, B., Decoulx, M., Wemeau, J.-L., Racadot, A. & Proye, C. Hypocalcemia following Thyroid Surgery: Incidence and Prediction of Outcome. *World J. Surg* **22**, 718–724 (1998).

8. McHenry, C. R., Speroff, T., Wentworth, D. & Murphy, T. Risk factors for postthyroidectomy hypocalcemia. *Surgery* **116**, 641–7; discussion 647-8 (1994).

9. Zahedi Niaki, N., Singh, H., Moubayed, S. P., Leboeuf, R., Tabet, J.-C., Christopoulos, A., Ayad, T., Olivier, M.-J., Guertin, L. & Bissada, E. The Cost of Prolonged Hospitalization due to Postthyroidectomy Hypocalcemia: A Case-Control Study. *Adv. Endocrinol.* **2014**, 1–4 (2014).

10. Naveh-Many, T. *Molecular Biology of the Parathyroid*. (Kluwer Academic / Plenum Publishers, 2005).

11. Mohebati, A. & Shaha, A. R. Anatomy of thyroid and parathyroid glands and neurovascular relations. *Clin. Anat.* **25**, 19–31 (2012).

12. Lo, C. Y. & Tam, S. C. Parathyroid autotransplantation during thyroidectomy: Documentation of graft function. *Arch. Surg.* **136**, 1381–1385 (2001).

13. Sierra, M., Herrera, M. F., Herrero, B., Jiménez, F., Sepúlveda, J., Lozano, R. R., Gamino, R., González, O. & Correa-Rotter, R. Prospective biochemical and scintigraphic evaluation of autografted normal parathyroid glands in patients undergoing thyroid operations. *Surgery* **124**, 1005–10 (1998).

14. Kuriloff, D. B. & Kizhner, V. Parathyroid gland preservation and selective autotransplantation utilizing topical lidocaine in total thyroidectomy. *Laryngoscope* **120**, 1342–1344 (2010).

15. Ezzat, W., Fathey, H., Fawaz, S., El-Ashri, A., Youssef, T. & Othman, H. Intraoperative parathyroid hormone as an indicator for parathyroid gland preservation in thyroid surgery. *Swiss Med. Wkly.* (2011) doi:10.4414/smw.2011.13299.

16. Fortuny, J. V., Belfontali, V., Sadowski, S. M., Karenovics, W., Guigard, S. & Triponez, F. Parathyroid gland angiography with indocyanine green fluorescence to predict parathyroid function after thyroid surgery. *Br. J. Surg.* **103**, 537–543 (2016).

17. Fercher, A. F. & Briers, J. D. Flow Visualization By Means Of Single-Exposure Speckle Photography. *Opt. Commun.* **37**, (1981).

18. Briers, J. D. & Webster, S. Laser Speckle Contrast Analysis (LASCA): A Nonscanning, Full-Field Technique for Monitoring Capillary Blood Flow. *J. Biomed. Opt.* **1**, 174–179 (1996).

19. Boas, D. A. & Dunn, A. K. Laser speckle contrast imaging in biomedical optics. *J. Biomed. Opt.* **15**, 011109 (2010).

20. Choi, B., Kang, N. M. & Nelson, J. S. Laser speckle imaging for monitoring blood flow dynamics in the in vivo rodent dorsal skin fold model. *Microvasc. Res.* **68**, 143–6 (2004).

21. Iredahl, F., Löfberg, A., Sjöberg, F., Farnebo, S. & Tesselaar, E. Non-Invasive Measurement of Skin Microvascular Response during Pharmacological and Physiological Provocations. *PLoS One*

10, e0133760 (2015).

22. Dunn, A. K., Bolay, H., Moskowitz, M. A. & Boas, D. A. Dynamic Imaging of Cerebral Blood Flow Using Laser Speckle. *J. Cereb. Blood Flow Metab.* **21**, 195–201 (2001).

23. Huang, Y.-C., Ringold, T. L., Nelson, J. S. & Choi, B. Noninvasive blood flow imaging for real-time feedback during laser therapy of port wine stain birthmarks. *Lasers Surg. Med.* **40**, 167–173 (2008).

24. Mirdell, R., Iredahl, F., Sjöberg, F., Farnebo, S. & Tesselaar, E. Microvascular blood flow in scalds in children and its relation to duration of wound healing: A study using laser speckle contrast imaging. *Burns* **42**, 648–654 (2016).

25. Richards, L. M., Kazmi, S. S., Olin, K. E., Waldron, J. S., Fox, D. J. & Dunn, A. K. Intraoperative multi-exposure speckle imaging of cerebral blood flow. *J. Cereb. Blood Flow Metab.* 0271678X1668698 (2017) doi:10.1177/0271678X16686987.

26. Kirkpatrick, S. J., Duncan, D. D. & Wells-Gray, E. M. Detrimental effects of speckle-pixel size matching in laser speckle contrast imaging. *Opt. Lett.* **33**, 2886 (2008).

27. Briers, D., Duncan, D. D., Hirst, E., Kirkpatrick, S. J., Larsson, M., Steenbergen, W., Stromberg, T. & Thompson, O. B. Laser speckle contrast imaging: theoretical and practical limitations. *J. Biomed. Opt.* **18**, 066018 (2013).

28. Kazmi, S. M. S., Faraji, E., Davis, M. a, Huang, Y.-Y., Zhang, X. J. & Dunn, A. K. Flux or speed? Examining speckle contrast imaging of vascular flows. *Biomed. Opt. Express* **6**, (2015).

29. Sexton, K. J., Zhao, Y., Davis, S. C., Jiang, S. & Pogue, B. W. Optimization of fluorescent imaging in the operating room through pulsed acquisition and gating to ambient background cycling. *Biomed. Opt. Express* **8**, 2635 (2017).

30. American College of Surgeons. Total Thyroidectomy Complication Rates and Costs Are Lower if Surgeon Performs 25 or More Cases Yearly. https://www.facs.org/media/press-releases/2015/sosa (2015).

31. Thompson, O., Andrews, M. & Hirst, E. Correction for spatial averaging in laser speckle contrast analysis. *Biomed. Opt. Express* **2**, 1021–9 (2011).

CHAPTER 4

ASSESSING INTRAOPERATIVE LASER SPECKLE CONTRAST IMAGING OF PARATHYROID GLANDS IN RELATION TO THYROIDECTOMY PATIENT OUTCOMES

Emmanuel A. Mannoh, BS[1,2], Giju Thomas, PhD[1,2], Naira Baregamian, MD[3], Sarah L. Rohde, MD[4], Carmen C. Solórzano, MD[3], Anita Mahadevan-Jansen, PhD[1,2]

[1] Vanderbilt Biophotonics Center, Vanderbilt University, Nashville, TN 37235

[2] Department of Biomedical Engineering, Vanderbilt University, Nashville, TN 37235

[3] Division of Surgical Oncology and Endocrine Surgery, Vanderbilt University Medical Center, Nashville, TN 37232

[4] Department of Otolaryngology – Head & Neck Surgery, Vanderbilt University Medical Center, Nashville, TN 37232

This chapter was adapted from:

"Assessing intraoperative laser speckle contrast imaging of parathyroid glands in relation to thyroidectomy patient outcomes"

In review at:

Thyroid

4.1 Abstract

BACKGROUND: Accurate assessment of parathyroid gland vascularity is important during thyroidectomy to preserve the function of parathyroid glands and prevent postoperative hypocalcemia. Laser speckle contrast imaging (LSCI) has been shown to be accurate in detecting differences in parathyroid vascularity. In this surgeon-blinded prognostic study, we evaluate the relationship between intraoperative LSCI measurements and postoperative outcomes of total thyroidectomy patients.

METHODS: Seventy-two thyroidectomy patients were included in this study. After thyroid resection, an LSCI device was used to image all parathyroid glands identified, and a speckle contrast value was calculated for each. An average value was calculated for each patient and the data was grouped according to whether the patient had normal (16-77 pg/mL) or low levels of parathyroid hormone (PTH) measured on postoperative day 1 (POD1). The aim of this study was to establish a speckle contrast threshold for classifying a parathyroid gland as adequately perfused, and to determine how many such glands are required for normal postoperative parathyroid function.

RESULTS: A speckle contrast limit of 0.186 separated the normoparathyroid and hypoparathyroid groups with 87.5% sensitivity and 84.4% specificity: 7 out of 8 patients with low PTH on POD1 had an average parathyroid speckle contrast above this limit, while 54 out of 64 patients with normal postoperative PTH had an average parathyroid speckle contrast below this limit. Taking this value as the threshold for adequate parathyroid perfusion, it was determined that only one vascularized gland was needed for normal postoperative parathyroid function: 64 out of 69 patients (92.8%) with at least one vascularized gland (determined by LSCI) had normal postoperative PTH, while all 3 patients (100%) with no vascularized glands had low postoperative PTH. Overall, the rates of temporary and permanent hypoparathyroidism in this study were 8.3% and 1.4% respectively.

CONCLUSION: Laser speckle contrast imaging is a promising technique for assessing parathyroid gland vascularity. It has the potential to help reduce the incidence of hypocalcemia after thyroidectomy by providing surgeons with additional information during surgery to aid in the preservation of parathyroid function.

4.2 Introduction

Post-surgical hypoparathyroidism is a major complication following thyroid surgery due to inadvertent damage to parathyroid glands or their blood supply. Loss of parathyroid function (termed hypoparathyroidism) leads to hypocalcemia – below normal levels of serum calcium, which is needed for a variety of functions such as muscle contraction and neuronal excitability[1]. Patients suffering from hypocalcemia must rely on calcium and vitamin D supplementation in order to avoid the associated negative effects which include numbness, muscle spasms, tetany and seizures. Reports on the rates of hypoparathyroidism or hypocalcemia after thyroidectomy vary widely[2–9]. The variation is due to differing definitions of post-surgical hypoparathyroidism and hypocalcemia[10], and differences in surgeon experience[11]. However, one review found the medians of reported rates to be 27% for temporary cases and 1% for permanent cases[12].

Since the discovery that parathyroid glands fluoresce in the near-infrared[13], numerous studies have utilized this phenomenon in optical fiber based[14–18] and imaging[19–26] approaches to help surgeons accurately identify the glands intraoperatively and avoid accidental excision. Two clinical devices employing near-infrared autofluorescence (NIRAF) have now received FDA clearance and CE marking for parathyroid detection[27]. However, numerous studies have shown that identifying the glands alone is insufficient to improve hypocalcemia rates post-thyroidectomy[28–31], and it is more crucial to preserve the vascularity of glands to ensure normoparathyroid/normocalcemic status after surgery. Assessing the vascularity of intact parathyroid glands remains a challenge and surgeons often rely on visual inspection and their experience in doing so. Accurate knowledge of the parathyroid glands' state of vascularity is also important as it guides decision-making on autotransplantation – when devascularized, autotransplantation of a parathyroid gland can help regain its function over time[32–34].

A few experimental techniques have been reported for assessing parathyroid vascularity including topical application of lidocaine[35], laser Doppler flowmetry[36], intraoperative parathyroid hormone assay[37], and confocal endomicroscopy using the dye fluorescein[38]. Recently, the use of Indocyanine Green (ICG) angiography has gained traction[39–44]. While there have been promising reports, there are a few limitations. First, while ICG is generally considered safe, a small percentage of patients can still suffer severe allergic reactions to the dye[45]. Secondly, it cannot be performed simultaneously with NIRAF detection for parathyroid identification. This is because the fluorescence of ICG is in the same spectral range as the parathyroid NIRAF and is much stronger in intensity, while also persisting for long periods. Once ICG

has been injected, NIRAF detection can no longer be used to localize other parathyroid glands. This creates a challenge for the surgeon who might want to make immediate decisions on preserving a parathyroid gland before continuing with the procedure. Lastly, current practice relies on qualitative scoring of ICG fluorescence intensity which makes it difficult to standardize measurements, though efforts have been made to make it more quantitative[46].

An alternative technique which overcomes these limitations is laser speckle contrast imaging (LSCI), a real-time label-free imaging technique that is sensitive to superficial blood flow. The technique was first used to image blood flow in the human retina[47]. It works by analyzing blurriness of the interference or speckle pattern produced when laser light illuminates a surface. To produce a flow map from an image of a speckle pattern, a quantity called the speckle contrast is calculated. In one form, it is calculated as the standard deviation of pixel intensities within local regions of the image divided by their corresponding mean intensities[48]. Lower speckle contrast values indicate more blurring of the speckle pattern and hence greater blood flow, while higher contrast values indicate the converse. The work presented in Chapter 3 showed that LSCI is able to differentiate with high accuracy between parathyroid glands classified as well-vascularized or devascularized by an experienced endocrine surgeon[49]. The purpose of this current work is to determine how intraoperative LSCI measurements relate to thyroidectomy patient outcomes, namely postoperative parathyroid hormone (PTH) levels since it has been suggested that PTH within the first 24 hours after surgery is indicative of hypoparathyroidism[50].

4.3 Methods

4.3.1 Laser speckle contrast imaging system

Imaging was performed using a modified version of the LSCI system described in Chapter 3. Briefly, the device consists of a 785 nm laser to provide illumination, and a near-infrared-optimized camera to image the speckle pattern produced which is then sent to a computer for real-time processing. The multimode 785 nm laser in the previous system was replaced with a single-mode equivalent (Innovative Photonics Solutions, Monmouth Junction, NJ) which improved speckle visibility. Additionally, a linear

polarizer was placed in front of the light source, and another in front of the camera with its axis of polarization oriented perpendicular to the first in order to reduce specular reflections in the images.

4.3.2 Patient recruitment and study design

This study was approved by the Vanderbilt University Medical Center (VUMC) Institutional Review Board. Seventy-nine patients scheduled to undergo thyroidectomy were recruited by three surgeons and informed written consent was obtained from each patient prior to participation. These included 58 patients who underwent total thyroidectomy alone, 10 who underwent total thyroidectomy with neck dissection, and 4 who underwent completion thyroidectomy. After resection of the thyroid, all parathyroid glands identified during the course of the operation were imaged with the LSCI system. Imaging took up to one minute per gland, including time for the surgeon to position the camera above the parathyroid. Since LSCI is label-free and poses no risk to the patient, imaging can be repeated as often as desired. Overall, imaging added about 5 minutes to each case. For each gland, ten frames were averaged and this averaged image was then segmented to obtain the average speckle contrast for that parathyroid. Only parathyroid glands identified with high confidence by the surgeon were included in analyses. No additional dissection was performed to look for missing parathyroid glands. Any parathyroid gland that was inadvertently or unavoidably (e.g. intrathyroidal parathyroid) resected with the thyroid was autotransplanted. Since *in situ* LSCI measurements were unobtainable for these excised glands, they were assigned the highest parathyroid speckle contrast value that was measured throughout the study. The surgeon's visual assessment of each parathyroid gland was also recorded into one of three categories: well-vascularized, compromised (e.g. bruised but still perfused), and devascularized (these glands were subsequently autotransplanted). Parathyroid speckle contrast measurements were grouped according to these classifications and a one-way analysis of variance was performed to look for significant differences. Throughout the study the surgeons were blinded from LSCI data so as not to influence patient care. Parathyroid hormone (PTH) and serum calcium levels on postoperative day 1 (POD1) were available for 72 patients, hence only these were included in further analyses. Patients with POD1 PTH below the accepted normal range at VUMC of 16-77 pg/mL were evaluated up to six months postop to look for recovery within that period. All patients received calcium supplementation postoperatively.

4.3.3 Data analysis

The goal of this study was to establish a speckle contrast threshold for classifying a parathyroid gland as adequately vascularized, and to determine how many vascularized glands are needed for a patient to have normal PTH levels postoperatively. This was achieved by first calculating the average parathyroid speckle contrast for each patient and grouping the data according to whether the patient had normal or low levels of PTH on POD1. Note, this is the average value of all parathyroid glands in each patient. An ROC curve was generated using average parathyroid speckle contrast as a classifier to separate the two groups of patients. The optimum point on the curve was taken to be the speckle contrast threshold for adequate parathyroid vascularity. The minimum number of vascularized parathyroid glands needed for normal postoperative function was then determined based on this value. This minimum required number of vascularized parathyroid glands is designated as n_{min}. Data analysis was conducted for two scenarios: $n_{min} = 1$ and $n_{min} = 2$. For each of these, the percentage of patients with less than n_{min} vascularized glands (as determined by the speckle contrast threshold) who then had low PTH levels on POD1 was calculated. This is also the positive predictive value of postoperative hypoparathyroidism. Additionally, the percentage of patients with n_{min} vascularized parathyroid glands who then had normal PTH levels on POD1 was calculated. This is the negative predictive value. Due to insufficient data, calculations could not be performed for $n_{min} = 3$ or $n_{min} = 4$. However, we do not anticipate that 3 or more vascularized parathyroid glands are crucial to maintain a normoparathyroid state, as there is ample evidence to show that the human body is able to compensate when one or more parathyroid glands are injured[51]. The calculations were performed on the dataset of 72 patients, as well as on groups determined by the number of parathyroid glands identified during the operation and left in the patient (including autotransplanted glands). These groups consist of cases where there were 4 glands (n = 25), 3 glands (n = 22), and 1 or 2 glands (n = 25).

4.4 Results

Patient demographics and clinical data for the 72 patients with postoperative PTH and calcium data are shown in Table 4.1. A multinomial logistic regression revealed that neither sex, race, age, nor body mass index significantly influenced whether or not a patient had low levels of PTH on POD1. Indication

for surgery similarly had no significant impact on patient outcome (though patients with Hashimoto's thyroiditis had to be excluded from this analysis due to insufficient data). Surgical procedure could not be included in the regression analysis due to insufficient data.

Table 4.1. Patient demographics

	Total population (*n* = 72)	**Low POD1 PTH (*n* = 8)**	**Normal POD1 PTH (*n* = 64)**
Sex			
Female	56 (78%)	7 (88%)	49 (77%)
Male	16 (22%)	1 (13%)	15 (23%)
Race/ethnicity			
White	51 (71%)	4 (50%)	47 (73%)
Non-white	21 (29%)	4 (50%)	17 (27%)
Indication for surgery			
Graves' disease	21 (29%)	2 (25%)	19 (30%)
Papillary thyroid carcinoma	13 (18%)	2 (25%)	11 (17%)
Other thyroid cancer	15 (21%)	1 (13%)	14 (22%)
Toxic/non-toxic thyroid nodule	20 (28%)	2 (25%)	18 (28%)
Hashimoto's thyroiditis	3 (4%)	1 (13%)	2 (3%)
Surgical procedure			
Total thyroidectomy	58 (81%)	4 (50%)	54 (84%)
Total thyroidectomy w/ neck dissection	10 (14%)	3 (38%)	7 (11%)
Completion thyroidectomy	4 (6%)	1 (13%)	3 (5%)
Age in years (mean ± s.d.)	48.8 ± 13.2	43.9 ± 11.6	49.4 ± 13.3
Body mass index in kg/m^2 (mean ± s.d.)	33.6 ± 8.4	31.9 ± 8.0	33.8 ± 8.5
Number of PGs per pt. (mean ± s.d.)	3 ± 0.9	3.4 ± 0.7	2.9 ± 0.9

POD1: postoperative day 1, PTH: parathyroid hormone, PG: parathyroid gland

Representative images of a well-vascularized, a compromised and a devascularized parathyroid gland are shown in Figure 4.1. Their average speckle contrast values were 0.11, 0.18, and 0.21 respectively. A total of 231 parathyroid glands were imaged in this study, yielding an average of ~2.9 glands per patient. The distribution of speckle contrast for these glands, grouped according to the surgeons' assessment of vascularity, is shown in Figure 4.2. Speckle contrast was lowest for well-vascularized glands and highest for devascularized glands. The range of parathyroid speckle contrast values for this instrument was 0.09 to 0.27, with a mean value of 0.17. Statistical testing using a one-way analysis of variance showed significant differences between well-vascularized, compromised, and autotransplanted parathyroid glands ($p < 0.05$). In spite of this significance, there were a number of cases where LSCI greatly disagreed with the surgeon. A few examples are shown in Figure 4.3, where glands that were considered well-vascularized by the surgeon had high speckle contrast values (indicating reduced perfusion), and glands that were considered devascularized had low speckle contrast. This further motivates the need to evaluate patient outcomes against intraoperative LSCI.

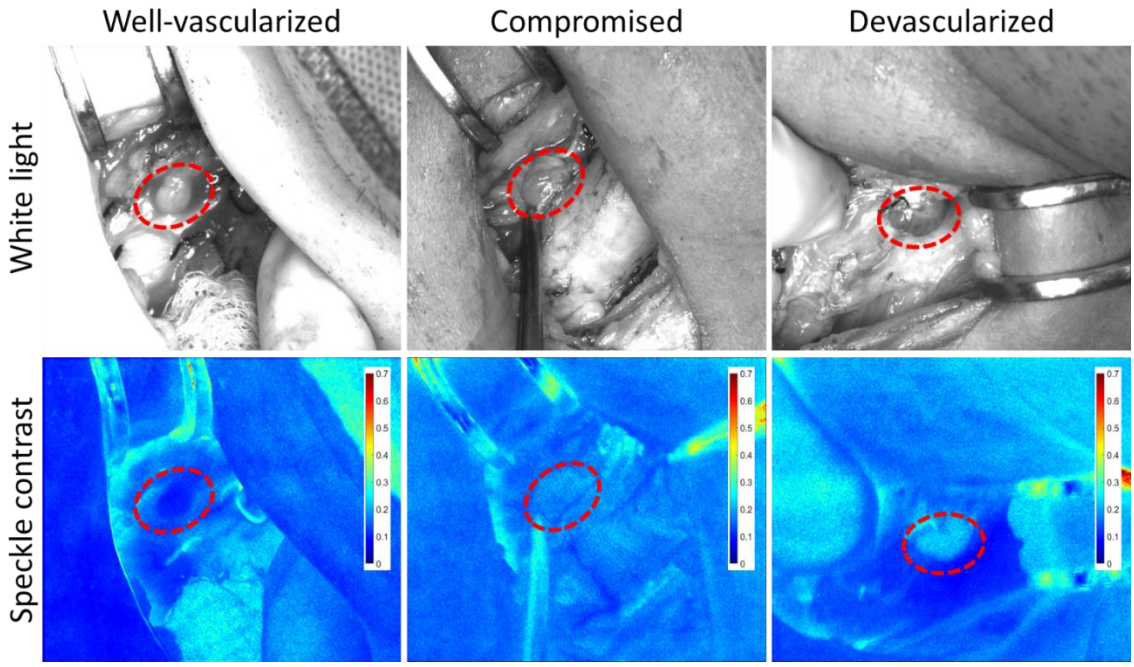

Figure 4.1. Representative white light and speckle contrast images of a well-vascularized, compromised, and a devascularized parathyroid gland. Parathyroid glands are indicated with ellipses. Speckle contrast values were respectively 0.11, 0.18, and 0.21.

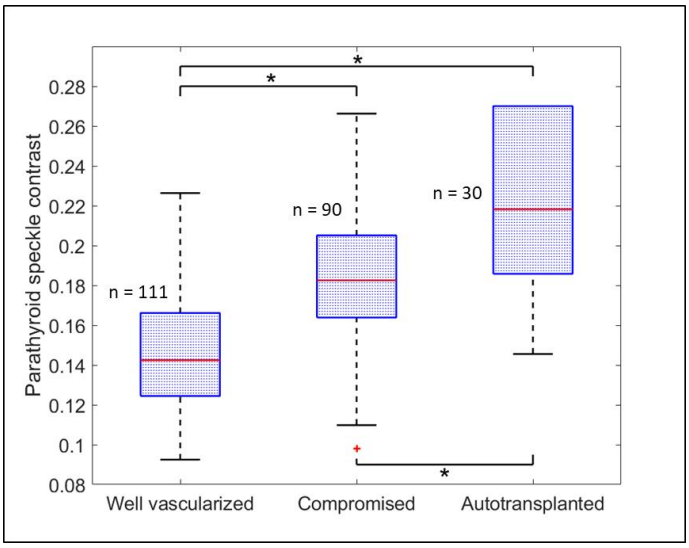

Figure 4.2. Speckle contrast of parathyroid glands grouped according to surgeons' classifications. Medians are indicated by the horizontal red line in each box, and each box spans the 25th to 75th percentile of that group. Whiskers extend to the most extreme point not considered outliers and outliers are indicated by red plus signs. All groups are significantly different (*: $p < 0.05$).

There were 8 patients out of 72 (11.1%) who had PTH levels below 16 pg/mL on POD1. Of these, 4 also had serum calcium levels below the normal range of 8.4-10.5 mg/dL. These 4 patients mostly had lower PTH levels than the other 4 patients. Data on all 8 patients is summarized in Table 4.2. These patients underwent surgery for a variety of conditions including thyroid cancers, Graves' disease, Hashimoto's thyroiditis and multinodular goiters. Three out of 10 patients who underwent neck dissection had low post-op PTH, suggesting an increased likelihood of postoperative hypoparathyroidism with more extensive surgical procedures. Four patients received autotransplantation and of these, in one case PTH levels did not return to normal within the first 6 months postoperatively. For two patients, data on subsequent PTH measurements was unavailable. However, their calcium levels returned to normal within the first 6 months after surgery and the patients no longer required calcium supplementation. The average parathyroid gland speckle contrast in most cases was at least 0.19, with the exception of Patient 8 who had a very transient drop in PTH to 13 pg/mL and rapid recovery to 31 pg/mL on POD4. For comparison, it took weeks to months for PTH to recover in the other patients suggesting this was not a case of true hypoparathyroidism. Altogether, the rate of temporary hypoparathyroidism in this study was 8.3%, and the rate of permanent hypoparathyroidism 1.4%.

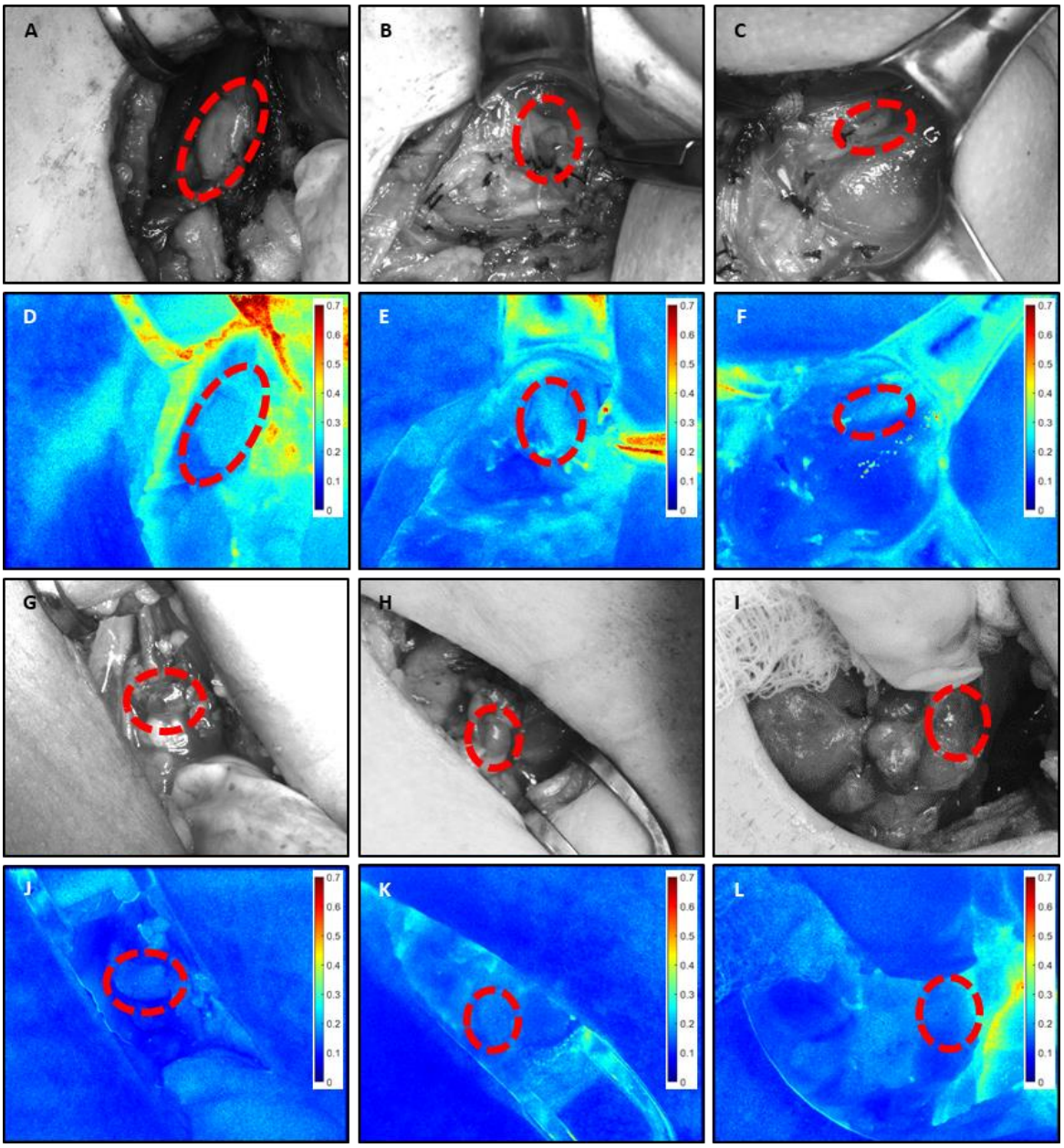

Figure 4.3. White light (A, B, C) and speckle contrast (D, E, F) images of PGs that were assessed to be well-vascularized but had high speckle contrast values of 0.22, 0.23, and 0.20 respectively; and white light (G, H, I) and speckle contrast (J, K, L) images of PGs that were autotransplanted but had low speckle contrast values of 0.15, 0.16, and 0.17 respectively. PGs indicated by red ellipses.

Table 4.2. Summary information on patients with low PTH on POD1

Patient	Diagnosis	Procedure	Post-op PTH[a]	Post-op Ca[b]	Average PG speckle contrast[c]	# of PG's found(left)	Auto-transplant?	PTH recovered?
1	Papillary thyroid carcinoma	Thyroidectomy w/ neck dissection	13	9.3	0.21 (0.21, 0.17, 0.24, 0.23)	4(4)	Yes	Yes
2	Multinodular goiter	Completion thyroidectomy	3	8.7	0.21 (0.19, 0.24, 0.20)	3(3)	No	Yes
3	Papillary thyroid carcinoma	Thyroidectomy w/ neck dissection	3	**8.1**	0.19 (0.22, 0.12, 0.21)	3(3)	Yes	No
4	Graves' disease	Total thyroidectomy	3	**8.2**	0.20 (0.24, 0.19, 0.16, 0.21)	4(4)	No	Yes
5	Toxic multinodular goiter	Total thyroidectomy	7	**8.2**	0.23 (0.20, 0.27, 0.21)	3(3)	Yes	Yes
6	Hashimoto's thyroiditis	Total thyroidectomy	6	8.6	0.20 (0.17, 0.19, 0.16, 0.27)	4(4)	Yes	--
7	Papillary thyroid carcinoma	Thyroidectomy w/ neck dissection	3	**7.5**	0.23 (0.23, 0.22)	2(2)	No	--
8	Graves' disease	Total thyroidectomy	13	9.1	0.15 (0.19, 0.11, 0.19, 0.13)	4(4)	No	Yes

[a] PTH: parathyroid hormone. Values are in pg/mL; normal range 16-77 pg/mL.
[b] Values are in mg/dL; normal range 8.4-10.5 mg/dL. Values below normal are bolded.
[c] PG: parathyroid gland. Values in parentheses indicate speckle contrast of individual parathyroid glands.

Average parathyroid speckle contrast was calculated for each of the 72 patients and grouped according to PTH status on POD1. The distribution of values is shown in Figure 4.4A. As expected, the average parathyroid speckle contrast values for patients with low postoperative PTH are higher than those for patients with normal postoperative PTH. This difference was statistically significant when evaluated with a two-sided two-sample t-test ($p < 10^{-4}$). Using average parathyroid speckle contrast as a classifier to separate the two groups, the ROC curve in Figure 4.4B was generated. The optimum point on this curve was at a speckle contrast of 0.186, which resulted in a sensitivity and specificity of 87.5% and 84.4% respectively. In other words, 87.5% of the patients with low PTH on POD1 had average parathyroid speckle contrast greater than 0.186, and 84.4% of the patients with normal PTH on POD1 had average parathyroid speckle contrast less than or equal to 0.186. This value of 0.186 was identified as the optimal cutoff point for adequate parathyroid vascularity.

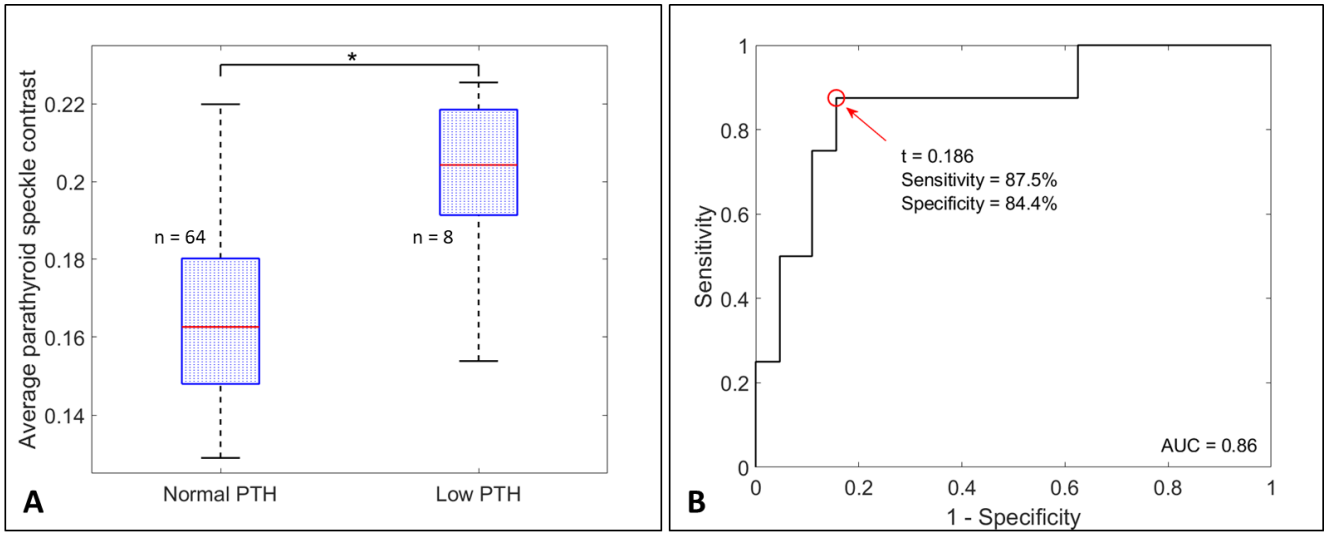

Figure 4.4. (A) Distribution of average parathyroid speckle contrast values in patients with normal and low levels of PTH on POD1. Medians are indicated by horizontal red lines and each box spans the 25th to 75th percentile of that group. Whiskers extend to the most extreme data points not considered outliers. (B) ROC curve resulting from using average speckle contrast as a classifier. The two groups were significantly different ($p < 10^{-4}$), and the optimum speckle contrast value (t) separating them was 0.186.

To determine how many vascularized glands are needed for normal postoperative PTH levels, positive and negative predictive values were calculated for $n_{min} = 1$ and $n_{min} = 2$. The results are shown in Table 4.3. Overall, requiring one vascularized gland for normal postoperative parathyroid function had the higher combined predictive values. All 3 patients with no vascularized parathyroid glands (i.e., no glands with speckle contrast below 0.186) had low PTH levels on POD1, corresponding to a positive predictive value of 100%. These were Patients 2, 5, and 7 in Table 2. On the other hand, 64 out of 69 patients who had at least one vascularized parathyroid gland had normal PTH levels on POD1, corresponding to a negative predictive value of 92.8%. The exceptions were Patients 1, 3, 4, 6, and 8 in Table 2, who also generally had high average values. This trend largely held regardless of the number of parathyroid glands identified during the surgery. This data is presented in Table 4.4.

Table 4.3. Minimum number of vascularized parathyroid glands needed for normal postoperative function

At least 1 vascularized PG required

	0 PGs with speckle contrast below 0.186	At least 1 PG with speckle contrast below 0.186
Patients with low POD1 PTH	3	5
Patients with normal POD1 PTH	0	64
	PPV: 100%	*NPV*: 92.8%

At least 2 vascularized PGs required

	< 2 PGs with speckle contrast below 0.186	At least 2 PGs with speckle contrast below 0.186
Patients with low POD1 PTH	5	3
Patients with normal POD1 PTH	19	45
	PPV: 20.8%	*NPV*: 93.8%

PG: parathyroid gland, PPV: positive predictive value, NPV: negative predictive value, POD1: postoperative day 1

Table 4.4. Predictive values of requiring one versus two vascularized parathyroid glands, broken down by number of glands identified in a case

At least 1 vascularized PG required

	1 or 2 PGs identified		3 PGs identified		4 PGs identified	
	0 vasc. PGs	≥ 1 vasc. PG	0 vasc. PGs	≥ 1 vasc. PG	0 vasc. PGs	≥ 1 vasc. PG
Low PTH	1	0	2	1	0	4
Normal PTH	0	24	0	19	0	21
	PPV: 100%	*NPV*: 100%	*PPV*: 100%	*NPV*: 95.0%	*PPV*: NA*	*NPV*: 84.0%

At least 2 vascularized PGs required

	1 or 2 PGs identified		3 PGs identified		4 PGs identified	
	< 2 vasc. PGs	≥ 2 vasc. PGs	< 2 vasc. PGs	≥ 2 vasc. PGs	< 2 vasc. PGs	≥ 2 vasc. PGs
Low PTH	1	0	3	0	1	3
Normal PTH	15	9	4	15	0	21
	PPV: 6.7%	*NPV*: 100%	*PPV*: 42.9%	*NPV*: 100%	*PPV*: 100%	*NPV*: 87.5%

* In cases where 4 glands were identified, there were no patients without a single vascularized gland and so PPV could not be calculated for that subset of data.

PG: parathyroid gland, PPV: positive predictive value, NPV: negative predictive value, vasc.: vascularized

4.5 Discussion

Parathyroid glands are crucial to maintaining normal serum calcium levels. Therefore it is critical during thyroidectomies for the surgeon to have accurate knowledge of the parathyroid glands' state of vascularity, to help preserve function postoperatively. We propose that LSCI can provide this information. In this study, an average parathyroid speckle contrast value of 0.186 was found to have the highest sensitivity and specificity in separating patients with normal from low postoperative PTH levels. Overall, 87.5% of patients with low POD1 PTH had average parathyroid speckle contrast greater than 0.186, while 84.4% of patients with normal POD1 PTH had average parathyroid speckle contrast less than 0.186. This value was taken to be the threshold for adequate parathyroid vascularization, i.e. a parathyroid gland with speckle contrast below 0.186 was considered to be vascularized. Requiring one such parathyroid gland for normal postoperative function produced much higher combined positive and negative predictive values than requiring two parathyroid glands, suggesting that only one gland is needed. All the patients who had

no parathyroids with speckle contrast below 0.186 had low POD1 PTH, while POD1 PTH was low for only 5 out of the 24 patients who had less than two vascularized glands. The calculations were also performed on groups determined by the number of parathyroid glands identified because the actions a surgeon might take in a case where they identified four parathyroid glands could differ from those in a case where only one was identified. The predictive values were consistently higher for $n_{min} = 1$; regardless of whether one, two or three parathyroid glands were identified during the surgery, only one gland needed to have speckle contrast below 0.186. A possible exception exists in the cases where four parathyroid glands were identified. However, it should be noted that the positive predictive value of requiring one vascularized gland in these cases could not be assessed as all of these patients had at least one vascularized gland. We nevertheless expect that it would be as high as in the other groups – if all four parathyroid glands have been identified and none are vascularized, the patient will most likely have low postoperative PTH levels.

Most surgeons currently rely on the subjective methods of visual inspection. In relying on visual inspection to assess the viability of a parathyroid gland, one property surgeons often evaluate is color. Generally, vascular compromise to a parathyroid gland results in the gland turning dark due to pooling of deoxygenated blood. However, this may not always be the case, particularly if the damage is arterial. On the other hand, vascular spasms may cause a gland to temporarily become dusky and even after flow returns to normal it could take a while for the typical pinkish color to return. The advantage of a technique like LSCI is that it is sensitive to the flow of blood rather than its presence, and so should be unaffected by these scenarios. As mentioned in the Results, there were a few cases of substantial disagreement between the surgeon and LSCI, some of which were shown in Figure 4.3. The parathyroid glands on the top row (Figure 4.3A-F) were classified by the surgeon as being well-vascularized, but had high speckle contrast values, all at least 0.2. On the other hand, the parathyroid glands on the bottom row (Figure 4.3G-L) were autotransplanted largely due to appearing very dusky, but had low speckle contrast values, at most 0.17. These examples highlight the importance of this study looking at postoperative outcomes as there is no good way to determine whether the surgeon or the instrument was more accurate in these instances. While this is the case, inferences can still be made supporting the superior accuracy of LSCI. A good example to look at is Patient 2 in Table 4.2, in which three parathyroid glands were identified intraoperatively. Two were visually assessed to be compromised and one to be well-vascularized by the surgeon (this is the gland in Figure 4.3C). However all had fairly high (at least 0.19) speckle contrast values, suggesting they were all compromised, and this patient had a PTH level of 3 pg/mL on POD1.

Altogether in this study, 89.5% (51 out of 57) of the patients that were visually assessed to have at least one well-vascularized parathyroid gland had normal PTH levels on POD1, and only 13.3% (2 out of 15) of those who were visually assessed to have none ended up with low POD1 PTH levels.

In a study using ICG angiography to evaluate parathyroid glands after thyroid surgery, Fortuny *et al*. reported that postoperative PTH levels were normal for all patients who had at least one well-vascularized parathyroid gland (evaluated by ICG fluorescence intensity)[39]. In a similar but slightly different vein, our study found that all patients who had no vascularized parathyroid glands had low PTH levels on POD1. However, not all patients who did have one vascularized gland had normal postoperative PTH levels. Overall, 7% of patients who had at least one vascularized gland still had low postoperative PTH. An exception is Patient 8 in Table 4.2, who had favorable assessments of their parathyroid glands by both LSCI and the surgeon. Though PTH was below the normal range on POD1, it recovered to normal within days whereas recovery took weeks to months in the other patients. Therefore it is possible that the transient PTH drop in this patient was due to postoperative swelling or other effects, rather than loss of parathyroid function.

Overall, 8.3% of patients experienced temporary hypoparathyroidism, compared to the median reported rate of 27%[12]. Additionally, while the rate of permanent hypoparathyroidism was 1.4%, it usually reported as up to 5%[2,3] or higher[5]. Incidence of hypoparathyroidism after thyroid surgery is largely dependent on surgeon experience and specialization, and at a high-volume institution there are less likely to be post-surgical complications. The three surgeons involved in this study are high-volume surgeons who perform over a hundred thyroidectomies annually, pointing to one limitation of this study – there were not many patients who experienced a negative outcome. Furthermore, in some patients, not all parathyroid glands may have been evaluated. While it is possible for a patient to naturally have more or less than four parathyroid glands, 84-87% have four[52]. Hence, for 47 out of 72 patients in this study there could have been parathyroid glands that were hidden and therefore not evaluated. It could be argued that these hidden glands were protected and therefore largely responsible for the patients' normal postoperative outcomes. To overcome this limitation, future studies need to evaluate all four parathyroid glands. In four cases, a parathyroid gland was not easily accessible for imaging with the current device. It should be noted that the presence of connective tissue or fat overlaying the parathyroid will artificially increase the speckle contrast measured, as it adds a layer of static scatterers. Due to this, the surgeons in our study made an

effort to expose parathyroid glands from beneath fat or connective tissue before imaging. Lastly, this study was entirely reliant on the visual assessment of the surgeon to identify the parathyroid glands.

Care should be taken in applying these results to different LSCI instruments. The visibility of speckles, and therefore the contrast that is calculated, depends on factors such as the coherence length of the laser and the pixel size of the camera used. To some degree this can be corrected for with a linear factor[53]. For instance, the switch from a multimode to a single-mode laser in our device caused a doubling of the speckle contrast, determined by imaging a microfluidic flow phantom. It has been shown however, that this linearity does not hold over large ranges of flow speed, and for that reason, a more accurate solution could be to acquire multiple speckle contrast images at different camera exposure times and calculate the speckle decorrelation time (a quantity that is inversely proportional to flow speed)[54]. Other important points to note are that LSCI is sensitive to other types of motion (e.g. movement of hands holding retractors), and to strong ambient illumination that is within the same wavelength range as the detected signal. The surgeons in this study made every effort to keep their hands still during the few seconds of image acquisition. Additionally, while the room lights remained on during measurements, the lights above the operating table had to be turned off or pointed away from the surgical field as they reduced the visibility of speckle patterns. Regardless of these considerations, we believe LSCI for parathyroid vascularity assessment is highly promising because it is label-free, real-time and can be performed simultaneously with NIRAF imaging, and work is already underway to develop clinical devices utilizing both techniques[55,56].

4.6 Conclusion

Laser speckle contrast imaging is a promising approach for label-free intraoperative assessment of parathyroid gland vascularity. It is quantitative, real-time, label-free, and does not interfere with NIRAF detection for localization of parathyroid glands. Based on this dataset, a thyroidectomy patient that does not have at least one vascularized parathyroid gland by LSCI will likely suffer hypoparathyroidism, while the vast majority of those who do will have normal PTH levels. Use of LSCI in thyroid surgery has the potential to help reduce long-term post-surgical hypoparathyroidism by providing surgeons with objective and accurate assessment of parathyroid gland vascularity.

4.7 Acknowledgements

The authors wish to acknowledge the financial support of the National Institutes of Health under Grant # 1R01CA212147-01A1. We also wish to express our gratitude to the operating room staff and patients recruited at the Vanderbilt University Medical Center for their accommodation and participation in the study.

4.8 References

1. Naveh-Many, T. Development of Parathyroid Glands. in *Molecular Biology of the Parathyroid* 1–2 (Landes Bioscience / Eurekah.com, 2005).
2. Ritter, K., Elfenbein, D., Schneider, D. F., Chen, H. & Sippel, R. S. Hypoparathyroidism after total thyroidectomy: incidence and resolution. *J. Surg. Res.* **197**, 348–53 (2015).
3. Cannizzaro, M. A., Lo Bianco, S., Picardo, M. C., Provenzano, D. & Buffone, A. How to avoid and to manage post-operative complications in thyroid surgery. *Updates Surg.* **69**, 211–215 (2017).
4. McHenry, C. R., Speroff, T., Wentworth, D. & Murphy, T. Risk factors for postthyroidectomy hypocalcemia. *Surgery* **116**, 641–7; discussion 647-8 (1994).
5. Dedivitis, R. A., Aires, F. T. & Cernea, C. R. Hypoparathyroidism after thyroidectomy: Prevention, assessment and management. *Current Opinion in Otolaryngology and Head and Neck Surgery* vol. 25 142–146 (2017).
6. Tredici, P., Grosso, E., Gibelli, B., Massaro, M. A., Arrigoni, C. & Tradati, N. Identification of patients at high risk for hypocalcemia after total thyroidectomy. *Acta Otorhinolaryngol. Ital.* **31**, 144–148 (2011).
7. Demeester-Mirkine, N., Hooghe, L., Van Geertruyden, J. & Maertelaer, V. Hypocalcemia After Thyroidectomy. *Arch. Surg.* **127**, 854–858 (1992).
8. Baldassarre, R. L., Chang, D. C., Brumund, K. T. & Bouvet, M. Predictors of Hypocalcemia after Thyroidectomy: Results from the Nationwide Inpatient Sample. *ISRN Surg.* **2012**, 1–7 (2012).
9. Sanabria, A., Kowalski, L. P. & Tartaglia, F. Inferior thyroid artery ligation increases hypocalcemia after thyroidectomy: A meta-analysis. *Laryngoscope* **128**, 534–541 (2018).
10. Edafe, O. & Balasubramanian, S. P. Incidence, prevalence and risk factors for post-surgical hypocalcaemia and hypoparathyroidism. *Gland Surgery* vol. 6 S59–S68 (2017).
11. American College of Surgeons. Total Thyroidectomy Complication Rates and Costs Are Lower if Surgeon Performs 25 or More Cases Yearly. https://www.facs.org/media/press-releases/2015/sosa (2015).

12. Edafe, O., Antakia, R., Laskar, N., Uttley, L. & Balasubramanian, S. P. Systematic review and meta-analysis of predictors of post-thyroidectomy hypocalcaemia. *Br. J. Surg.* **101**, 307–320 (2014).

13. Paras, C., Keller, M., White, L., Phay, J. & Mahadevan-Jansen, A. Near-infrared autofluorescence for the detection of parathyroid glands. *J. Biomed. Opt.* **16**, 067012 (2011).

14. McWade, M. A., Paras, C., White, L. M., Phay, J. E., Mahadevan-Jansen, A. & Broome, J. T. A novel optical approach to intraoperative detection of parathyroid glands. *Surgery* **154**, 1371–7; discussion 1377 (2013).

15. McWade, M. A., Sanders, M. E., Broome, J. T., Solórzano, C. C. & Mahadevan-Jansen, A. Establishing the clinical utility of autofluorescence spectroscopy for parathyroid detection. *Surgery* **159**, 193–202 (2016).

16. Thomas, G., McWade, M. A., Paras, C., Mannoh, E. A., Sanders, M. E., White, L. M., Broome, J. T., Phay, J. E., Baregamian, N., Solórzano, C. C. & Mahadevan-Jansen, A. Developing a Clinical Prototype to Guide Surgeons for Intraoperative Label-Free Identification of Parathyroid Glands in Real Time. *Thyroid* **28**, 1517–1531 (2018).

17. Thomas, G., McWade, M. A., Nguyen, J. Q., Sanders, M. E., Broome, J. T., Baregamian, N., Solórzano, C. C. & Mahadevan-Jansen, A. Innovative surgical guidance for label-free real-time parathyroid identification. *Surgery* **165**, 114–123 (2019).

18. Thomas, G., Squires, M. H., Metcalf, T., Mahadevan-Jansen, A. & Phay, J. E. Imaging or Fiber Probe-Based Approach? Assessing Different Methods to Detect Near Infrared Autofluorescence for Intraoperative Parathyroid Identification. *J. Am. Coll. Surg.* **229**, 596-608.e3 (2019).

19. McWade, M. A., Paras, C., White, L. M., Phay, J. E., Solórzano, C. C., Broome, J. T. & Mahadevan-Jansen, A. Label-free Intraoperative Parathyroid Localization With Near-Infrared Autofluorescence Imaging. *J. Clin. Endocrinol. Metab.* **99**, 4574–4580 (2014).

20. Kim, S. W., Song, S. H., Lee, H. S., Noh, W. J., Oak, C., Ahn, Y.-C. & Lee, K. D. Intraoperative Real-Time Localization of Normal Parathyroid Glands With Autofluorescence Imaging. *J. Clin. Endocrinol. Metab.* **101**, 4646–4652 (2016).

21. Ladurner, R., Sommerey, S., Arabi, N. Al, Hallfeldt, K. K. J., Stepp, H. & Gallwas, J. K. S. Intraoperative near-infrared autofluorescence imaging of parathyroid glands. *Surg. Endosc.* **31**, 3140–3145 (2017).

22. Kim, S. W., Lee, H. S., Ahn, Y. C., Park, C. W., Jeon, S. W., Kim, C. H., Ko, J. B., Oak, C., Kim, Y. & Lee, K. D. Near-Infrared Autofluorescence Image-Guided Parathyroid Gland Mapping in Thyroidectomy. *J. Am. Coll. Surg.* **226**, 165–172 (2018).

23. Dip, F., Falco, J., Verna, S., Prunello, M., Loccisano, M., Quadri, P., White, K. & Rosenthal, R. Randomized Controlled Trial Comparing White Light with Near-Infrared Autofluorescence for Parathyroid Gland Identification During Total Thyroidectomy. *J. Am. Coll. Surg.* **228**, 744–751 (2019).

24. De Leeuw, F., Breuskin, I., Abbaci, M., Casiraghi, O., Mirghani, H., Ben Lakhdar, A., Laplace-Builhé, C. & Hartl, D. Intraoperative Near-infrared Imaging for Parathyroid Gland Identification by Auto-fluorescence: A Feasibility Study. *World J. Surg.* **40**, 2131–2138 (2016).

25. Kahramangil, B., Dip, F., Benmiloud, F., Falco, J., de La Fuente, M., Verna, S., Rosenthal, R. & Berber, E. Detection of Parathyroid Autofluorescence Using Near-Infrared Imaging: A Multicenter Analysis of Concordance Between Different Surgeons. *Ann. Surg. Oncol.* **25**, 957–962 (2018).

26. Kose, E., Kahramangil, B., Aydin, H., Donmez, M. & Berber, E. Heterogeneous and low-intensity parathyroid autofluorescence: Patterns suggesting hyperfunction at parathyroid exploration. *Surgery* **165**, 431–437 (2019).

27. FDA. FDA permits marketing of two devices that detect parathyroid tissue in real-time during surgery | FDA. https://www.fda.gov/news-events/press-announcements/fda-permits-marketing-two-devices-detect-parathyroid-tissue-real-time-during-surgery.

28. Serra, C., Silveira, L. & Canudo, A. Identification of inadvertently removed parathyroid glands during thyroid surgery using autofluorescence. *Gland Surg.* **9**, 893–898 (2020).

29. Serra, C., Canudo, A. & Silveira, L. Intraoperative identification of parathyroid glands by autofluorescence on total thyroidectomy – Does it really reduces post-operative hypocalcemia? *Surg. Pract. Sci.* **2**, 100011 (2020).

30. Papavramidis, T. S., Chorti, A., Tzikos, G., Anagnostis, P., Pantelidis, P., Pliakos, I., Panidis, S., Papaioannou, M., Bakkar, S., Unal, E. & Michalopoulos, A. The effect of intraoperative autofluorescence monitoring on unintentional parathyroid gland excision rates and postoperative PTH concentrations—a single-blind randomized-controlled trial. *Endocrine* (2021) doi:10.1007/s12020-020-02599-5.

31. Kim, Y. S., Erten, O., Kahramangil, B., Aydin, H., Donmez, M. & Berber, E. The impact of near infrared fluorescence imaging on parathyroid function after total thyroidectomy. *J. Surg. Oncol.* **122**, jso.26098 (2020).

32. Sierra, M., Herrera, M. F., Herrero, B., Jiménez, F., Sepúlveda, J., Lozano, R. R., Gamino, R., González, O. & Correa-Rotter, R. Prospective biochemical and scintigraphic evaluation of autografted normal parathyroid glands in patients undergoing thyroid operations. *Surgery* **124**, 1005–10 (1998).

33. Lo, C. Y. & Tam, S. C. Parathyroid autotransplantation during thyroidectomy: Documentation of graft function. *Arch. Surg.* **136**, 1381–1385 (2001).

34. Ahmed, N., Aurangzeb, M., Muslim, M. & Zarin, M. Routine parathyroid autotransplantation during total thyroidectomy: A procedure with predictable outcome. *J. Pakistan Med. Assoc.* **63**, 190–3 (2013).

35. Kuriloff, D. B. & Kizhner, V. Parathyroid gland preservation and selective autotransplantation utilizing topical lidocaine in total thyroidectomy. *Laryngoscope* **120**, 1342–1344 (2010).

36. Ander, S., Johansson, K. & Smeds, S. In situ preservation of the parathyroid glands during operations on the Thyroid. *Eur. J. Surg.* **163**, 33–7 (1997).

37. Ezzat, W., Fathey, H., Fawaz, S., El-Ashri, A., Youssef, T. & Othman, H. Intraoperative parathyroid hormone as an indicator for parathyroid gland preservation in thyroid surgery. *Swiss Med. Wkly.* (2011) doi:10.4414/smw.2011.13299.

38. Chang, T.-P., Palazzo, F., Tolley, N., Constantinides, V., Yang, G.-Z. & Darzi, A. Vascularity assessment of parathyroid glands using confocal endomicroscopy: Towards an intraoperative imaging tool for real-time in situ viability assessment. *Eur. J. Surg. Oncol.* **40**, S3 (2014).

39. Fortuny, J. V., Belfontali, V., Sadowski, S. M., Karenovics, W., Guigard, S. & Triponez, F. Parathyroid gland angiography with indocyanine green fluorescence to predict parathyroid function after thyroid surgery. *Br. J. Surg.* **103**, 537–543 (2016).

40. Vidal Fortuny, J., Karenovics, W., Triponez, F. & Sadowski, S. M. Intra-Operative Indocyanine Green Angiography of the Parathyroid Gland. *World J. Surg.* **40**, 2378–2381 (2016).

41. Demarchi, M. S., Karenovics, W., Bédat, B. & Triponez, F. Intraoperative Autofluorescence and Indocyanine Green Angiography for the Detection and Preservation of Parathyroid Glands. *J. Clin. Med.* **9**, 830 (2020).

42. Vidal Fortuny, J., Sadowski, S. M., Belfontali, V., Guigard, S., Poncet, A., Ris, F., Karenovics, W. & Triponez, F. Randomized clinical trial of intraoperative parathyroid gland angiography with indocyanine green fluorescence predicting parathyroid function after thyroid surgery. *Br. J. Surg.* **105**, 350–357 (2018).

43. Zaidi, N., Bucak, E., Yazici, P., Soundararajan, S., Okoh, A., Yigitbas, H., Dural, C. & Berber, E. The feasibility of indocyanine green fluorescence imaging for identifying and assessing the perfusion of parathyroid glands during total thyroidectomy. *J. Surg. Oncol.* **113**, (2016).

44. Gálvez-Pastor, S., Torregrosa, N. M., Ríos, A., Febrero, B., González-Costea, R., García-López, M. A., Balsalobre, M. D., Pastor-Pérez, P., Moreno, P., Vázquez-Rojas, J. L. & Rodríguez, J. M. Prediction of hypocalcemia after total thyroidectomy using indocyanine green angiography of parathyroid glands: A simple quantitative scoring system. *Am. J. Surg.* **218**, 993–999 (2019).

45. Chu, W., Chennamsetty, A., Toroussian, R. & Lau, C. Anaphylactic Shock After Intravenous Administration of Indocyanine Green During Robotic Partial Nephrectomy. *Urol. Case Reports* **12**, 37–38 (2017).

46. Lang, B. H. H., Wong, C. K. H., Hung, H. T., Wong, K. P., Mak, K. L. & Au, K. B. Indocyanine green fluorescence angiography for quantitative evaluation of in situ parathyroid gland perfusion and function after total thyroidectomy. in *Surgery (United States)* vol. 161 87–95 (Mosby Inc., 2017).

47. Fercher, A. F. & Briers, J. D. Flow Visualization By Means Of Single-Exposure Speckle Photography. *Opt. Commun.* **37**, (1981).

48. Boas, D. A. & Dunn, A. K. Laser speckle contrast imaging in biomedical optics. *J. Biomed. Opt.* **15**, 011109 (2010).

49. Mannoh, E. A., Thomas, G., Solórzano, C. C. & Mahadevan-Jansen, A. Intraoperative Assessment of Parathyroid Viability using Laser Speckle Contrast Imaging. *Sci. Rep.* **7**, 14798 (2017).

50. Julián, M. T., Balibrea, J. M., Granada, M. L., Moreno, P., Alastrué, A., Puig-Domingo, M. & Lucas, A. Intact parathyroid hormone measurement at 24 hours after thyroid surgery as predictor of parathyroid function at long term. *Am. J. Surg.* **206**, 783–789 (2013).

51. Anastasiou, O. E., Yavropoulou, M. P., Papavramidis, T. S., Tzouvara, C., Triantafyllopoulou, K., Papavramidis, S. & Yovos, J. G. Secretory Capacity of the Parathyroid Glands after Total Thyroidectomy in Normocalcemic Subjects. *J. Clin. Endocrinol. Metab.* **97**, 2341–2346 (2012).

52. Mohebati, A. & Shaha, A. R. Anatomy of thyroid and parathyroid glands and neurovascular relations. *Clin. Anat.* **25**, 19–31 (2012).

53. Thompson, O., Andrews, M. & Hirst, E. Correction for spatial averaging in laser speckle contrast analysis. *Biomed. Opt. Express* **2**, 1021–9 (2011).

54. Parthasarathy, A. B., James Tom, W., Gopal, A., Zhang, X. & Dunn, A. K. Robust flow measurement with multi-exposure speckle imaging. *OSA Opt. EXPRESS* **16**, 1975–1989 (2008).

55. Mannoh, E. A., Luo, M., Thomas, G., Solórzano, C. C. & Mahadevan-Jansen, A. A combined autofluorescence and laser speckle contrast imaging system for parathyroid surgical guidance (Conference Presentation). in *Advanced Biomedical and Clinical Diagnostic and Surgical Guidance Systems XVII* (ed. Mahadevan-Jansen, A.) vol. 10868 20 (SPIE, 2019).

56. Oh, E., Kim, W. W., Nam, S.-H., Cheon, G. W., Ning, B. & Cha, J. Development of a portable imager for intraoperative real-time localization of parathyroid glands. in *Advanced Biomedical and Clinical Diagnostic and Surgical Guidance Systems XVIII* (ed. Mahadevan-Jansen, A.) vol. 11229 7 (SPIE, 2020).

CHAPTER 5

DEVELOPMENT OF AN IMAGING DEVICE FOR LABEL-FREE PARATHYROID GLAND IDENTIFICATION AND VASCULARITY ASSESSMENT

Emmanuel A. Mannoh[1,2], Logan B. Parker[1,2], Giju Thomas[1,2], Carmen C. Solórzano[3], Anita Mahadevan-Jansen[1,2]

[5] Vanderbilt Biophotonics Center, Nashville, TN 37235

[6] Department of Biomedical Engineering, Vanderbilt University, Nashville, TN 37235

[7] Division of Surgical Oncology and Endocrine Surgery, Vanderbilt University Medical Center, Nashville, TN 37232

This chapter was adapted with permission from:

"Development of an imaging device for label-free parathyroid gland identification and vascularity assessment"

Journal of Biophotonics. 2021

5.1 Abstract

During thyroid surgeries, it is important for surgeons to accurately identify healthy parathyroid glands and assess their vascularity to preserve their function postoperatively, thus preventing hypoparathyroidism and hypocalcemia. Near infrared autofluorescence detection enables parathyroid identification, while laser speckle contrast imaging allows assessment of parathyroid vascularity. Here, we present an imaging system combining the two techniques to perform both functions, simultaneously and label-free. An algorithm to automate the segmentation of a parathyroid gland in the fluorescence image to determine its average speckle contrast is also presented, reducing a barrier to clinical translation. Results from imaging ex vivo tissue samples show that the algorithm is equivalent to manual segmentation. Intraoperative images from representative procedures are presented showing successful implementation of the device to identify and assess vascularity of healthy and diseased parathyroid glands.

5.2 Introduction

Hypocalcemia is a common occurrence after total thyroidectomy. Reported rates vary partly due to differences in definitions[1–3], with some as high as 47%[4], however one review places the median reported rate at 27%[5]. Post-thyroidectomy hypocalcemia occurs when healthy parathyroid glands, which are the human body's main calcium regulators[6], are accidentally excised, injured or have their blood supply disrupted during thyroid resection. This leads to a loss of parathyroid hormone (hypoparathyroidism), which is responsible for signaling the body to increase calcium levels in the bloodstream when they are low. Calcium is required for a host of functions including muscle contraction and neuronal excitability. Hence, patients with prolonged low levels will suffer from tetany, cardiac arrhythmias and muscle spasms [6]. These patients therefore require calcium supplementation and repeated hospital visits in order to maintain normal calcium levels, and in about 5% of total thyroidectomy patients the condition is lifelong[2], making this a huge economic burden for these patients[7].

The two main challenges in the preservation of healthy parathyroid glands during thyroidectomy are the ability to identify the glands and assess their vascularity. The parathyroid glands are small (on the order of 3-8 mm[8]) and appear visually similar to adjacent tissues in the neck, making identification challenging. Paras *et al.* were the first to report autofluorescence of parathyroid glands under near-infrared illumination[9]. Using 785 nm excitation, they obtained fluorescence spectra peaking between 820-830 nm that were at least twice as intense as the spectra from the thyroid. Further work showed that the ratio of the parathyroid fluorescence to that of the thyroid ranges from 1.2 to above 20[10, 11]. These studies relied on point measurements of fluorescence spectra using a fiber-optic probe and led to the development of a clinical device for probe-based parathyroid detection[12]. Another approach to detecting the parathyroid near-infrared autofluorescence (NIRAF) is based on imaging, typically using a long-pass filter in front of a camera in order to visualize the fluorescence[13–17]. On one hand, the probe-based approach provides spectral information and lends itself more readily to quantifying fluorescence intensity. Measurements are made by being in contact with the tissue of interest, and therefore it is more likely to detect weaker fluorescence signals. It is also quite similar in handling to nerve-monitoring devices used routinely in thyroid surgeries, making it easier for surgeons to adopt. On the other hand, the imaging approach provides spatial information which can be very useful when surveying the surgical field. There is also evidence to suggest that the imaging approach can detect parathyroid glands obscured by fat or connective tissue[18].

Both approaches have demonstrated the consistency of parathyroid NIRAF and its utility in helping prevent accidental parathyroidectomy.

The second challenge of assessing parathyroid gland vascularity is just as important for positive postoperative outcomes. If a parathyroid gland is devascularized, that is, its blood supply is completely severed during the surgery, it will not be able to produce and secrete parathyroid hormone postoperatively. A devascularized parathyroid gland can however be salvaged intraoperatively by autotransplantation, a process whereby the gland is cut into tiny pieces and inserted into a muscle pouch[19]. Accurate knowledge of parathyroid vascularity is therefore needed to aid decision-making regarding autotransplantation. Visual assessment and perturbation of the parathyroid to elicit bleeding are the most commonly used methods to assess parathyroid vascularity. Indocyanine green (ICG) angiography is a method that is currently gaining acceptance in this field. It has been reported that observing one parathyroid gland with strong ICG fluorescence is sufficient for the patient to have normal parathyroid hormone levels post-thyroidectomy[20]. However, since this method relies on the fluorescence of ICG which is in a similar spectral region and much stronger than the parathyroid autofluorescence, autofluorescence-based parathyroid detection cannot be accomplished post ICG injection. Current use of ICG to assess parathyroid viability also faces a few other challenges. With a half-life of 3.4 minutes, repeated injections of ICG may sometimes be required depending on the duration of the surgery[20]. Another problem is that the current method of evaluation relies on a qualitative scoring of fluorescence intensity by the surgeon, which makes it difficult to standardize measurements across surgeons[20]. Finally, a small percentage of patients can suffer allergic reactions to the dye[21]. There is therefore still a need for a label-free objective approach to assess parathyroid vascularity.

An alternative method to assess parathyroid vascularity without the use of contrast agents is laser speckle contrast imaging (LSCI). This technique analyzes the interference pattern produced when coherent light is incident on a surface. Motion causes blurring of this interference or speckle pattern, which can be analyzed spatially or temporally to produce, for instance, blood flow maps in biological tissue. To analyze the speckle pattern, speckle contrast, which represents the ratio of the standard deviation of pixel intensities within local regions to their corresponding mean intensities, is calculated. For temporal analysis, standard deviations and means are calculated for each pixel over a number of images, while for spatial analysis, they are calculated per image within a sliding window (typically 5-by-5 or 7-by-7 pixels)[22]. Lower speckle contrast is indicative of greater blurring of the speckle pattern and therefore

greater blood flow. We have recently demonstrated that LSCI is able to accurately distinguish between parathyroid glands classified as well-vascularized versus vascularly damaged, as compared to the eye of an experienced surgeon. Well-vascularized glands consistently had lower speckle contrast[23].

The purpose of this work is to demonstrate a device – the parathyroid speckle and autofluorescence imager (ParaSPAI) – that combines NIRAF imaging with LSCI to enable simultaneous label-free parathyroid identification and vascularity assessment. An added benefit of this combination is the ability to use fluorescence images to automatically segment parathyroid glands and determine their speckle contrast. Previous work required manually segmenting speckle contrast images in order to obtain this information[23], which could be a barrier to clinical translation. Here, we present a combined autofluorescence and LSCI system, as well as a segmentation algorithm developed to automate the process of determining parathyroid gland speckle contrast. The device and algorithm were evaluated first on *ex vivo* tissue samples, and then intraoperatively in 3 patients.

5.3 Methods

5.3.1 Device design

The ParaSPAI was developed in-house and is depicted in Figure 1. The device was constructed on a cart that can be wheeled into and out of the operating room (Figure 5.1A). It has a single mode 785 nm diode laser with 60 mW power output (Innovative Photonics Solutions, Monmouth Junction, NJ) as its illumination source. An articulated arm (ICWUSA, Medford, OR) is attached to the cart, capable of extending about 4 feet from its edge, with an attachment for a sterile handle to allow maneuvering by the surgeon. The imaging head that acquires both LSCI and autofluorescence images is attached to the end of this articulated arm. A single mode fiber optic patch cable (Thorlabs, Newton, NJ) couples light from the laser to a lens tube attached on the exterior of the imaging head, illuminating a ~30 mm diameter spot at a distance of 400 mm from the imaging head. A linear polarizer (Thorlabs, Newton, NJ) in the lens tube is used to polarize its output to enable reduction of specular reflection in acquired images. The illumination has an approximately Gaussian profile and the maximum power density across the spot was measured to

be 6.8 mW/cm^2. Two laser pointers, one green and one red (Digi-Key, Thief River Falls, MN), attached on the sides of the imaging head guide the surgeon in positioning the device so that the tissue of interest in roughly in the center of the field of view and in focus when imaging. The laser pointers are angled such that their beams overlap at a distance of 400 mm from the imaging head.

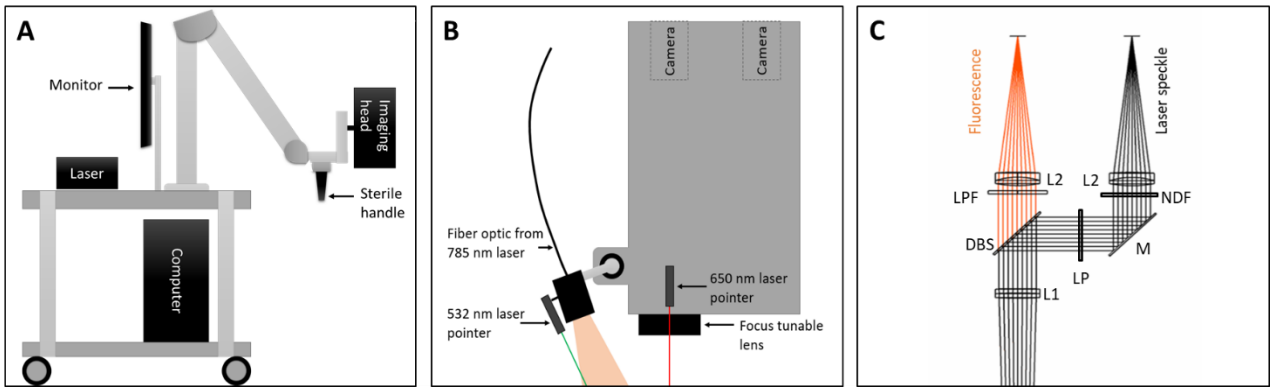

Figure 5.1. Schematic of the ParaSPAI (A); schematic of imaging head (B); optical layout of system (C). DBS, dichroic beamsplitter; L1, lens 1; L2, lens 2; LP, linear polarizer; LPF, longpass filter; M, mirror; NDF, neutral density filter.

Light scattered from the tissue is detected by the imaging head through the LSCI or NIRAF path (Figure 5.1C). Both paths share a collection lens (Edmund Optics, Barrington, NJ) which collimates light from the imaging plane onto a ~800 nm dichroic beamsplitter (Semrock, Rochester, NY). In the LSCI path, the laser light scattered from the tissue reflects off the dichroic and is focused onto a near-infrared-optimized CMOS camera (acA1300-60gmNIR, Basler AG, Ahrensburg, Germany), operated at 8-bit depth. After the dichroic mirror, there is a linear polarizer with its axis of polarization oriented perpendicular to the polarizer on the illumination leg. Its purpose is to reduce specular reflections from the illuminated site. Additionally, there is a 1.3 O.D. neutral density filter (Thorlabs, Newton, NJ) in front of the lens in order to improve visualization of speckles on the sensitive camera (i.e. avoid saturation). This optical path is folded by inserting a silver mirror (Thorlabs, Newton, NJ) after the polarizer to achieve a compact layout of the system. Modeling in Zemax 13 (Zemax Inc., Kirkland, WA) showed that this configuration results in a minimum detectable speckle size that is roughly twice the camera pixel size,

matching the sampling criterion for performing LSCI[24]. In the NIRAF path, the longer wavelength fluorescence is transmitted through the dichroic mirror and is further filtered by a ~800 nm longpass filter (Semrock, Rochester, NY) before being focused onto a second near-infrared-optimized camera operated at 12-bit depth. Lastly, there is a focus tunable lens (Optotune, Dietikon, Switzerland) in front of the assembly, to enable fine adjustments in focus for images acquired during surgery. The field of view of the imaging system at the working distance of 400 mm is approximately 26 x 32 mm. This platform is computer controlled, via a custom image acquisition and analysis program created in LabVIEW 2017 (National Instruments, Austin, TX).

5.3.2 Imaging procedure & parameters

Transportation of the imaging system over time results in slight shifts in the positions of the two cameras relative to each other. Therefore, there is a need to quantify the degree of image overlap between the cameras are prior to each imaging session. This was achieved by imaging an irregular grid and using these images to determine the rigid transformation that aligns the fields of view of the two cameras together. An efficient solution was engineered through the control software to acquire these images and subsequently perform intensity-based image registration to determine this transformation, with a single click. Fluorescence images are generated by first capturing a background image with the laser off, then a second image with the laser on, and then subtracting the former from the latter. Similar to image registration, this is executed by a single click. Due to the comparatively long exposure time required for parathyroid NIRAF, background-subtracted autofluorescence images are only generated as stills. Speckle contrast images are generated using the spatial method with a 5-by-5 pixel window, and displayed in real time at ~24 fps. The first 30 speckle contrast images after generating a fluorescence image are saved for post-processing. Sensor integration times were 100 ms and 5 ms for NIRAF and LSCI, respectively.

5.3.3 Fluorescence sensitivity & resolution measurement

Parathyroid autofluorescence is weak in intensity, and so to evaluate the capability of the imaging system to detect it, dilute solutions of ICG were made and imaged. Diluting with water, concentrations of 1, 0.7, 0.5, 0.3, 0.2, 0.1, 0.07, 0.05, 0.03, 0.02, and 0.01 μg/mL were made. Clinically, 3.5 mL of a 2.5 mg/mL ICG solution is administered to assess parathyroid vascularity[20]. Assuming 5 L of blood in the

human body, and given that ICG remains entirely within the blood until it is broken down by hepatic cells, the above-listed concentrations represent signal levels about 2 to 200 times smaller than would be expected for intraoperative imaging of ICG fluorescence. The solutions were pipetted into two 24-well plates, with one empty well in all directions separating each sample in order to prevent signal contamination. The last well was filled with water. Fluorescence images were acquired and the average intensity across each well was calculated from these images.

To measure spatial resolution, light from an 810 nm LED was collimated onto a negative 1951 United States Air Force resolution test target (Thorlabs, Newton, NJ). The negative test target transmits light only through the engraved patterns, allowing this setup to result in the lines mimicking fluorescent sources. An image was acquired of the test target from the opposite end of the light source. The image of the resolution test target is shown in Figure 5.2A. The largest set of unresolvable horizontal and vertical lines indicates the resolving power of the system. This was element 1 of group 4 (Figure 5.2C), indicating a spatial resolution of 62.5 µm.

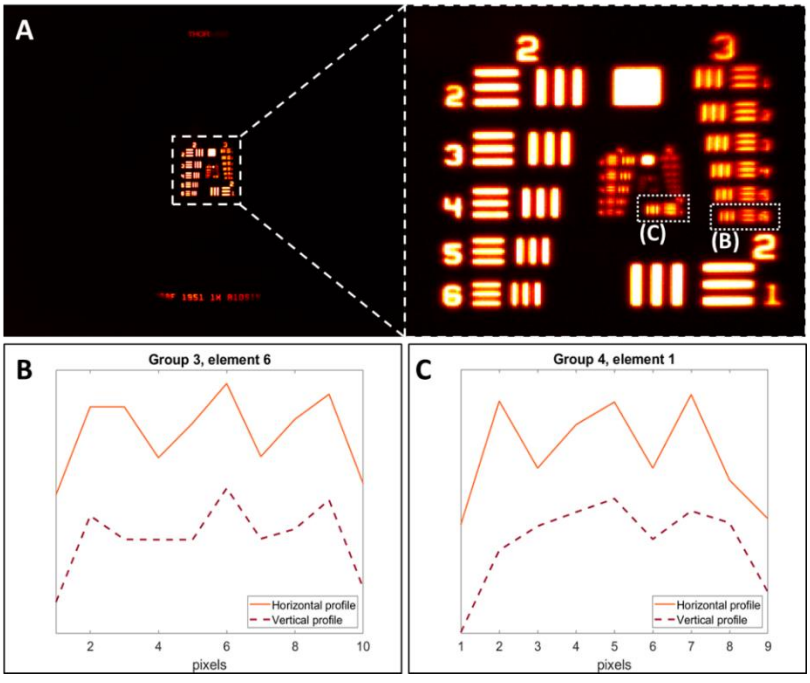

Figure 5.2. Resolution of the NIRAF imaging system measured by imaging a negative 1951 USAF resolution test target (A) placed in front of a collimated 810 nm beam. Comparing element 6 of group 3 (B) with element

1 of group 4 (C) shows that the latter is the largest set of unresolvable horizontal and vertical lines. This corresponds to a spatial resolution of 62.5 µm.

5.3.4 Development of parathyroid segmentation algorithm

Previous work using LSCI to assess parathyroid vascularity required manual segmentation of the images in order to determine a parathyroid gland's speckle contrast[23]. This is time-consuming and a potential barrier to clinical translation, and therefore would benefit greatly from a method to automate the segmentation. Combining LSCI with NIRAF imaging allows the parathyroid gland to be automatically segmented in the fluorescence image (where it is generally the most fluorescent organ). This information can then be used to automate determination of the parathyroid speckle contrast. Following is a description of the algorithm developed to automatically segment the parathyroid gland after acquiring autofluorescence and speckle contrast images. The first step is to crop the autofluorescence image (Figure 3.A) to remove the first 200 pixels on each edge (original image size is 1024 x 1280 pixels). Given that the parathyroid gland is expected to be in the center of the image, this step reduces the size of the data and speeds up computation for later steps. This image is then thresholded into three levels using a multiple thresholding scheme based on Otsu's method[25] (Figure 3.B). The reason for choosing three levels is that, while the parathyroid is generally the strongest auto-fluorescing tissue in the neck at this wavelength, other tissues such as the thyroid also emit fluorescence; choosing three levels allows separation of parathyroid, thyroid (and other less fluorescent tissues), and the non-fluorescent background. After thresholding, the middle intensity level (thyroid) is set equal to the low intensity background (Figure 3.C). By this point, there should ideally be a clear distinction between the tissue of interest and everything else, however noise due to specular reflections and imperfect thresholding may still contaminate the image. To reduce these effects, the dominant cluster of high intensities is located through an iterative process of finding the centroid of the high intensity pixels and removing outliers to a two-dimensional Gaussian centered on the centroid until the mean and covariance of the pixel coordinates converge (Figure 3.D). This filtered image is then converted to an edge map (Figure 3.E) using Canny edge detection[26], and an active contour model is fit to this edge map to obtain the contour demarcating the parathyroid gland (Figure 3.F). The force used to drive the active contour towards the parathyroid boundary is based on gradient vector flow[27]. After obtaining the contour, the transformation that aligns the two cameras

(determined from imaging the irregular grid) is applied to demarcate the parathyroid in the first of the acquired series of speckle contrast images. Nine subsequent speckle contrast images are registered to the first using a discrete Fourier transform registration that only accounts for translation[28] – since these images are acquired at 24 fps, there is not much motion from frame to frame and a transformation that only relies on translation is sufficient to register them. These ten images are then averaged to improve spatial resolution and the average speckle contrast of the parathyroid (area within the transformed contour) is obtained. The entire process described above takes about 5 seconds to run on the system computer.

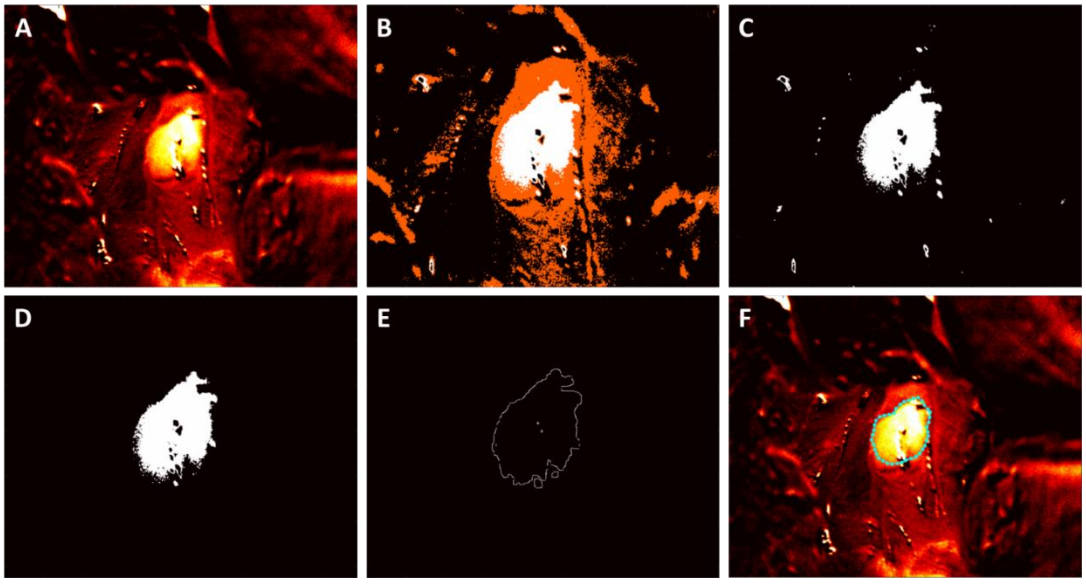

Figure 5.3. Parathyroid localization steps: background-subtracted fluorescence image (A) is thresholded into 3 levels (B). The second intensity level is set equal to the background (C), then the dominant cluster of high intensities is located (D). An edge map is created from this cluster of points (E) and used to fit an active contour model to demarcate the parathyroid (F). The image shown is of a healthy parathyroid gland in a parathyroidectomy case.

5.3.5 Evaluation of segmentation algorithm

To test the device and algorithm, two thyroid and five parathyroid ex vivo tissue samples, all from different patients, were imaged in the laboratory. The specimens were obtained from the Cooperative

Health Tissue Network at the Vanderbilt University Medical Center. The parathyroid specimens were obtained from cases of parathyroid adenoma, while the thyroid specimens were from non-malignant thyroid tissue. One thyroid specimen was obtained from cauterized tissue and was therefore more optically absorbing than the other. Each parathyroid specimen was placed next to each thyroid specimen for imaging, resulting in a total of ten pairings. The tissue samples were placed in a flat container with just enough phosphate-buffered saline to keep them hydrated without submerging them. Autofluorescence images were acquired of each pairing and the automated parathyroid segmentation algorithm was then run on these images. Blinded from the segmentation results, three different users manually segmented the autofluorescence images to demarcate the parathyroid. The performance of the algorithm was evaluated by calculating the Hausdorff distances between the contour generated by the algorithm and the contours manually segmented by the three users. The Hausdorff distance is the longest of all the distances from a point on one contour to its closest point on the other contour[29]. Calculations were performed for both the forward and backward direction and the maximum value was taken. Hausdorff distances between the manually segmented contours were also calculated. Two sample t-tests were performed on the two sets of data to determine if the Hausdorff distances from the contours produced by the algorithm to the manually segmented contours were significantly different from the inter-user Hausdorff distances.

Finally, a simulation was performed to evaluate the impacts of (1) parathyroid to thyroid fluorescence ratio, and (2) parathyroid signal-to-background ratio, on the segmentation algorithm. An image of a parathyroid specimen next to a thyroid specimen was simulated by manually drawing the specimens onto a blank figure in MATLAB (The MathWorks Inc., Natick, MA) and assigning intensities to the three different portions of the image: parathyroid, thyroid and background. The intensity of the thyroid was fixed, while the intensities of the background and parathyroid were varied to achieve signal to background ratios of 5, 3.5, 3 and 2, and parathyroid to thyroid fluorescence ratios of 1, 1.1, 1.2, 1.5 and 2. Normally-distributed random noise was generated with standard deviation equal to 10% of the thyroid intensity and added to each image prior to running the segmentation algorithm. Success or failure was determined by whether or not the resulting contour bounded just the simulated parathyroid.

5.3.6 Intraoperative imaging

One patient undergoing thyroid lobectomy and two patients undergoing parathyroidectomy at Vanderbilt University Medical Center were recruited under a larger study approved by the Institutional

Review Board, and written informed consent was obtained prior to their participation. In the thyroid lobectomy case, speckle contrast images of both the superior and inferior parathyroid glands were acquired after resection of the thyroid lobe. Following this, 1 mL of a 2.5 mg/mL ICG solution was administered to the patient and fluorescence images were acquired for comparison with the speckle contrast data. In the parathyroidectomy cases, imaging followed one of two protocols depending on the health of the gland being imaged. For a diseased gland, one set of images (a single autofluorescence image and a series of speckle contrast images) was first acquired after the surgeon located and exposed the gland. Then, the surgeon ligated the blood supply to the diseased parathyroid in preparation for excision and a second set of images was acquired. For a healthy gland, only one set of autofluorescence and speckle contrast images was acquired and this occurred at any point during the surgery at the discretion of the surgeon. No more than 5 minutes was added to each surgical procedure due to imaging. Imaging was performed with the room lights on, but with the overhead OR lamps and the surgeon's headlamp pointed away from the surgical field to avoid saturating the cameras.

5.4 Results

5.4.1 Fluorescence sensitivity

Figure 5.4A shows the fluorescence images obtained of ICG solutions ranging in concentration from 0.01 µg/mL to 1 µg/mL. Water is also shown (0 µg/mL). The average intensity across the channels appears to follow an exponential curve (Figure 5.4B). Figure 5.4C is a log-log plot of just the ICG data (excluding water), showing a good fit to a straight line with R^2 value of 0.98. As mentioned previously, the concentrations measured range from 2 to 200 times smaller than the expected ICG concentration intraoperatively.

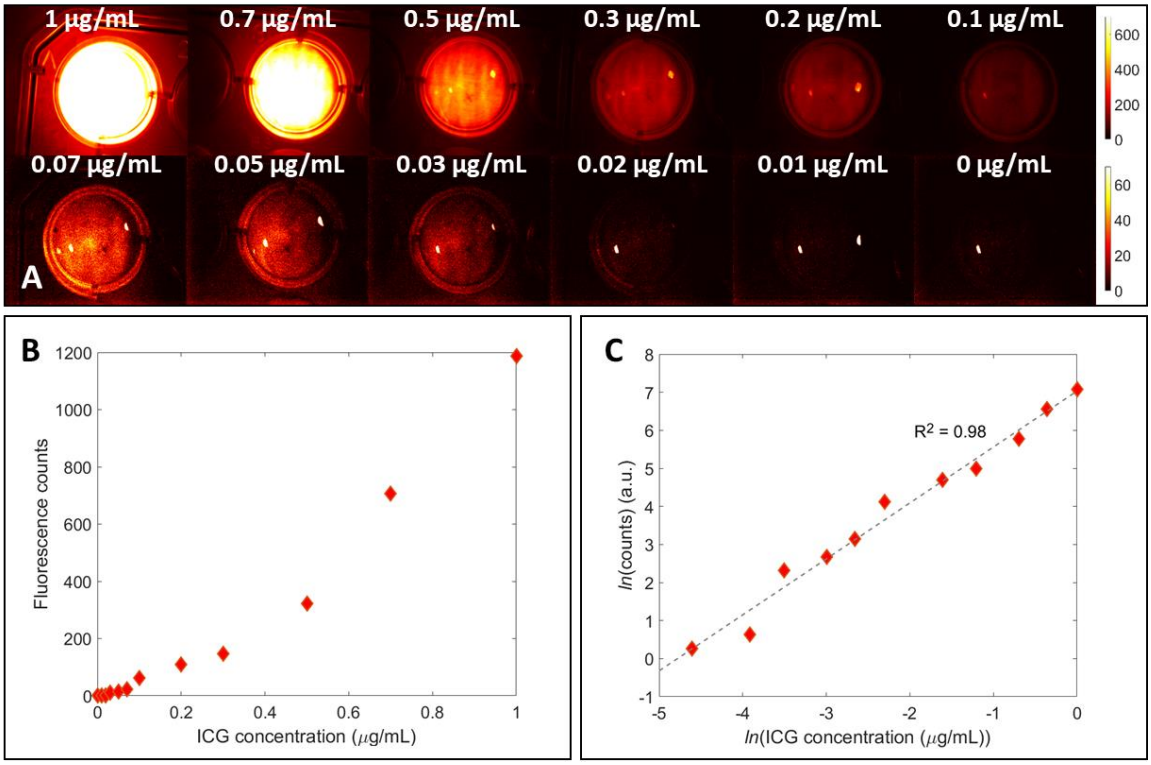

Figure 5.4. Fluorescence images of ICG solutions ranging in concentration from 1 µg/mL down to 0 µg/mL (water) in wells (A). The average intensity across each well was calculated and appeared to follow an exponential pattern (B). A logarithmic plot of the data fits a straight line with R^2 value of 0.98 (C).

5.4.2 Evaluation of segmentation algorithm

The segmentation algorithm was evaluated on autofluorescence images acquired from ten different pairings of ex vivo thyroid and parathyroid tissue samples, shown in Figure 5.5. The unique parathyroid specimens are sorted along the columns in order of increasing fluorescence intensity, while the two thyroid specimens are separated by the rows. The results of the automated parathyroid segmentation algorithm are indicated by the dotted cyan contours. Visually assessing the results, the algorithm correctly identified the parathyroid gland in each of the pairings. Hausdorff distances, the longest of all the distances from a point on one contour to its closest point on the other contour, were calculated in pixel numbers and converted to millimeters using the known dimensions of the field of view. The maximum inter-user Hausdorff distance in all ten pairings was 1.5 mm, while the maximum Hausdorff distance between the results of the

algorithm and any user was 1.7 mm. For reference, a normal parathyroid gland is up to 8 mm in length[8]. In general, the brighter the parathyroid sample, the more similar the segmentations were to each other and therefore the smaller the Hausdorff distances. Grouping the Hausdorff distances into inter-user, and between the algorithm and each user, two sample t-tests were performed (results shown in Figure 5.6). Only one significant difference was found ($p < 0.05$) and this was for the dimmest parathyroid specimen: while the users generally conformed to each other with an average inter-user Hausdorff distance of 0.6 mm, the algorithm generated a significantly different contour resulting in the maximum Hausdorff distance of 1.7 mm. A closer look at the top left panel of Figure 5.5 shows that a bright spot close to the top edge of the parathyroid may have had a large influence in pulling the active contour further away from the edge, resulting in the disparity.

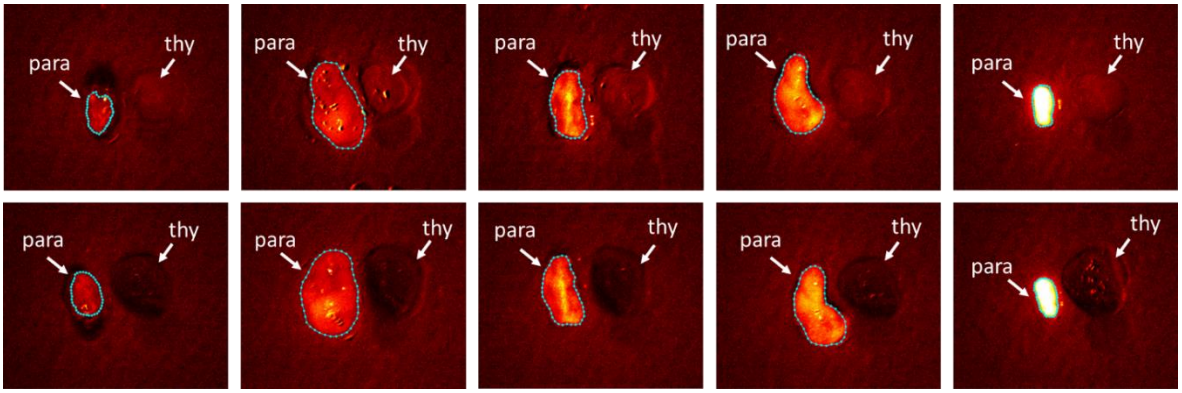

Figure 5.5. Autofluorescence images of *ex vivo* parathyroid (para) and thyroid (thy) tissue samples. Five parathyroid samples are sorted along the columns in order of increasing fluorescence intensity, each paired with two thyroid samples sorted along rows. Results of automated segmentation are shown by the dotted cyan contour.

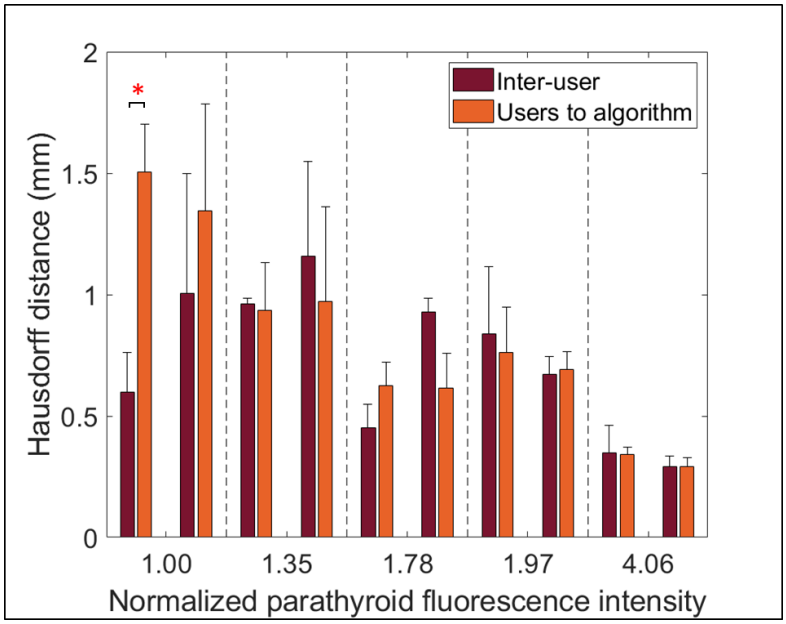

Figure 5.6. Hausdorff distances between parathyroid contours manually segmented by three different users (Inter-user), and between contours produced by the algorithm and their corresponding manually segmented contours (Users to algorithm). Data is sorted according to parathyroid fluorescence intensity normalized to the dimmest parathyroid and data from each unique parathyroid is separated from the others with dashed vertical lines. Hausdorff distances decrease the brighter the parathyroid. There is no significant difference in segmentation results except in the case of the dimmest parathyroid sample.

Simulation results (Figure 5.7) showed that at a parathyroid signal to background ratio of 5, the algorithm correctly segments out a parathyroid with a fluorescence intensity as low as 1.1 times that of the thyroid. At lower signal to background ratios, success of the algorithm requires stronger parathyroid fluorescence as would be expected. In the case of a parathyroid signal to background ratio of 2, success was only achieved when the background and thyroid intensities were the same.

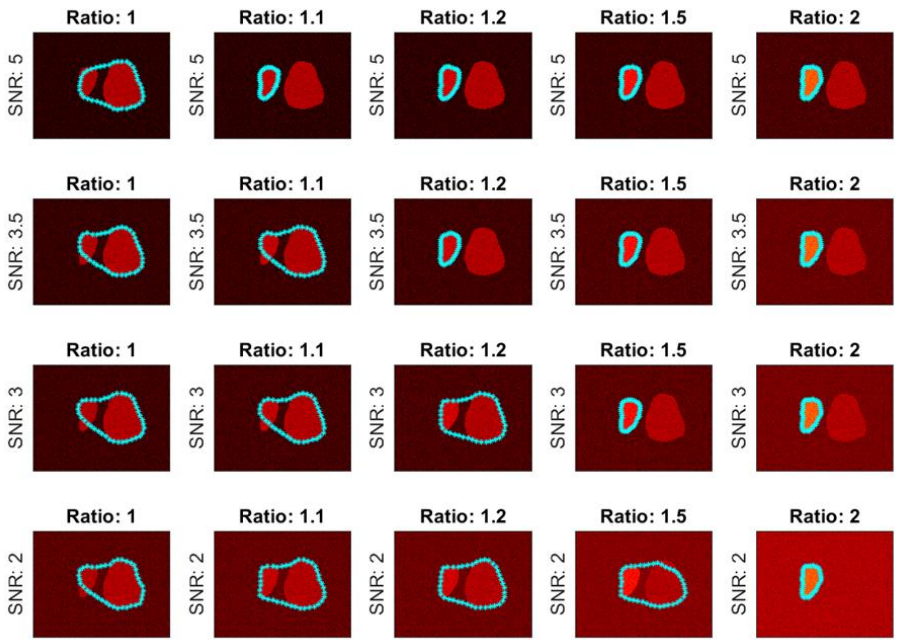

Figure 5.7. Results of varying parathyroid signal to background ratio (SNR) and parathyroid to thyroid fluorescence ratio on a simulated image. At higher SNR, successful segmentation is achieved at parathyroid to thyroid fluorescence ratios as low as 1.1. Stronger parathyroid fluorescence is needed at lower SNR.

5.4.3 Intraoperative images

Two parathyroid glands were identified by the surgeon during the thyroid lobectomy case, after removal of the diseased lobe. The surgeon considered the superior gland to be very well vascularized, and the inferior gland to be damaged but not completely devascularized as it did not appear visually dark. The average speckle contrast (calculated after manual segmentation) of the superior gland was 0.072, and that of the inferior gland was much higher at 0.128, indicating worse perfusion. The ICG fluorescence images supported this data, with the superior gland exhibiting very strong ICG fluorescence while the inferior gland had very little. These results are shown in Figure 5.8.

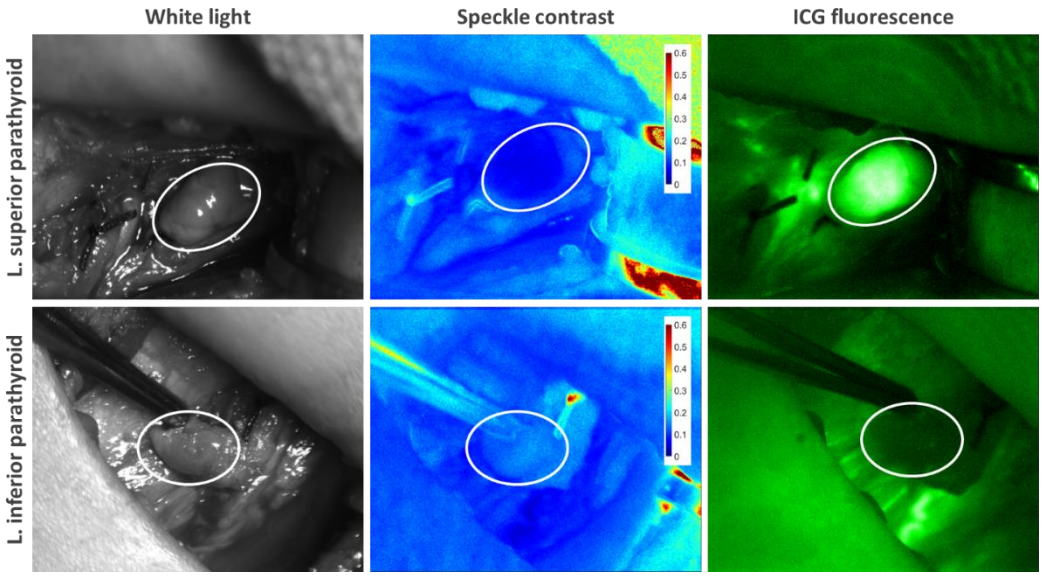

Figure 5.8. White light, speckle contrast and ICG fluorescence images of a well-vascularized left superior parathyroid gland and a partially devascularized left inferior parathyroid gland, taken during a thyroid lobectomy case. The low speckle contrast of the superior gland is supported by strong ICG fluorescence in the gland, and the high speckle contrast of the inferior gland is supported by its minimal ICG fluorescence. Parathyroid glands are indicated by white ellipses.

A healthy parathyroid gland observed during parathyroidectomy is shown in Figure 5.9. Strong autofluorescence of the gland facilitated successful segmentation (visually assessed) by the algorithm. The average speckle contrast within the transformed contour in the speckle contrast image was 0.175. For comparison, the value was 0.172 within the contour produced by manual segmentation. In Figure 5.10, a diseased parathyroid gland is shown before and immediately after ligation of its blood supply. Visually, there is no appreciable change in either white light or autofluorescence images from before to after blood supply ligation. The only noticeable change is in speckle contrast which increased as expected, indicating a decrease in blood flow. Figure 5.10 highlights the heterogeneity in autofluorescence of some diseased parathyroid glands. This heterogeneity caused the segmentation algorithm to demarcate the more fluorescent portion of the gland, rather than its entirety. The resulting average speckle contrast values obtained from these contours were 0.072 before blood supply ligation and 0.188 after ligation. The uniformity of speckle contrast across the gland however, resulted in these values not being too different from the results of manual segmentation: 0.066 before and 0.186 after blood supply ligation. The larger difference (0.072 minus 0.066) was only 5% of the change in speckle contrast from pre- to post-ligation.

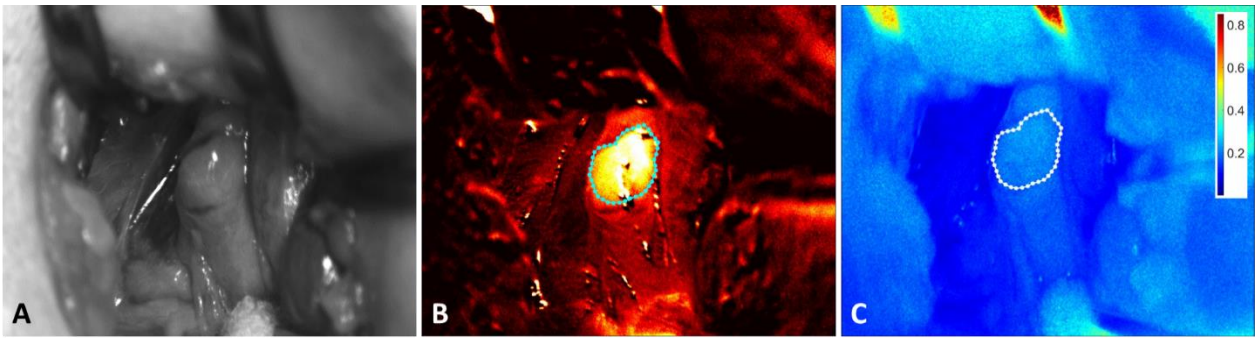

Figure 5.9. White light (A), autofluorescence (B), and speckle contrast (C) images of a healthy parathyroid gland observed in a parathyroidectomy case. The dotted cyan contour in the autofluorescence image is the result of the segmentation algorithm, and the dotted white contour in the speckle contrast image is the transformed contour within which average speckle contrast is calculated.

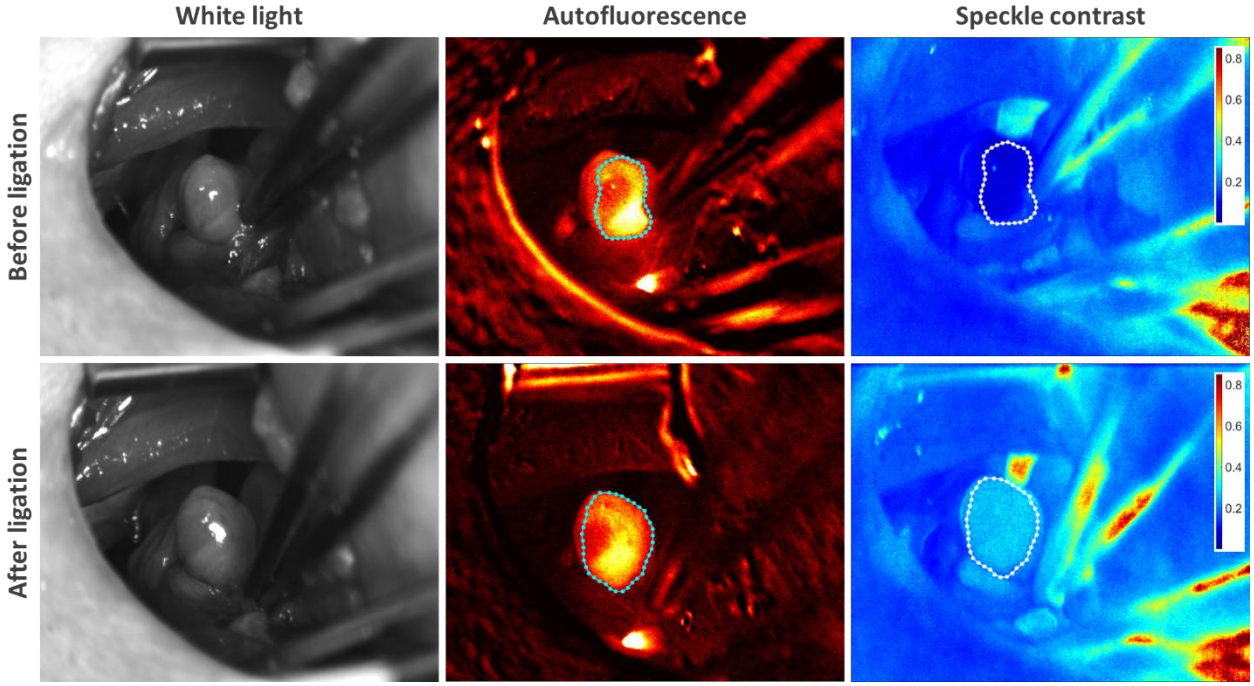

Figure 5.10. White light, autofluorescence and speckle contrast images of a diseased parathyroid gland before and immediately after blood supply ligation. As expected, the only appreciable change is the increase in speckle contrast, indicating a decrease in blood flow. Heterogeneity of autofluorescence resulted in a sub-total segmentation of the parathyroid gland, however speckle contrast values within the resulting contours were still similar to manual segmentation.

5.5 Discussion

It is crucial during thyroid and parathyroid surgical procedures for the surgeon to be able to not only identify but also assess the state of vascularity of parathyroid glands. This work presents a device that performs both functions without the need for exogenous contrast agents. Near-infrared autofluorescence imaging has been shown in numerous studies to be capable of identifying parathyroid glands[9–17], and this was demonstrated in this work as well. Other methods of parathyroid identification include preoperative sestamibi scans[30], frozen section histology[31], intraoperative methylene blue administration[32], and optical coherence tomography[33]. In comparison to these, NIRAF imaging has advantages in that it is label-free, can be done in real time, and does not require expensive or complex instrumentation. On its own, the use of LSCI to assess parathyroid gland vascularity would require input from the surgeon or another member of the surgical team to identify the region of interest. By combining NIRAF imaging with LSCI, the fluorescence of the parathyroid can be used to automatically determine its location in the speckle contrast images and enable more direct relay of information to the surgeon, reducing a barrier to clinical translation. The ParaSPAI achieves this.

Given that parathyroid NIRAF is a relatively weak signal, it was important to evaluate the capability of the ParaSPAI to detect this signal. To this end, ICG solutions that were 2 to 200 times less concentrated than the levels expected after a standard administration were imaged. The fit to the data in Figure 5.4C shows that the device is sensitive to this range of fluorescence intensities. For comparison, ongoing work suggests that parathyroid NIRAF is 10 to 100 smaller than the ICG fluorescence from the same gland after the dye has been injected (unpublished data). This indicates that the device should be sensitive to parathyroid NIRAF. Tiny fluorescent sources were mimicked by collimating 810 nm light through a 1951 USAF resolution test target. The resolution of the imaging system (62.5 μm) was well below the normal size of parathyroid glands, indicating that size should not hinder the detection of the parathyroid NIRAF.

In this work, we demonstrated that LSCI performs similar to ICG angiography in the same thyroid lobectomy case (Figure 5.8). Both methods agreed with the surgeon's assessment that the left superior parathyroid gland was very well vascularized, and the left inferior gland was at least partially devascularized. In comparison with ICG angiography, using LSCI to assess parathyroid gland vascularity has a few advantages: the technique can be performed simultaneously with autofluorescence imaging, is more readily quantifiable, and does not require exogenous contrast. Another potential advantage is in avoiding certain false positive situations that may arise. With a half-life of about 3.4 minutes[20], it will take

about 17 minutes for a bolus of ICG to washout to 3% of its initial concentration. A scenario can be envisioned in which a parathyroid gland becomes devascularized after initially demonstrating strong ICG fluorescence, due to additional surgery being performed. This gland would likely still exhibit strong ICG fluorescence, while LSCI would be able to detect the devascularization as it is sensitive to the flow of blood. On the other hand, ICG angiography has an advantage over LSCI in that it can delineate the arterial blood supply to the parathyroid gland, allowing the surgeon to avoid injury to it. While this is technically also possible with LSCI, the blood vessel would have to be very superficial.

In the ParaSPAI, a three-level thresholding scheme and active contour model were used to automatically segment the parathyroid. While in some cases, thresholding alone (followed by locating the dominant cluster of high intensities) would be sufficient to determine the pixels in the image containing parathyroid tissue, the additional step of fitting an active contour model to the parathyroid boundary helps overcome limitations in obtaining accurate speckle contrast averages across the gland due to noise and autofluorescence heterogeneity. The contours in Figure 5.10 did not encompass the entire parathyroid gland due to heterogeneity, however a larger area was still segmented than would have been with just thresholding. An alternative segmentation approach that might overcome this problem would be to use machine learning, which has been employed to segment features in real time during laparoscopic surgical procedures[34]. While this could be a future approach, there is currently insufficient data from the ParaSPAI to train such a model.

The mechanism for localizing the parathyroid in fluorescence images was found to not differ substantially from manual segmentation. Hausdorff distances are a measure of the similarity of two segmentations – the lower the value, the more similar the two contours in question are to each other. The results of segmenting NIRAF images of *ex vivo* tissue specimens showed that the stronger the parathyroid fluorescence, the more similar the segmentation contours produced manually and by the algorithm. The largest difference was between the algorithm and one user, producing a Hausdorff distance of 1.7 mm for a parathyroid tissue sample 8 mm in length. This was the least fluorescent parathyroid specimen, 1.5 times as fluorescent as the thyroid tissue next to it. More importantly however, with the exception of this one case, the Hausdorff distances between the algorithm and users did not differ significantly from the distances between the users. In other words, the segmentation produced by the algorithm was equivalent to having a fourth user manually segment the images. The algorithm is however highly dependent on the ratio of parathyroid to thyroid fluorescence, as well as the level of background noise. The smallest

parathyroid to thyroid fluorescence ratio among the *ex vivo* tissue specimens imaged was 1.5. However, in studies using a fiber optic probe to measure parathyroid gland fluorescence, it was reported that this ratio can range anywhere from 1.2 to above 20[11]. Simulations show that the segmentation algorithm can localize a parathyroid gland that is only 1.1 times as fluorescent as the thyroid, provided the background noise level is low enough. From the values tested, this occurred when the background noise was 5 times smaller than the parathyroid fluorescence intensity. When the background noise was 3.5 times smaller than the parathyroid fluorescence intensity, segmentation was successful at a parathyroid to thyroid fluorescence ratio of 1.2. The background noise level intraoperatively will differ from case to case due to factors such as the other tissues present in the field of view, and the intensity and type of room lighting in the operating room as the filters employed in this instrument do not completely eliminate their contribution.

The ParaSPAI could be useful in both parathyroidectomies and thyroidectomies. In parathyroidectomies, its main utility would be in confirming the diseased gland(s) as parathyroid and identifying and assessing vascularity of any normal parathyroid glands encountered. For this reason, the subtotal segmentation in Figure 5.10 is acceptable as autofluorescence heterogeneity occurs in diseased parathyroid glands while healthy parathyroid glands tend to be more homogeneous in autofluorescence[16], as can be seen in Figure 5.9. Such a device would be even more useful in thyroidectomies however, where healthy parathyroid glands are more at risk of being accidentally excised or devascularized. Following is a description of its envisioned use in a thyroidectomy. During thyroid resection, autofluorescence images can be acquired to confirm parathyroid candidates identified by the surgeon. After the thyroid has been removed, the device could once again be used to image previously identified parathyroid glands and any new candidates. With the push of a button, the segmentation algorithm would localize the parathyroid in the fluorescence image and its corresponding location in the speckle contrast image would be used to determine its average speckle contrast value. This information can then be conveyed to the surgeon in some form (e.g. as a binary output or a probability of parathyroid devascularization). Work is currently ongoing to establish clinically relevant criteria for assessing parathyroid vascularity after thyroidectomy using LSCI.

In summary, we present ParaSPAI, a device capable of label-free parathyroid gland identification and vascularity assessment through the combination of NIRAF imaging with LSCI. This device overcomes limitations associated with the use of ICG angiography to assess parathyroid vascularity. The parathyroid

segmentation algorithm developed for use with the device proved to be equivalent to manual segmentation and allows automated determination of parathyroid speckle contrast to simplify use of the device in the operating room. Such a device has the potential to help reduce hypoparathyroidism and hypocalcemia arising from complications in thyroid surgery.

5.6 Acknowledgements

The authors wish to acknowledge the members of the Vanderbilt Biophotonics Center for helpful discussion and feedback during the preparation of this manuscript, as well as the operating room staff and patients at the Vanderbilt University Medical Center for their accommodation and participation in the study. This work was funded by NIH 1R01CA212147-01A1.

5.7 References

1. Ritter, K., Elfenbein, D., Schneider, D. F., Chen, H. & Sippel, R. S. Hypoparathyroidism after total thyroidectomy: incidence and resolution. *J. Surg. Res.* **197**, 348–53 (2015).
2. Cannizzaro, M. A., Lo Bianco, S., Picardo, M. C., Provenzano, D. & Buffone, A. How to avoid and to manage post-operative complications in thyroid surgery. *Updates Surg.* **69**, 211–215 (2017).
3. Dedivitis, R. A., Aires, F. T. & Cernea, C. R. Hypoparathyroidism after thyroidectomy: Prevention, assessment and management. *Current Opinion in Otolaryngology and Head and Neck Surgery* vol. 25 142–146 (2017).
4. McHenry, C. R., Speroff, T., Wentworth, D. & Murphy, T. Risk factors for postthyroidectomy hypocalcemia. *Surgery* **116**, 641–7; discussion 647-8 (1994).
5. Edafe, O., Antakia, R., Laskar, N., Uttley, L. & Balasubramanian, S. P. Systematic review and meta-analysis of predictors of post-thyroidectomy hypocalcaemia. *Br. J. Surg.* **101**, 307–320 (2014).
6. Naveh-Many, T. Development of Parathyroid Glands. in *Molecular Biology of the Parathyroid* 1–2 (Landes Bioscience / Eurekah.com, 2005).
7. Zahedi Niaki, N., Singh, H., Moubayed, S. P., Leboeuf, R., Tabet, J.-C., Christopoulos, A., Ayad, T., Olivier, M.-J., Guertin, L. & Bissada, E. The Cost of Prolonged Hospitalization due to

Postthyroidectomy Hypocalcemia: A Case-Control Study. *Adv. Endocrinol.* **2014**, 1–4 (2014).

8. Mohebati, A. & Shaha, A. R. Anatomy of thyroid and parathyroid glands and neurovascular relations. *Clin. Anat.* **25**, 19–31 (2012).

9. Paras, C., Keller, M., White, L., Phay, J. & Mahadevan-Jansen, A. Near-infrared autofluorescence for the detection of parathyroid glands. *J. Biomed. Opt.* **16**, 067012 (2011).

10. McWade, M. A., Paras, C., White, L. M., Phay, J. E., Mahadevan-Jansen, A. & Broome, J. T. A novel optical approach to intraoperative detection of parathyroid glands. *Surgery* **154**, 1371–7; discussion 1377 (2013).

11. McWade, M. A., Sanders, M. E., Broome, J. T., Solórzano, C. C. & Mahadevan-Jansen, A. Establishing the clinical utility of autofluorescence spectroscopy for parathyroid detection. *Surgery* **159**, 193–202 (2016).

12. Thomas, G., McWade, M. A., Paras, C., Mannoh, E. A., Sanders, M. E., White, L. M., Broome, J. T., Phay, J. E., Baregamian, N., Solórzano, C. C. & Mahadevan-Jansen, A. Developing a Clinical Prototype to Guide Surgeons for Intraoperative Label-Free Identification of Parathyroid Glands in Real Time. *Thyroid* **28**, 1517–1531 (2018).

13. McWade, M. A., Paras, C., White, L. M., Phay, J. E., Solórzano, C. C., Broome, J. T. & Mahadevan-Jansen, A. Label-free Intraoperative Parathyroid Localization With Near-Infrared Autofluorescence Imaging. *J. Clin. Endocrinol. Metab.* **99**, 4574–4580 (2014).

14. Ladurner, R., Sommerey, S., Arabi, N. Al, Hallfeldt, K. K. J., Stepp, H. & Gallwas, J. K. S. Intraoperative near-infrared autofluorescence imaging of parathyroid glands. *Surg. Endosc.* **31**, 3140–3145 (2017).

15. Dip, F., Falco, J., Verna, S., Prunello, M., Loccisano, M., Quadri, P., White, K. & Rosenthal, R. Randomized Controlled Trial Comparing White Light with Near-Infrared Autofluorescence for Parathyroid Gland Identification During Total Thyroidectomy. *J. Am. Coll. Surg.* **228**, 744–751 (2019).

16. Kose, E., Kahramangil, B., Aydin, H., Donmez, M. & Berber, E. Heterogeneous and low-intensity parathyroid autofluorescence: Patterns suggesting hyperfunction at parathyroid exploration. *Surgery* **165**, 431–437 (2019).

17. De Leeuw, F., Breuskin, I., Abbaci, M., Casiraghi, O., Mirghani, H., Ben Lakhdar, A., Laplace-Builhé, C. & Hartl, D. Intraoperative Near-infrared Imaging for Parathyroid Gland Identification by Auto-fluorescence: A Feasibility Study. *World J. Surg.* **40**, 2131–2138 (2016).

18. Kim, S. W., Song, S. H., Lee, H. S., Noh, W. J., Oak, C., Ahn, Y.-C. & Lee, K. D. Intraoperative Real-Time Localization of Normal Parathyroid Glands With Autofluorescence Imaging. *J. Clin. Endocrinol. Metab.* **101**, 4646–4652 (2016).

19. Lo, C. Y. & Tam, S. C. Parathyroid autotransplantation during thyroidectomy: Documentation of graft function. *Arch. Surg.* **136**, 1381–1385 (2001).

20. Fortuny, J. V., Belfontali, V., Sadowski, S. M., Karenovics, W., Guigard, S. & Triponez, F. Parathyroid gland angiography with indocyanine green fluorescence to predict parathyroid function after thyroid surgery. *Br. J. Surg.* **103**, 537–543 (2016).

21. Chu, W., Chennamsetty, A., Toroussian, R. & Lau, C. Anaphylactic Shock After Intravenous Administration of Indocyanine Green During Robotic Partial Nephrectomy. *Urol. Case Reports* **12**, 37–38 (2017).

22. Boas, D. A. & Dunn, A. K. Laser speckle contrast imaging in biomedical optics. *J. Biomed. Opt.* **15**, 011109 (2010).

23. Mannoh, E. A., Thomas, G., Solórzano, C. C. & Mahadevan-Jansen, A. Intraoperative Assessment of Parathyroid Viability using Laser Speckle Contrast Imaging. *Sci. Rep.* **7**, 14798 (2017).

24. Kirkpatrick, S. J., Duncan, D. D. & Wells-Gray, E. M. Detrimental effects of speckle-pixel size matching in laser speckle contrast imaging. *Opt. Lett.* **33**, 2886 (2008).

25. Reddi, S. S., Rudin, S. F. & Keshavan, H. R. An optimal multiple threshold scheme for image segmentation. *IEEE Trans. Syst. Man. Cybern.* **SMC-14**, 661–665 (1984).

26. Canny, J. A Computational Approach to Edge Detection. *IEEE Trans. Pattern Anal. Mach. Intell.* **PAMI-8**, 679–698 (1986).

27. Xu, C. & Prince, J. L. Snakes, shapes, and gradient vector flow. *IEEE Trans. Image Process.* **7**, 359–369 (1998).

28. Guizar-Sicairos, M., Thurman, S. T. & Fienup, J. R. Efficient subpixel image registration algorithms. *Opt. Lett.* **33**, 156 (2008).

29. Taha, A. A. & Hanbury, A. An Efficient Algorithm for Calculating the Exact Hausdorff Distance. *IEEE Trans. Pattern Anal. Mach. Intell.* **37**, 2153–2163 (2015).

30. Westerdahl, J. & Bergenfelz, A. Sestamibi scan-directed parathyroid surgery: Potentially high failure rate without measurement of intraoperative parathyroid hormone. *World J. Surg.* **28**, 1132–1138 (2004).

31. Westra, W. H., Pritchett, D. D. & Udelsman, R. Intraoperative confirmation of parathyroid tissue during parathyroid exploration: A retrospective evaluation of the frozen section. *Am. J. Surg. Pathol.* **22**, 538–544 (1998).

32. Bewick, J. & Pfleiderer, A. The value and role of low dose methylene blue in the surgical management of hyperparathyroidism. *Ann. R. Coll. Surg. Engl.* **96**, 526–529 (2014).

33. Conti De Freitas, L. C., Phelan, E., Liu, L., Gardecki, J., Namati, E., Warger, W. C., Tearney, G. J. & Randolph, G. W. Optical coherence tomography imaging during thyroid and parathyroid surgery: A novel system of tissue identification and differentiation to obviate tissue resection and frozen section. *Head Neck* **36**, 1329–1334 (2014).

34. Volkov, M., Hashimoto, D. A., Rosman, G., Meireles, O. R. & Rus, D. Machine learning and coresets for automated real-time video segmentation of laparoscopic and robot-assisted surgery. in *Proceedings - IEEE International Conference on Robotics and Automation* 754–759 (Institute of Electrical and Electronics Engineers Inc., 2017). doi:10.1109/ICRA.2017.7989093.

CHAPTER 6

COMPARING LASER SPECKLE CONTRAST IMAGING AND INDOCYANINE GREEN ANGIOGRAPHY FOR ASSESSMENT OF PARATHYROID VASCULARITY

Emmanuel A. Mannoh[1,2], Naira Baregamian[3], Giju Thomas[1,2], Carmen C. Solórzano[3], Anita Mahadevan-Jansen[1,2]

[8] Vanderbilt Biophotonics Center, Vanderbilt University, Nashville, TN 37235

[9] Department of Biomedical Engineering, Vanderbilt University, Nashville, TN 37235

[10] Division of Surgical Oncology and Endocrine Surgery, Vanderbilt University Medical Center, Nashville, TN 37232

This chapter is in preparation for submission as:

"Comparing laser speckle contrast imaging and indocyanine green angiography for assessment of parathyroid vascularity"

At:

Journal of the American College of Surgeons

6.1 Abstract

BACKGROUND: Hypoparathyroidism is a major concern after thyroidectomy. To reduce the incidence, accurate intraoperative assessment of parathyroid gland vascularity is crucial as it helps preserve the function of parathyroid glands postoperatively. Indocyanine green (ICG) angiography is emerging as a promising technique to assess parathyroid vascularity, however it has a few limitations. A label-free method would overcome these limitations, and laser speckle contrast imaging (LSCI) is one such method which has been shown to be accurate in detecting differences in parathyroid vascularity. In this study, we examine the relationship between LSCI measurements and ICG fluorescence in the same parathyroid glands intraoperatively.

STUDY DESIGN: Twenty-one patients undergoing thyroidectomy or parathyroidectomy were included in this study. A combined LSCI and fluorescence imaging device was used to image a total of 37 parathyroid glands, and an average speckle contrast value was calculated for each parathyroid. This was followed by injection of ICG and fluorescence imaging of the same glands. ICG scores (0, 1, 2) were assigned by three observers and the speckle contrast values were grouped according to these scores. Analyses of variance were performed to detect significant differences between groups. Lastly, the ICG fluorescence intensity was calculated for each parathyroid gland and compared with speckle contrast in a linear regression.

RESULTS: Ambiguity in assigning ICG score 1 was evident from the scores of the three observers and highlights a limitation of a qualitative scoring system. Nevertheless, significant differences in speckle contrast were observed between the groups such that parathyroids in the ICG 0 group had higher speckle contrast than parathyroids in the ICG 1 group, which in turn had higher speckle contrast than those in the ICG 2 group. This was further supported by a strong correlation coefficient of -0.81 between mean-normalized ICG fluorescence intensity and speckle contrast. Results suggest that ICG angiography and LSCI detect similar differences in parathyroid gland vascularity.

CONCLUSION: Laser speckle contrast imaging provides similar assessments of vascularity to ICG angiography in the same parathyroid glands intraoperatively. It shows promise as a label-free alternative that overcomes the current limitations of ICG angiography for parathyroid vascularity assessment.

6.2 Introduction

Preserving healthy parathyroid glands is of critical importance during endocrine neck surgeries. Failure to do so could result in an inability to produce sufficient levels of parathyroid hormone (PTH) for normal calcium regulation, termed hypoparathyroidism[1]. Consequently, the patient is likely to suffer from hypocalcemia – low levels of calcium circulating in the bloodstream. This causes increased neuromuscular irritability resulting in tingling, muscle cramps, cardiac arrhythmias and seizures[1,2]. Reports on the incidence of hypoparathyroidism after thyroidectomy vary based on surgeon experience and disease definition[3–5], however a review of 115 studies found the rates of temporary and permanent hypoparathyroidism to be between 19-38% and 0-3% respectively (interquartile ranges)[6]. Conventional treatment of hypoparathyroidism involves supplementation with calcium and activated vitamin D, however there is evidence to suggest that long-term treatment can lead to nephrocalcinosis, kidney stones and brain calcifications[1]. PTH replacement therapy is an alternative treatment that reduces the need for calcium and activated vitamin D supplements[7]. Nevertheless, further studies are required to determine if it reduces the risk of long-term complications and improves quality of life[7]. Efforts should therefore also be focused on developing tools to provide additional guidance to surgeons intraoperatively to help reduce the incidence of post-surgical hypoparathyroidism.

There are two main challenges surgeons face in the preservation of healthy parathyroid glands during surgery. The first involves identification of the glands. Due to their small size[8], visual similarity to other tissues such as lymph nodes[9], and variability in location[10,11], intraoperative localization of parathyroid glands can be challenging. Near-infrared autofluorescence (NIRAF) detection has emerged as a reliable technique to localize or confirm identification of parathyroid glands intraoperatively[12,13,22,14–21]. There are currently two clinical devices with FDA clearance and CE marking for parathyroid identification using NIRAF detection[23]. Nevertheless, identification alone is insufficient to improve rates of post-surgical hypoparathyroidism[24–27].

The second challenge involves preserving the blood supply to the parathyroid glands and accurately assessing their perfusion status at the end of the surgery. Correctly assessed, the function of a devascularized parathyroid gland can be salvaged by autotransplantation[28]. Indocyanine green (ICG) angiography is emerging as a promising technique to aid in preservation of the parathyroid blood supply and assessing the parathyroids' perfusion status[29–33]. It has been reported that a minimum of one parathyroid gland with strong ICG fluorescence is sufficient for normal postoperative parathyroid

function[29], though other studies report there is no benefit to the technique[34]. Part of the reason for this discrepancy is that the current method relies on qualitative scoring of the ICG fluorescence intensity[29]. Furthermore, the timeline of imaging is extremely important as offsets between the injection of ICG and the commencement of imaging could result in inaccurate scores. Other limitations to the technique include the fact that it cannot be simultaneously combined with NIRAF detection for parathyroid localization, and the possibility for severe allergic reactions to the dye[35]. These limitations would be overcome by a label-free method to assess parathyroid vascularity.

In Chapters 3 and 4, laser speckle contrast imaging (LSCI) was presented as a label-free approach to assess parathyroid vascularity. The technique analyzes blurring of the speckle pattern produced when coherent laser light illuminates a tissue surface, providing contrast between regions of varying blood flow. The speckle contrast is calculated as the standard deviation of pixel intensities within local regions of the speckle pattern, divided by their corresponding mean intensities, with smaller values indicating greater blood flow[36]. In Chapter 5, an imaging device was presented combining LSCI with NIRAF imaging for simultaneous identification of parathyroid glands and assessment of their vascularity. Using this device, the purpose of the proceeding study is to examine the relationship between intraoperative LSCI and ICG angiography of the same parathyroid glands.

6.3 Methods

6.3.1 Patient recruitment and imaging protocol

This study was approved by the Vanderbilt University Medical Center (VUMC) Institutional Review Board. Twenty-one patients undergoing either thyroidectomy (partial or total) or parathyroidectomy were recruited and informed written consent was obtained from each patient prior to participation. Label-free imaging (LSCI & NIRAF) and ICG imaging were performed using the ParaSPAI developed in Chapter 5. The imaging procedure varied according to the type of surgery being performed. In thyroidectomy cases, imaging would begin after the thyroid lobe(s) had been excised. The attending surgeon positioned the device above each parathyroid gland they identified during the course of the operation and label-free

images were acquired. Following this, the anesthesiologist administered 1 mL of a 2.5 mg/mL ICG solution intravenously, followed by a saline flush. With the device still positioned above a parathyroid gland, ICG fluorescence images were recorded after the saline flush. Images were recorded until the ICG fluorescence intensity peaked and plateaued or began to gradually decrease (20-30 seconds after saline flush), then the device was quickly positioned above any other parathyroid glands to record at least 5 seconds of data for each. In parathyroidectomy cases, imaging began after the diseased parathyroid gland had been localized by the attending surgeon. Before ligating the parathyroid blood supply in preparation for excision, label-free imaging of the diseased gland was performed. Next, the parathyroid blood supply was ligated and label-free images of the diseased gland were again acquired. Additionally, any other unligated parathyroid glands identified by the surgeon were then imaged. After label-free imaging, 1 mL of a 2.5 mg/mL ICG solution was administered intravenously, followed by a saline flush. ICG fluorescence images were recorded as described above. The imaging procedure added no more than 10 minutes to the operating time for each patient and no repeat ICG injections were performed. In order to avoid influencing patient care, the attending surgeon was blinded from images acquired by the device intraoperatively. While imaging was performed with the room lights on, the overhead OR lamps and the surgeon's headlamp had to be pointed away from the surgical field.

6.4.2 Data analysis

Average speckle contrast was calculated for each parathyroid gland that had a noticeable NIRAF intensity. For each of these parathyroid glands, an image was selected from the ICG recording (after peaking of the fluorescence intensity) and a qualitative score of fluorescence intensity was assigned by three different scorers (including one of the surgeons that participated in the study). The scoring system used was similar to that reported by Fortuny *et al.* in their demonstration of ICG angiography for assessment of parathyroid viability[29]. A parathyroid gland with little to no ICG fluorescence received a score of 0, a parathyroid gland with moderate or patchy ICG fluorescence received a score of 1, and a parathyroid gland with strong ICG fluorescence received a score of 2. The speckle contrast data was grouped according to these scores for each observer. A two-way analysis of variance, followed by multiple comparison testing was performed on these groupings to identify any significant differences in speckle contrast between the groups given by ICG scores and scorers. The test was performed using MATLAB software (The MathWorks Inc., Natick, MA).

Given that the ParaSPAI described in Chapter 5 images from a fixed distance, fluorescence intensity can also be quantified instead of simply assigning qualitative scores. This was done by manually segmenting the ICG fluorescence images and calculating the average intensity for each parathyroid gland. In order to account for variability between patients in the amount of ICG entering the surgical field, and variability due to ICG draining from the surgical field, the average intensity of each parathyroid gland was normalized to the average intensity for that entire image. This mean-normalized fluorescence intensity was then compared against the parathyroid speckle contrast in a regression, and a linear correlation coefficient was calculated.

6.4 Results

Representative images of a vascularized and a devascularized parathyroid gland are displayed in Figure 6.1. Both sets of images were acquired in a thyroid lobectomy case.

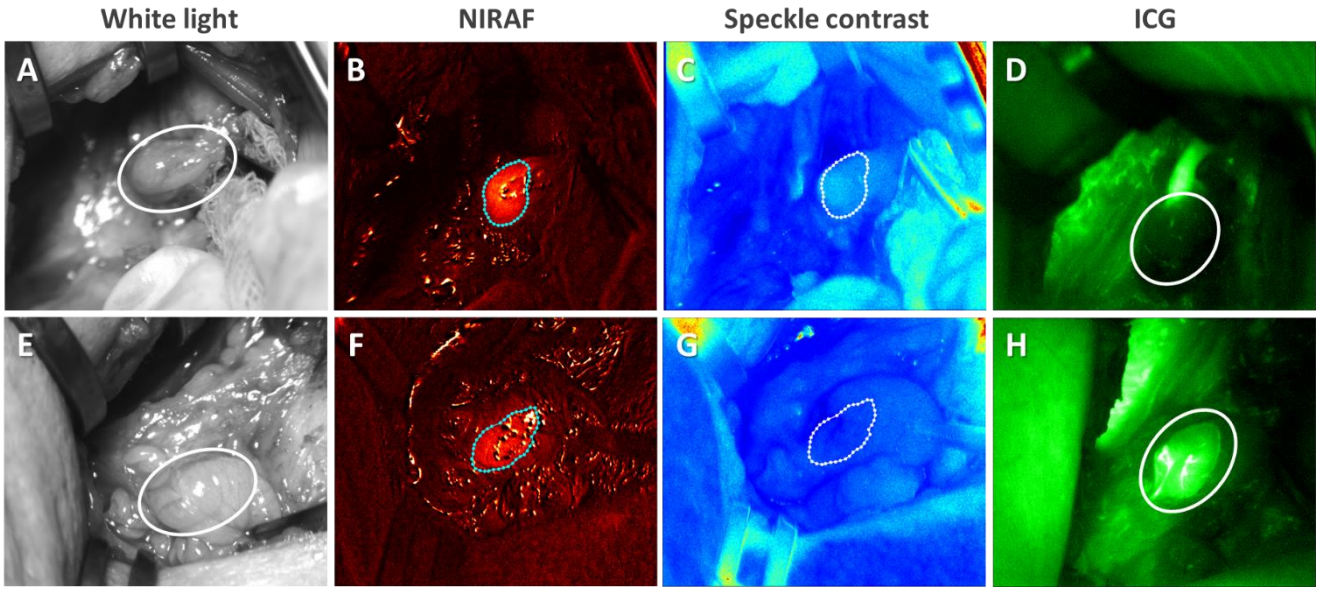

Figure 6.1. Representative white light, NIRAF, speckle contrast, and ICG fluorescence images of a devascularized (A – D) and a vascularized (E – F) parathyroid gland, acquired with the ParaSPAI device. The parathyroid glands are indicated with

white ellipses in white light and ICG fluorescence images, and with dotted contours generated by automated segmentation in NIRAF and speckle contrast images.

A total of 37 parathyroid glands were imaged in this study. The distribution of ICG scores assigned to each gland by the three scorers is shown in Figure 6.2. For 31 out of the 37 glands, all scorers assigned the same scores. The exceptions are indicated within red boxes in Figure 6.2 and always involve a discrepancy with assigning ICG score 1. In fact, of the 11 parathyroid glands that received an ICG score of 1 from any scorer, only 5 had all scorers in agreement. An example of a parathyroid gland that received disparate scores is shown in Figure 6.3, indicated by a white ellipse. One scorer assigned a value of 2, another scored it as 1, and the third scored it as being between 1 and 2 (1 was chosen to fit with the 3-level scoring system). There were no discrepancies where one scorer assigned an ICG score of 0 and another, an ICG score of 2.

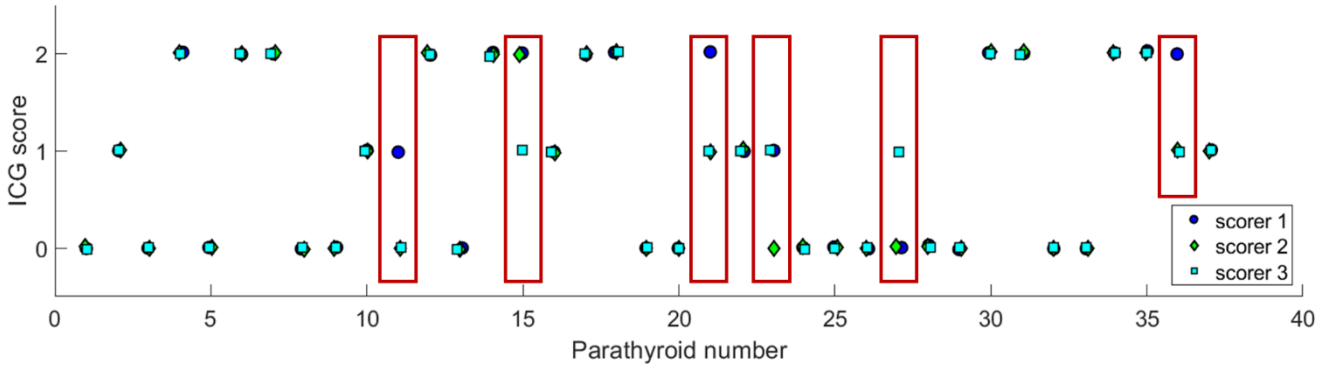

Figure 6.2. ICG scores assigned to 37 parathyroid glands imaged intraoperatively, assigned by 3 different scorers. Red boxes indicate instances of disagreement between the scorers. These all involve discrepancies in assigning ICG score 1.

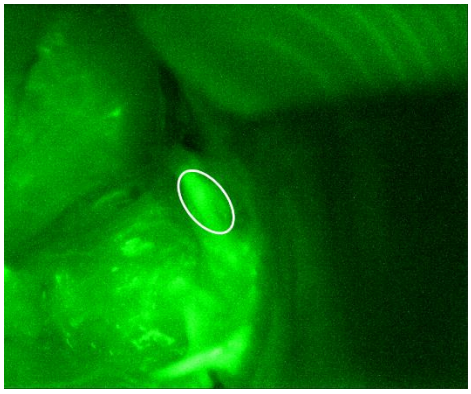

Figure 6.3. An example ICG image showing a parathyroid gland that received differing scores. One scorer assigned a score of 2, and the other two assigned a score of 1.

Average speckle contrast for each of the 37 parathyroid glands was then grouped according to the ICG scores provided by each scorer. A two-way analysis of variance on the speckle contrast data revealed that the interaction term assessing interaction between ICG score and scorer was not statistically significant ($p = 0.98$). Additionally, regardless of the differences observable in Figure 6.2, overall there was no significant influence of the scorer on the model ($p = 0.77$). The influence of ICG score was however significant ($p < 10^{-4}$). Consequently, three separate one-way analyses of variance were performed for each scorer, followed by multiple comparisons between ICG scores. The results are shown as the boxplots in Figure 6.4. For scorer 1, the speckle contrast of parathyroid glands assigned ICG score 0 were significantly different ($p < 0.05$) from the speckle contrast of parathyroid glands assigned ICG score 2. Similarly, the speckle contrast of parathyroid glands assigned ICG score 1 were significantly different from those assigned ICG score 2. However, there was no significant difference in speckle contrast between ICG score 0 and ICG score 1. For scorers 2 and 3, on the other hand, all groups had significantly different speckle contrast from one another. For all scorers, there is a notable trend where speckle contrast is lower for higher ICG scores. This makes sense since lower speckle contrast and higher ICG score both indicate greater perfusion.

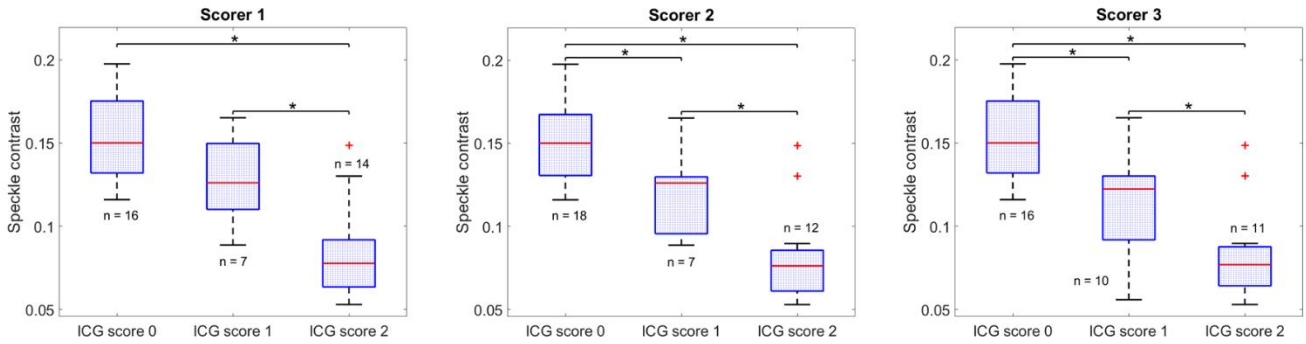

Figure 6.4. Boxplots showing distribution of speckle contrast for parathyroid glands assigned ICG scores 0, 1 and 2 by three different scorers. Each box represents the interquartile range for data in that group, the red horizontal line indicates the median for the group, whiskers extend to the most extreme data point not considered an outlier, and outliers are represented by red crosses. Significant differences ($p < 0.05$) between groups are indicated with black asterisks (*).

In order to compare LSCI and ICG angiography more quantitatively, the ICG fluorescence intensity was calculated for each parathyroid gland. This was possible because the imaging distance remained fixed for all data acquisition. To account for variability in patient anatomy influencing the amount of ICG reaching the surgical field, and variability in the timing of imaging, each fluorescence intensity value was normalized to the mean fluorescence intensity of the image it was extracted from. Figure 6.5 shows the speckle contrast of all 37 parathyroid glands, plotted against their mean-normalized ICG fluorescence intensity. Again, there is a notable trend in which speckle contrast decreases as ICG fluorescence intensity increases. A linear correlation coefficient of -0.81 relating the two measures was obtained from analysis.

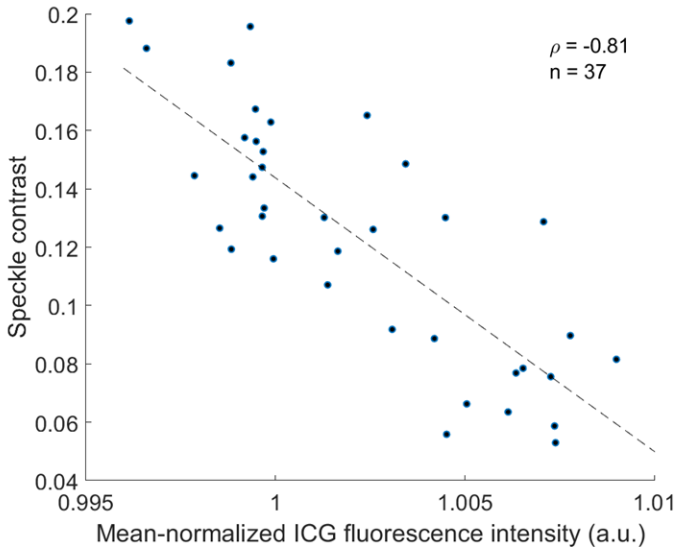

Figure 6.5. Scatterplot of speckle contrast of 37 parathyroid glands against their respective mean-normalized ICG fluorescence intensity. The line of best fit relating the two quantities is indicated by the dashed line. A linear correlation coefficient of -0.81 was obtained, suggesting strong similarity between the two techniques.

6.5 Discussion

Accurate assessment of blood flow to the parathyroid glands is important for ensuring normoparathyroid and normocalcemic outcomes for patients after endocrine neck surgeries. Currently, the assessment is primarily made by visual inspection of the glands and confirmation of bright red bleeding after needle prick[37]. Recently, ICG angiography has emerged as a promising technique to help improve the accuracy of surgeons' assessments of parathyroid vascularity. However, the technique has a number of limitations that would be overcome with the use of a label-free method, such as LSCI. In this study, we compared intraoperative speckle contrast with ICG scores and ICG fluorescence intensity for 37 parathyroid glands in 21 thyroidectomy and parathyroidectomy patients. Using a previously-developed imaging device (detailed in Chapter 5), both sets of data could be acquired for the same parathyroid glands using the same instrument.

Three observers scored the ICG images while blinded from each other's scores and speckle contrast data. Though there was no significant influence of the choice of scorer on the speckle contrast of

parathyroid glands assigned different scores, the results made evident the ambiguity in assigning an ICG score of 1 in a qualitative 3-level system. For instance, the parathyroid gland in Figure 6.3 received a score of 2 from one scorer, and a score of 1 from the other two. Imagining a scenario where this parathyroid gland was the best perfused or only gland identified after a total thyroidectomy, its ICG score could influence decisions made by the surgeon. In a study involving 36 thyroidectomy patients, Fortuny *et al*. reported normal postoperative PTH levels for all patients in whom at least one parathyroid gland with an ICG score of 2 was identified. Depending on the scorer, the patient in the above hypothetical scenario could either be expected to have normal or low postoperative PTH. It is possible that similar ambiguities in scoring contributed to the findings in another study that parathyroid ICG scores are not associated with post-thyroidectomy patient outcomes[34].

For all scorers, the median speckle contrast of parathyroid glands assigned ICG score 0 was higher than the median of parathyroids assigned ICG score 1, which in turn was higher than the median of parathyroids assigned ICG score 2. Smaller speckle contrast values indicate greater blood flow, therefore this trend makes sense. In all but one instance, these differences in speckle contrast across the ICG score groups were statistically significant, suggesting that LSCI and ICG angiography detect similar differences in parathyroid vascularity. To more quantitatively evaluate the similarity between the two techniques, the average fluorescence intensity of each parathyroid gland was calculated from ICG images. This was a valid approach due to the fixed imaging distance of the device used. Quantification of ICG fluorescence with handheld cameras currently on the market is challenging as variability in distance to the target and angle of imaging result in variability of fluorescence intensity[38]. Performing this quantification revealed a strong negative correlation between speckle contrast and mean-normalized ICG fluorescence intensity, again suggesting that the two techniques provide similar information. Further supporting the similarity of the two techniques is the fact that two previous studies, one using ICG angiography[29], and the other using LSCI (study in Chapter 4), both concluded that a minimum of one vascularized parathyroid gland is needed for normal parathyroid function after total thyroidectomy.

While there are similarities in the results of parathyroid assessment using the two techniques, it is important to note their differences. ICG angiography detects the presence of blood containing the dye, while LSCI simply detects the flow of blood. For this reason, if imaging is timed appropriately, the arterial supply to a vascularized parathyroid gland can be unequivocally highlighted after an injection of ICG – the fluorescence of the dye can be tracked as it enters the parathyroid gland. This can be extremely useful

early on in the operation to alert the surgeon to the location of the blood vessel and help them avoid damage to it. Since LSCI detects the flow of all blood, while it might highlight blood vessels, it will not provide an indication as to which blood vessel is directly supplying the parathyroid. Another result of the difference between the two methods is that ICG angiography is susceptible to false positives if a blood vessel is damaged after injection of the dye, while LSCI is not. If a blood vessel is cut and the dye leaks out, it could result in the entire surgical field fluorescing, giving the impression of adequate perfusion. Furthermore, since the dye persists for several minutes[29], damage to a previously well-vascularized gland will not be detectable until the fluorescence levels have dropped low enough for a subsequent ICG injection. Due to its label-free nature, LSCI also has an advantage over ICG angiography in that it can be performed multiple times throughout the course of surgery without the risk of increasing toxicity. The intensity and wavelength of light used in this study pose no harm to the patient. Finally, LSCI can be seamlessly integrated with NIRAF detection for parathyroid localization, as was demonstrated in Chapter 5, whereas NIRAF detection is no longer possible after ICG angiography.

6.6 Conclusion

In this study, we demonstrated that speckle contrast correlates strongly with ICG fluorescence in the same parathyroid glands intraoperatively. While ICG scoring can be ambiguous, LSCI provides objective quantitative values on blood flow to a parathyroid gland. It also allows seamless integration with NIRAF detection to provide complete assessment of parathyroid glands in endocrine neck surgeries. Laser speckle contrast imaging is a promising label-free alternative to ICG angiography for intraoperative parathyroid vascularity assessment.

6.7 Acknowledgements

We would like to express our thanks to the operating room staff at the Vanderbilt University Medical Center for being very accommodating throughout this study. We would also like to thank the patients that

participated. This work would not have been possible without funding from the National Institutes of Health through Grant # 1R01CA212147-01A1.

6.8 References

1. Mannstadt, M., Bilezikian, J. P., Thakker, R. V., Hannan, F. M., Clarke, B. L., Reijnmark, L., Mitchell, D. M., Vokes, T. J., Winer, K. K. & Shoback, D. M. Hypoparathyroidism. *Nat. Rev. Dis. Prim.* **3**, 1–21 (2017).

2. Naveh-Many, T. Development of Parathyroid Glands. in *Molecular Biology of the Parathyroid* 1–2 (Landes Bioscience / Eurekah.com, 2005).

3. American College of Surgeons. Total Thyroidectomy Complication Rates and Costs Are Lower if Surgeon Performs 25 or More Cases Yearly. https://www.facs.org/media/press-releases/2015/sosa (2015).

4. Edafe, O. & Balasubramanian, S. P. Incidence, prevalence and risk factors for post-surgical hypocalcaemia and hypoparathyroidism. *Gland Surgery* vol. 6 S59–S68 (2017).

5. Meltzer, C., Hull, M., Sundang, A. & Adams, J. L. Association between Annual Surgeon Total Thyroidectomy Volume and Transient and Permanent Complications. *JAMA Otolaryngol. - Head Neck Surg.* **145**, 830–837 (2019).

6. Edafe, O., Antakia, R., Laskar, N., Uttley, L. & Balasubramanian, S. P. Systematic review and meta-analysis of predictors of post-thyroidectomy hypocalcaemia. *Br. J. Surg.* **101**, 307–320 (2014).

7. Rejnmark, L., Underbjerg, L. & Sikjaer, T. Hypoparathyroidism: Replacement therapy with parathyroid hormone. *Endocrinology and Metabolism* vol. 30 436–442 (2015).

8. Mohebati, A. & Shaha, A. R. Anatomy of thyroid and parathyroid glands and neurovascular relations. *Clin. Anat.* **25**, 19–31 (2012).

9. Johnson, N. A., Tublin, M. E. & Ogilvie, J. B. Parathyroid Imaging: Technique and Role in the Preoperative Evaluation of Primary Hyperparathyroidism. *Am. J. Roentgenol.* **188**, 1706–1715 (2007).

10. Akerström, G., Malmaeus, J. & Bergström, R. Surgical anatomy of human parathyroid glands. *Surgery* **95**, 14–21 (1984).

11. Wang, C. The anatomic basis of parathyroid surgery. *Ann. Surg.* **183**, 271–5 (1976).

12. Paras, C., Keller, M., White, L., Phay, J. & Mahadevan-Jansen, A. Near-infrared autofluorescence for the detection of parathyroid glands. *J. Biomed. Opt.* **16**, 067012 (2011).

13. McWade, M. A., Paras, C., White, L. M., Phay, J. E., Mahadevan-Jansen, A. & Broome, J. T. A novel optical approach to intraoperative detection of parathyroid glands. *Surgery* **154**, 1371–7;

discussion 1377 (2013).

14. McWade, M. A., Sanders, M. E., Broome, J. T., Solórzano, C. C. & Mahadevan-Jansen, A. Establishing the clinical utility of autofluorescence spectroscopy for parathyroid detection. *Surgery* **159**, 193–202 (2016).

15. Thomas, G., McWade, M. A., Nguyen, J. Q., Sanders, M. E., Broome, J. T., Baregamian, N., Solórzano, C. C. & Mahadevan-Jansen, A. Innovative surgical guidance for label-free real-time parathyroid identification. *Surg. (United States)* **165**, 114–123 (2019).

16. Thomas, G., McWade, M. A., Paras, C., Mannoh, E. A., Sanders, M. E., White, L. M., Broome, J. T., Phay, J. E., Baregamian, N., Solórzano, C. C. & Mahadevan-Jansen, A. Developing a Clinical Prototype to Guide Surgeons for Intraoperative Label-Free Identification of Parathyroid Glands in Real Time. *Thyroid* **28**, 1517–1531 (2018).

17. Ladurner, R., Sommerey, S., Arabi, N. Al, Hallfeldt, K. K. J., Stepp, H. & Gallwas, J. K. S. Intraoperative near-infrared autofluorescence imaging of parathyroid glands. *Surg. Endosc.* **31**, 3140–3145 (2017).

18. Dip, F., Falco, J., Verna, S., Prunello, M., Loccisano, M., Quadri, P., White, K. & Rosenthal, R. Randomized Controlled Trial Comparing White Light with Near-Infrared Autofluorescence for Parathyroid Gland Identification During Total Thyroidectomy. *J. Am. Coll. Surg.* **228**, 744–751 (2019).

19. Kose, E., Kahramangil, B., Aydin, H., Donmez, M. & Berber, E. Heterogeneous and low-intensity parathyroid autofluorescence: Patterns suggesting hyperfunction at parathyroid exploration. *Surgery* **165**, 431–437 (2019).

20. Benmiloud, F., Godiris-Petit, G., Gras, R., Gillot, J. C., Turrin, N., Penaranda, G., Noullet, S., Chéreau, N., Gaudart, J., Chiche, L. & Rebaudet, S. Association of Autofluorescence-Based Detection of the Parathyroid Glands during Total Thyroidectomy with Postoperative Hypocalcemia Risk: Results of the PARAFLUO Multicenter Randomized Clinical Trial. in *JAMA Surgery* vol. 155 106–112 (American Medical Association, 2020).

21. Kim, S. W., Lee, H. S., Ahn, Y. C., Park, C. W., Jeon, S. W., Kim, C. H., Ko, J. B., Oak, C., Kim, Y. & Lee, K. D. Near-Infrared Autofluorescence Image-Guided Parathyroid Gland Mapping in Thyroidectomy. *J. Am. Coll. Surg.* **226**, 165–172 (2018).

22. De Leeuw, F., Breuskin, I., Abbaci, M., Casiraghi, O., Mirghani, H., Ben Lakhdar, A., Laplace-Builhé, C. & Hartl, D. Intraoperative Near-infrared Imaging for Parathyroid Gland Identification by Auto-fluorescence: A Feasibility Study. *World J. Surg.* **40**, 2131–2138 (2016).

23. FDA. FDA permits marketing of two devices that detect parathyroid tissue in real-time during surgery | FDA. https://www.fda.gov/news-events/press-announcements/fda-permits-marketing-two-devices-detect-parathyroid-tissue-real-time-during-surgery.

24. Serra, C., Silveira, L. & Canudo, A. Identification of inadvertently removed parathyroid glands during thyroid surgery using autofluorescence. *Gland Surg.* **9**, 893–898 (2020).

25. Serra, C., Canudo, A. & Silveira, L. Intraoperative identification of parathyroid glands by autofluorescence on total thyroidectomy – Does it really reduces post-operative hypocalcemia? *Surg. Pract. Sci.* **2**, 100011 (2020).

26. Papavramidis, T. S., Chorti, A., Tzikos, G., Anagnostis, P., Pantelidis, P., Pliakos, I., Panidis, S., Papaioannou, M., Bakkar, S., Unal, E. & Michalopoulos, A. The effect of intraoperative autofluorescence monitoring on unintentional parathyroid gland excision rates and postoperative PTH concentrations—a single-blind randomized-controlled trial. *Endocrine* (2021) doi:10.1007/s12020-020-02599-5.

27. Kim, Y. S., Erten, O., Kahramangil, B., Aydin, H., Donmez, M. & Berber, E. The impact of near infrared fluorescence imaging on parathyroid function after total thyroidectomy. *J. Surg. Oncol.* **122**, jso.26098 (2020).

28. Lo, C. Y. & Tam, S. C. Parathyroid autotransplantation during thyroidectomy: Documentation of graft function. *Arch. Surg.* **136**, 1381–1385 (2001).

29. Fortuny, J. V., Belfontali, V., Sadowski, S. M., Karenovics, W., Guigard, S. & Triponez, F. Parathyroid gland angiography with indocyanine green fluorescence to predict parathyroid function after thyroid surgery. *Br. J. Surg.* **103**, 537–543 (2016).

30. Vidal Fortuny, J., Karenovics, W., Triponez, F. & Sadowski, S. M. Intra-Operative Indocyanine Green Angiography of the Parathyroid Gland. *World J. Surg.* **40**, 2378–2381 (2016).

31. Vidal Fortuny, J., Sadowski, S. M., Belfontali, V., Guigard, S., Poncet, A., Ris, F., Karenovics, W. & Triponez, F. Randomized clinical trial of intraoperative parathyroid gland angiography with indocyanine green fluorescence predicting parathyroid function after thyroid surgery. *Br. J. Surg.* **105**, 350–357 (2018).

32. Gálvez-Pastor, S., Torregrosa, N. M., Ríos, A., Febrero, B., González-Costea, R., García-López, M. A., Balsalobre, M. D., Pastor-Pérez, P., Moreno, P., Vázquez-Rojas, J. L. & Rodríguez, J. M. Prediction of hypocalcemia after total thyroidectomy using indocyanine green angiography of parathyroid glands: A simple quantitative scoring system. *Am. J. Surg.* **218**, 993–999 (2019).

33. Zaidi, N., Bucak, E., Yazici, P., Soundararajan, S., Okoh, A., Yigitbas, H., Dural, C. & Berber, E. The feasibility of indocyanine green fluorescence imaging for identifying and assessing the perfusion of parathyroid glands during total thyroidectomy. *J. Surg. Oncol.* **113**, 775–778 (2016).

34. Razavi, A. C., Ibraheem, K., Haddad, A., Saparova, L., Shalaby, H., Abdelgawad, M. & Kandil, E. Efficacy of indocyanine green fluorescence in predicting parathyroid vascularization during thyroid surgery. *Head Neck* **41**, 3276–3281 (2019).

35. Chu, W., Chennamsetty, A., Toroussian, R. & Lau, C. Anaphylactic Shock After Intravenous Administration of Indocyanine Green During Robotic Partial Nephrectomy. *Urol. Case Reports* **12**, 37–38 (2017).

36. Boas, D. A. & Dunn, A. K. Laser speckle contrast imaging in biomedical optics. *J. Biomed. Opt.* **15**, 011109 (2010).

37. Kuriloff, D. B. & Kizhner, V. Parathyroid gland preservation and selective autotransplantation utilizing topical lidocaine in total thyroidectomy. *Laryngoscope* **120**, 1342–1344 (2010).

38. Gebhart, S. C. Liquid-Crystal Tunable Filter Spectra Imaging for Discrimination between Normal and Neoplastic Tissues in the Brain. (Vanderbilt University, 2006).

CHAPTER 7

CONCLUSIONS AND FUTURE DIRECTIONS

7.1 Summary and Major Conclusions

The overall goals of this dissertation were to propose and develop a real-time label-free method for evaluating blood flow to parathyroid glands intraoperatively, and to integrate that with near-infrared autofluorescence (NIRAF) detection to improve surgical guidance during endocrine neck surgeries. Hypoparathyroidism primarily results from inadvertent damage to healthy parathyroid glands during thyroidectomy, and leads to hypocalcemia with its accompanying debilitating effects[1]. There are two challenges in addressing this problem. First is the intraoperative identification of parathyroid glands, a difficult challenge due to their small size[2], variability in location[3,4], and visual similarity to other tissues such as lymph nodes[5]. The discovery made in our lab that parathyroid glands autofluorescence under near-infrared illumination[6] has helped address the first challenge, with two clinical devices currently having received FDA clearance for intraoperative parathyroid identification[7]. However, as has been reported in several studies, identifying the parathyroid glands alone is not sufficient to improve rates of postoperative hypoparathyroidism[8–11]. The second challenge involves preserving adequate blood flow to the parathyroid glands and accurately detecting when blood flow is compromised in order to perform autotransplantation if needed. Because the parathyroid glands derive their blood supply from the same vessels that supply the thyroid[2,12], it is difficult to resect the thyroid without damaging the arterial vessels leading to each parathyroid. There is only a single delicate arteriole to each parathyroid gland, causing them to be famously likened to cherries on a stem[13]. If this blood supply is completely damaged during surgery, termed devascularization, the calcium-regulating function of the parathyroid gland can be salvaged if the gland is autotransplanted[14]. However, since autotransplantation is not guaranteed to succeed[15], the decision to autotransplant should only be made with accurate information on the state of vascularity of the parathyroid glands. To date, surgeons primarily rely on visual inspection of the glands and personal experience in making judgements on parathyroid vascularity. This dissertation proposes laser speckle contrast imaging (LSCI) as an objective technique for intraoperative assessment of parathyroid vascularity.

The underlying hypothesis of this work was that intraoperative LSCI can provide objective and accurate assessment of the state of vascularity of a parathyroid gland and therefore its viability. This was validated by the work conducted under specific aims 1 and 2. In Chapter 3, the first ever report on the use of LSCI for intraoperative parathyroid vascularity assessment was presented. This work involved the design and construction of an LSCI device for intraoperative imaging of parathyroid glands. It showed

that imaging could be performed in real-time and in the presence of low-level ambient lighting, making it an attractive technique for clinical translation. By comparing speckle contrast values with the visual assessments of an experienced high-volume endocrine surgeon, LSCI was found to be 91.5% accurate in detecting differences in parathyroid vascularity on a dataset of 59 parathyroid glands. The findings of this study also suggested that LSCI is able to detect vascular damage to parathyroid glands in cases where it is not visually apparent to the surgeon. To provide further support for the technique, images were acquired in parathyroidectomy cases before and immediately following ligation of the blood supply to the diseased gland. In all cases, an increase in speckle contrast was observed, indicating a loss of blood flow. This study concluded work under specific aim 1 and showed the promise of LSCI as an objective real-time label-free method for assessing parathyroid vascularity.

Specific aim 2 sought to evaluate the relationship between intraoperative parathyroid speckle contrast and the postoperative outcomes of thyroidectomy patients. Chapter 2 presented a prognostic study on 72 patients who underwent thyroidectomy and whose parathyroid glands were imaged with LSCI after thyroid resection. This study demonstrated that intraoperative parathyroid speckle contrast values are indeed related to postoperative parathyroid hormone (PTH) levels, supporting the underlying hypothesis of this dissertation. Patients with normal postoperative PTH levels were separable from patients with low postoperative PTH levels with 87.5% sensitivity and 84.4% specificity, based on average parathyroid speckle contrast after thyroid resection. The speckle contrast value that provided this classification accuracy was taken to be the maximum value for an adequately perfused parathyroid gland. This study also found that a minimum of one such adequately perfused gland is needed for normal postoperative PTH levels, supporting findings from another study involving the use of indocyanine green (ICG) angiography[16]. Completing work under specific aim 2, this study demonstrated the potential of LSCI to help reduce the incidence of post-surgical hypoparathyroidism by providing accurate intraoperative assessment of parathyroid vascularity.

The primary goal of specific aim 3 was to develop a device combining NIRAF detection with LSCI for complete surgical guidance involving the parathyroid gland: identification/localization and assessment of vascularity. Chapter 5 detailed the design, development and characterization of ParaSPAI, an imaging device combining the two techniques. Prior to the work presented in this chapter, determination of parathyroid speckle contrast required manual segmentation of images. Thus, even though the imaging technique itself was real-time, extracting quantitative information on the parathyroid glands was not, and

required additional human input. In a clinical scenario, this could cause disruptions to the surgical workflow and therefore is a barrier to translation. In this chapter, an automated segmentation algorithm to overcome this problem was reported. Leveraging the simultaneous acquisitions of LSCI and NIRAF images by the ParaSPAI, the location of parathyroid glands could be determined from NIRAF images and used to automatically calculate parathyroid speckle contrast. The performance of the algorithm was determined to be equivalent to manual segmentation, eliminating the need to have a human segment speckle contrast images in the operating room. Nevertheless, limitations to the algorithm's performance were identified, and in Appendix A, an alternate approach to segmentation based on convolutional neural networks was presented. Initial results suggest that this is a valid approach to automated segmentation and further work is required to realize a more effective network.

Finally, in Chapter 6, LSCI was compared with ICG angiography, a fluorescent-dye-based imaging technique that is seeing increasing use in thyroid surgery[16–20]. Given that the ParaSPAI developed in Chapter 5 images both fluorescence and LSCI, it was used to compare the two techniques on the same parathyroid glands. Results showed strong correlation between the two techniques when ICG fluorescence intensity was quantified, suggesting that they detect similar differences in parathyroid vascularity. The study highlighted the ambiguity of qualitative scoring of ICG fluorescence (which is the current practice). In contrast to ICG angiography, LSCI is label-free and can be readily integrated with NIRAF imaging for parathyroid detection. Concluding work under specific aim 3 demonstrated, for the first time, a single tool for real-time label-free complete assessment of the parathyroid gland. Further development and commercialization of such a device has the potential to help reduce the incidence of post-surgical hypoparathyroidism by improving the current state of surgical guidance in endocrine neck surgeries.

The major conclusions and outcomes of this dissertation are summarized as follows:

- Laser speckle contrast imaging is capable of detecting differences in parathyroid vascularity with 91.5% accuracy when evaluated against the visual assessment of an experienced high-volume endocrine surgeon.
- Patients who have low PTH levels after thyroidectomy have significantly higher average parathyroid speckle contrast intraoperatively, than patients with normal postoperative PTH levels. Average parathyroid speckle contrast classifies these two groups with 87.5% sensitivity and 84.4% specificity.

- A speckle contrast value was identified for classifying a parathyroid gland as adequately vascularized. A minimum of one such parathyroid gland observed intraoperatively is needed for normal levels of PTH production post-thyroidectomy.
- A single device combining LSCI with NIRAF imaging was developed, providing a tool for real-time label-free complete surgical guidance regarding the parathyroid gland.
- An automated segmentation scheme was developed for use with the combined imaging device to automate the calculation of parathyroid speckle contrast. This reduces a barrier to clinical translation of the technology into endocrine neck surgeries.

7.2 Recommendations for Future Directions

The process of achieving the goals laid out in this dissertation raised a number of questions and highlighted a few problems along the way. The following are my recommendations on avenues that future work could take to address some of these issues.

7.2.1 Establishing a method for standardizing parathyroid speckle contrast measurement

Speckle contrast is influenced by parameters such as the coherence length of the light source used to illuminate the target, and the pixel size of the camera sensor detecting the speckle pattern[21]. As a result, two different instruments imaging the same object can provide two very different speckle contrast values. For instance, when the device developed in Chapter 3 was modified in Chapter 4 to replace the multimode laser with a single-mode equivalent, the speckle contrast of a microfluidic phantom used in testing roughly doubled. For this reason, the value of 0.186 identified in Chapter 4 as the maximum for adequate vascularity of a parathyroid gland only holds for that LSCI device. Unlike the NIRAF signal of the parathyroid, which can be compared to the thyroid in a ratio and can therefore be uninfluenced by device differences such as illumination intensity, it may not be advisable to compare the speckle contrast of parathyroid glands to other tissues. This is because imaging takes place during surgery, which affects the blood supply to tissues and would therefore introduce an unknown amount of variability. A major blood vessel such as the carotid could potentially be used for comparison with the parathyroids, however this

might introduce unnecessary complexity as the vessel would first have to be exposed to avoid the influence of variation in thicknesses of any fat or connective tissue layers that might cover it. It is theorized that a linear factor can allow for comparison between different LSCI devices[22]. In the case of imaging the microfluidic phantom mentioned above, multiplying by a linear factor produced comparable results (Figure 7.1). Practically speaking, the limits of this linearity need to be explored, and a physical standard for relating measurements between devices needs to be realized.

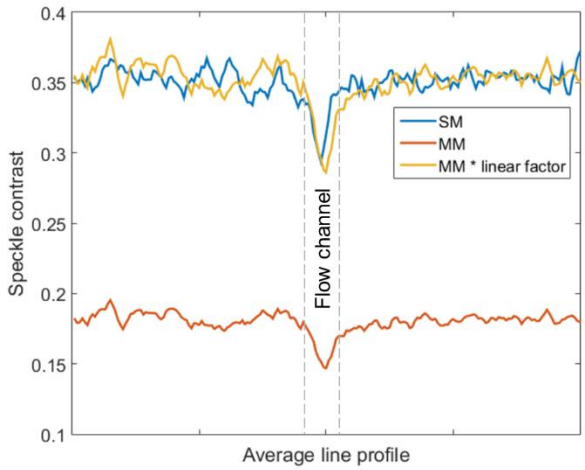

Figure 7.1. Speckle contrast line profiles across a microfluidic phantom calculated from images acquired with a single-mode (SM) and multimode (MM) laser. The profiles appear visually comparable after multiplication by a linear factor.

Should that fail, the use of speckle correlation time rather than speckle contrast is worth investigating. Correlation times are measures of how quickly a speckle pattern loses correlation with itself[21]. This decorrelation is due to movement of particles, causing the speckle pattern to shift. Correlation time is inversely proportional to flow speed, whereas speckle contrast does not directly relate to flow speed. However, the two quantities are related through the equation:

$$K = \beta^{0.5}\left\{\frac{\tau_c}{T} + \frac{\tau_c^2}{2T^2}\left[\exp\left(-\frac{2T}{\tau_c}\right) - 1\right]\right\}^{0.5} \quad (7.1)$$

where K represents speckle contrast, τ_c represents correlation time, T is the exposure time of the camera, and β is a factor that accounts for effects of polarization and differences in pixel versus speckle size[21]. The reason for suggesting the use of correlation time is that work on multi-exposure speckle imaging has shown that it extends the range over which relative blood flow measures (based on correlation time) are linear[23]. Multi-exposure speckle imaging could therefore provide more robust inter-device comparison.

7.2.2 Improving automated parathyroid segmentation using convolutional neural networks

The automated parathyroid segmentation algorithm developed in Chapter 5 has limited performance when the fluorescence intensity of the parathyroid is low, or there are bright spots of specular reflection and cotton ball sponges in the NIRAF image. An alternate approach based on training a convolutional neural network was proposed and initial results presented in Appendix A. After training on an augmented dataset of just 60 samples, a relatively small network is able to localize parathyroid glands in images not seen during training. These results warrant further development of the network, adding more layers to increase complexity. Added complexity should help the network learn to avoid false positives like bright edges, specular reflections and the fluorescence from cotton ball sponges, all of which have a distinct fluorescence pattern from parathyroid autofluorescence. In addition to increasing network complexity, more intraoperative NIRAF images of parathyroid glands are needed to expand the size of the training dataset. This should help improve the accuracy and robustness of the trained network. These images should also include the false positives mentioned above so the network can be trained to avoid them. In addition to potentially overcoming the limitations of the algorithm presented in Chapter 5, once an appropriate network has been trained, producing segmentation maps for new images could be instantaneous (as opposed to the ~5 seconds required in the earlier algorithm). This would make it possible for segmentation to be incorporated into real-time image acquisition, providing continuous information on the speckle contrast of a parathyroid gland.

7.2.3 Developing a handheld LSCI device for intraoperative parathyroid assessment

Throughout the process of designing, developing and testing the imaging devices described in this dissertation, it became evident to me that endocrine surgeons are generally more familiar and comfortable with smaller handheld devices. These allow for smaller surgical incisions while still having access to interrogate targets of interest. An example of a handheld device used in thyroidectomies is the NIM nerve monitoring system by Medtronic (Dublin, Ireland), which includes a pencil-like probe for mapping the recurrent laryngeal nerve and monitoring its electrical activity. There is also the recently FDA-cleared PTEye by AiBiomed (Santa Barabara, CA, USA), including a pencil-like probe for identifying parathyroid glands using NIRAF detection. Even with wide-field NIRAF imaging devices like the Fluobeam by Fluoptics (Grenoble, France), the device is handheld and operated much closer to the surgical incision than the research-grade instruments developed in this dissertation. It is therefore my recommendation that a handheld LSCI device be developed for parathyroid vascularity assessment. This will help improve the likelihood of adoption of the technique by endocrine surgeons.

The task of developing a handheld LSCI instrument for parathyroid assessment is not trivial however, and would require further research. The main challenge to overcome is the introduction of motion artifacts by handheld operation. Since LSCI is sensitive to motion, any extraneous motion by the hands of the instrument operator will lead to further blurring of the speckle pattern and therefore a global decrease in speckle contrast. Efforts to address motion artifacts in LSCI include: (1) attaching an adhesive opaque patch to the surface being imaged, assuming that any change in speckle contrast of the patch is due to motion artifacts and therefore this change can be subtracted from the rest of the image[24]; (2) employing a fiducial marker with high speckle contrast and setting a threshold to reject images that have an unacceptable decrease in the contrast of the marker[25]; (3) incorporating a gimbal stabilizer into the hardware to dampen movement[26]; and (4) image registration prior to averaging series of images to improve contrast[27,28]. Use of the adhesive opaque patch was reported in cases of skin imaging and may not be suitable for intraoperative imaging. Furthermore, a recent exploration of the effects of hand motion on handheld LSCI showed that the magnitude of the change in contrast is not just dependent on the speed of motion (translation and tilt), but also on the optical properties of the tissue, and therefore a simple look-up table may not be sufficient to correct for blurring[29]. While a gimbal stabilizer might be effective in dampening motion, it increases complexity of the device and makes it more difficult to create a pencil-like form for imaging deep-seated and aberrantly-located parathyroid glands. Image registration improves

the spatial resolution of averaged images, however it does not necessarily correct the global decrease in speckle contrast resulting from hand motion. To illustrate this, a 2% Intralipid solution flowing through a microfluidic phantom was imaged with the LSCI device developed in Chapter 3, in a static and then handheld manner. Since the device was fixed in position, the handheld scenario was mimicked by holding the microfluidic phantom in one free hand. As seen in Figure 7.2, the global speckle contrast of the phantom decreases in the handheld case, and contrast between the flow channel and the rest of the phantom is greatly reduced. After image registration, the distinction between the flow channel and the rest of the phantom is amplified, however the global speckle contrast is still less than in the static case. Since different operators might introduce different degrees of motion and therefore different magnitudes of speckle contrast decrease, image registration alone is an insufficient correction.

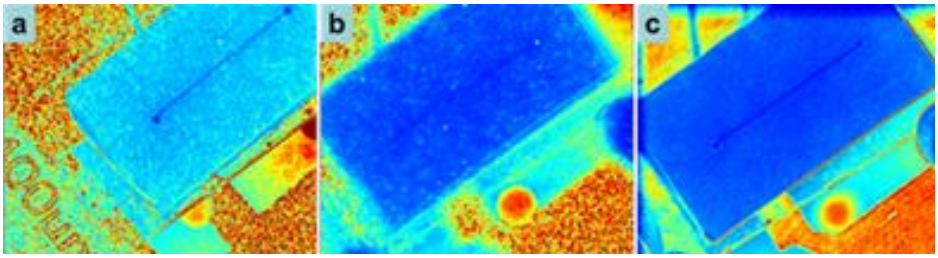

Figure 7.2. Speckle contrast images (average of 10) of a microfluidic phantom clamped (a) and handheld (b). Intensity based image registration is used to align handheld speckle contrast images before averaging (c).

A potential alternative approach which has not yet been attempted would be to correct the image of the raw speckle pattern prior to calculating speckle contrast. The global decrease in speckle contrast is due to a global blurring of the speckle pattern. Therefore, if the image of the speckle pattern can be appropriately deblurred, then the calculated speckle contrast would resemble that of a static imaging case. Current neural networks are capable of restoring detail to blurry images[30]. By training a model on the blurring patterns resulting from hand motion, raw speckle images could potentially be corrected before calculating speckle contrast. This could be the subject of future research.

7.3 Contributions to the Field and Societal Impact

I am grateful to have had the opportunity to make meaningful contributions to the fields of endocrine surgery and biophotonics by working with the Mahadevan-Jansen lab at Vanderbilt University. Overall, the process of learning to identify a clinical problem and coming up with an appropriate solution to it has been invaluable training that I will carry forward with me in my career as a biomedical engineer. These contributions are summarized below.

7.3.1 Impact on endocrine surgery

In the field of endocrine surgery, there are currently no objective and accurate means to assess blood flow to parathyroid glands intraoperatively. Surgeons often rely on their visual assessment and personal experience, which may not be very accurate depending on years of practice and frequency of performing surgeries. Consequently, a patient can undergo surgery to be treated for one condition, and leave the operating room having developed a whole new debilitating condition – hypoparathyroidism. Between 70-80% of patients with hypoparathyroidism developed the condition due to damage to the parathyroid glands during surgery[31]. It is no wonder that this is the most common cause of malpractice litigation after endocrine surgeries[32]. While calcium and vitamin D supplements help maintain healthy blood calcium levels in the absence of PTH, affected patients have a significantly reduced quality of life, and in cases of permanent hypoparathyroidism, long-term use can lead to nephrocalcinosis, kidney stones and brain calcifications[1]. Alternate therapies involving PTH replacement have been developed, however more studies are needed to evaluate their impact on quality of life[33]. Regardless, treatment of hypoparathyroidism places a physical, mental and financial burden on patients, where it could have been altogether avoided in the first place with better intraoperative guidance.

This dissertation presents a promising technique to improve intraoperative guidance in endocrine neck surgeries. By demonstrating that LSCI is highly accurate in detecting differences in parathyroid vascularity, and is also strongly related to the postoperative outcomes of thyroidectomy patients, this work provides the basis for development of medical devices utilizing the technique. Being quantitative and label-free, LSCI has advantages over other proposed methods like ICG angiography and fluorescein-based confocal endomicroscopy. Adoption of the technique as an adjunct by endocrine surgeons has the potential to transform the landscape of thyroid and parathyroid surgery. Clinical LSCI devices will particularly be

useful for less-experienced or lower-volume surgeons, and could lead to marked reduction in the rates of hypoparathyroidism after surgery. They would also be useful as training tools, helping surgical residents better evaluate differences in parathyroid gland vascularity intraoperatively.

This dissertation also demonstrates the feasibility of combining LSCI with NIRAF imaging in a relatively simple device, providing the basis for future development of a single medical device for complete assessment of the parathyroid gland. Such a device would fill a critical gap in the field as there are currently no medical devices employing label-free approaches for this purpose. NIRAF detection systems for parathyroid identification can be used with ICG angiography to assess parathyroid vascularity, however use of the dye has a few drawbacks. Furthermore, from personal discussions and observation, it appears that most surgeons, at least in the United States, prefer to avoid using the dye if possible. This work provides a completely label-free approach for parathyroid surgical guidance that poses no added risk to the patient. Throughout my time working on this project, I have had the opportunity to present at a number of conferences, including twice at the annual Symposium on Parathyroid Fluorescence which gathered over a hundred international endocrine and general surgeons. Discussions generated from my presentations made evident the excitement for the final outputs of this project, and I believe this shows promise for clinical adoption of LSCI in endocrine neck surgery.

7.3.2 Impact on biophotonics

No novel optical techniques were developed over the course of this dissertation, nor were any novel scientific discoveries made. However, I believe this body of work provides a good example to biophotonics researchers and biomedical engineers on the process of identifying clinical problems and developing appropriate solutions to them, pooling resources from different external fields if needed. Seeking out the right tool for the job led me to learn about LSCI, a technique I had no prior experience with. I also had to build on previous skills and learn new ones. I learned enough computer aided design (Solidworks) for designing the imaging devices, optical design (Zemax) for planning the layout of optical elements, electronic circuit design for remotely controlling elements of the imaging systems, image segmentation techniques used in computer science, and towards the end, a programming language (Python) for GPU-accelerated implementation of a deep-learning-based segmentation technique. While I do not consider myself a master of any of these, I learned enough to produce a successful solution to the identified clinical problem. I consider this to be a hallmark of biomedical engineering, and am grateful to

have had this experience working under Dr. Mahadevan-Jansen. Throughout the process, I also had frequent interaction with endocrine surgeons. I believe this was of great benefit to the success of the work, and contributed in no small part to the two patent applications resulting from it.

7.3.3 Commercialization of technology

During the course of this PhD, I was involved in small part with the commercialization of a fiber-optic probe-based NIRAF detection system for parathyroid identification (PTEye by AiBiomed). This device originated from previous work done in the lab, and after licensing the technology to AiBiomed, the lab remained involved in efforts to commercialize the final product. The PTEye has now received FDA clearance and CE marking for use in intraoperative parathyroid detection. During the De Novo application to the FDA, my contribution was to help determine the influence of blood on the NIRAF signal detected by the PTEye. This process taught me about the rigorousness required for data presented to the FDA, and was invaluable training for my career moving forward as a biomedical engineer.

I have also been involved in the protection of newer intellectual property. Working with patent lawyers, I helped with the drafting of two patent applications based on the work presented in this dissertation. This gave me valuable insight into the patent process and legal language involved. The intellectual property has been licensed to AiBiomed, and I look forward to seeing the eventual clinical translation of LSCI for intraoperative parathyroid assessment.

7.4 References

1. Mannstadt, M., Bilezikian, J. P., Thakker, R. V., Hannan, F. M., Clarke, B. L., Reijnmark, L., Mitchell, D. M., Vokes, T. J., Winer, K. K. & Shoback, D. M. Hypoparathyroidism. *Nat. Rev. Dis. Prim.* **3**, 1–21 (2017).
2. Mohebati, A. & Shaha, A. R. Anatomy of thyroid and parathyroid glands and neurovascular relations. *Clin. Anat.* **25**, 19–31 (2012).
3. Akerström, G., Malmaeus, J. & Bergström, R. Surgical anatomy of human parathyroid glands. *Surgery* **95**, 14–21 (1984).
4. Wang, C. The anatomic basis of parathyroid surgery. *Ann. Surg.* **183**, 271–5 (1976).

5. Johnson, N. A., Tublin, M. E. & Ogilvie, J. B. Parathyroid Imaging: Technique and Role in the Preoperative Evaluation of Primary Hyperparathyroidism. *Am. J. Roentgenol.* **188**, 1706–1715 (2007).

6. Paras, C., Keller, M., White, L., Phay, J. & Mahadevan-Jansen, A. Near-infrared autofluorescence for the detection of parathyroid glands. *J. Biomed. Opt.* **16**, 067012 (2011).

7. FDA. FDA permits marketing of two devices that detect parathyroid tissue in real-time during surgery | FDA. https://www.fda.gov/news-events/press-announcements/fda-permits-marketing-two-devices-detect-parathyroid-tissue-real-time-during-surgery.

8. Serra, C., Silveira, L. & Canudo, A. Identification of inadvertently removed parathyroid glands during thyroid surgery using autofluorescence. *Gland Surg.* **9**, 893–898 (2020).

9. Serra, C., Canudo, A. & Silveira, L. Intraoperative identification of parathyroid glands by autofluorescence on total thyroidectomy – Does it really reduces post-operative hypocalcemia? *Surg. Pract. Sci.* **2**, 100011 (2020).

10. Papavramidis, T. S., Chorti, A., Tzikos, G., Anagnostis, P., Pantelidis, P., Pliakos, I., Panidis, S., Papaioannou, M., Bakkar, S., Unal, E. & Michalopoulos, A. The effect of intraoperative autofluorescence monitoring on unintentional parathyroid gland excision rates and postoperative PTH concentrations—a single-blind randomized-controlled trial. *Endocrine* (2021) doi:10.1007/s12020-020-02599-5.

11. Kim, Y. S., Erten, O., Kahramangil, B., Aydin, H., Donmez, M. & Berber, E. The impact of near infrared fluorescence imaging on parathyroid function after total thyroidectomy. *J. Surg. Oncol.* **122**, jso.26098 (2020).

12. Nobori, M., Saiki, S., Tanaka, N., Harihara, Y., Shindo, S. & Fujimoto, Y. Blood supply of the parathyroid gland from the superior thyroid artery. *Surgery* **115**, 417–23 (1994).

13. Halsted, W. S. & Evans, H. M. The parathyroid glandules. Their blood supply, and their preservation in operation upon the thyroid gland. *Ann. Surg.* **XLVI**, 489–506 (1907).

14. Lo, C. Y. & Tam, S. C. Parathyroid autotransplantation during thyroidectomy: Documentation of graft function. *Arch. Surg.* **136**, 1381–1385 (2001).

15. Sierra, M., Herrera, M. F., Herrero, B., Jiménez, F., Sepúlveda, J., Lozano, R. R., Gamino, R., González, O. & Correa-Rotter, R. Prospective biochemical and scintigraphic evaluation of autografted normal parathyroid glands in patients undergoing thyroid operations. *Surgery* **124**, 1005–10 (1998).

16. Fortuny, J. V., Belfontali, V., Sadowski, S. M., Karenovics, W., Guigard, S. & Triponez, F. Parathyroid gland angiography with indocyanine green fluorescence to predict parathyroid function after thyroid surgery. *Br. J. Surg.* **103**, 537–543 (2016).

17. Vidal Fortuny, J., Karenovics, W., Triponez, F. & Sadowski, S. M. Intra-Operative Indocyanine Green Angiography of the Parathyroid Gland. *World J. Surg.* **40**, 2378–2381 (2016).

18. Vidal Fortuny, J., Sadowski, S. M., Belfontali, V., Guigard, S., Poncet, A., Ris, F., Karenovics, W. & Triponez, F. Randomized clinical trial of intraoperative parathyroid gland angiography with indocyanine green fluorescence predicting parathyroid function after thyroid surgery. *Br. J. Surg.*

105, 350–357 (2018).

19. Gálvez-Pastor, S., Torregrosa, N. M., Ríos, A., Febrero, B., González-Costea, R., García-López, M. A., Balsalobre, M. D., Pastor-Pérez, P., Moreno, P., Vázquez-Rojas, J. L. & Rodríguez, J. M. Prediction of hypocalcemia after total thyroidectomy using indocyanine green angiography of parathyroid glands: A simple quantitative scoring system. *Am. J. Surg.* **218**, 993–999 (2019).

20. Zaidi, N., Bucak, E., Yazici, P., Soundararajan, S., Okoh, A., Yigitbas, H., Dural, C. & Berber, E. The feasibility of indocyanine green fluorescence imaging for identifying and assessing the perfusion of parathyroid glands during total thyroidectomy. *J. Surg. Oncol.* **113**, 775–778 (2016).

21. Boas, D. A. & Dunn, A. K. Laser speckle contrast imaging in biomedical optics. *J. Biomed. Opt.* **15**, 011109 (2010).

22. Thompson, O., Andrews, M. & Hirst, E. Correction for spatial averaging in laser speckle contrast analysis. *Biomed. Opt. Express* **2**, 1021–9 (2011).

23. Parthasarathy, A. B., James Tom, W., Gopal, A., Zhang, X. & Dunn, A. K. Robust flow measurement with multi-exposure speckle imaging. *OSA Opt. EXPRESS* **16**, 1975–1989 (2008).

24. Mahé, G., Rousseau, P., Durand, S., Bricq, S., Leftheriotis, G. & Abraham, P. Laser speckle contrast imaging accurately measures blood flow over moving skin surfaces. *Microvasc. Res.* **81**, 183–188 (2011).

25. Lertsakdadet, B., Yang, B. Y., Dunn, C. E., Ponticorvo, A., Crouzet, C., Bernal, N., Durkin, A. J. & Choi, B. Correcting for motion artifact in handheld laser speckle images. *J. Biomed. Opt.* **23**, 1 (2018).

26. Lertsakdadet, B., Dunn, C., Bahani, A., Crouzet, C. & Choi, B. Handheld motion stabilized laser speckle imaging. *Biomed. Opt. Express* **10**, (2019).

27. Richards, L. M., Towle, E. L., Fox, D. J. & Dunn, A. K. Intraoperative laser speckle contrast imaging with retrospective motion correction for quantitative assessment of cerebral blood flow. *Neurophotonics* **1**, 1 (2014).

28. Miao, P., Rege, A., Li, N., Thakor, N. V, Thakor, N. V & Tong, S. High Resolution Cerebral Blood Flow Imaging by Registered Laser Speckle Contrast Analysis. *IEEE Trans. Biomed. Eng.* **57**, (2010).

29. Chizari, A., Knop, T., Sirmacek, B., Van Der Heijden, F. & Steenbergen, W. Exploration of movement artefacts in handheld laser speckle contrast perfusion imaging. *Biomed. Opt. Express* **11**, 2352 (2020).

30. Nimisha, T. M., Singh, A. K. & Rajagopalan, A. N. Blur-Invariant Deep Learning for Blind-Deblurring A N Rajagopalan. in *Proceedings of the IEEE International Conference on Computer Vision (ICCV)* 4752–4760 (2017).

31. Vokes, T. Quality of life in hypoparathyroidism. *Bone* **120**, 542–547 (2019).

32. Pattou, F., Combemale, F., Fabre, S., Carnaille, B., Decoulx, M., Wemeau, J.-L., Racadot, A. & Proye, C. Hypocalcemia following Thyroid Surgery: Incidence and Prediction of Outcome. *World J. Surg* **22**, 718–724 (1998).

33. Rejnmark, L., Underbjerg, L. & Sikjaer, T. Hypoparathyroidism: Replacement therapy with parathyroid hormone. *Endocrinology and Metabolism* vol. 30 436–442 (2015).

APPENDIX A

AUTOMATED PARATHYROID SEGMENTATION WITH CONVOLUTIONAL NEURAL NETWORKS

A.1 Abstract

The following presents unpublished work towards the development of an alternate automated parathyroid segmentation method. In Chapter 5, a few limitations of the segmentation algorithm developed were highlighted, namely its reliance on strong signal-to-background ratio, and sensitivity to bright spots in fluorescence images. Here, a fully-convolutional neural network is trained to segment parathyroid glands, and tested on images not seen by the network during training. Results show promise for future development and use of this approach for automated parathyroid segmentation.

A.2 Background and Motivation

In Chapter 5, a segmentation algorithm was developed to segment the parathyroid gland in near-infrared autofluorescence (NIRAF) images. This was used to automate calculation of the parathyroid gland's average speckle contrast. Overall, the algorithm was based on a three-level thresholding followed by an active contour model to fit the boundaries of the identified parathyroid. As mentioned in Chapter 5, the performance of this algorithm relies on the NIRAF intensity of the parathyroid gland, as well as its signal-to-background ratio. It is also affected by the presence of bright spots such as specular reflections in the image. Figure A.1 shows four intraoperative NIRAF images of parathyroid glands that caused the segmentation algorithm to fail. Results of segmentation are indicated with dotted cyan contours. The images make it evident that the algorithm is thrown off by specular reflection from metal tools such as retractors, fluorescence from cotton ball sponges used in surgery, autofluorescence heterogeneity of the parathyroid gland, and weak parathyroid NIRAF intensity. In these scenarios, manual segmentation of images is required to determine parathyroid speckle contrast, and this could hinder clinical adoption. Further motivating this work is the fact that automated segmentation took about 5 seconds for the method described in Chapter 5. While this is comparable to the time it would take for manual segmentation, there is the possibility for instantaneous/real-time segmentation with deep learning[1].

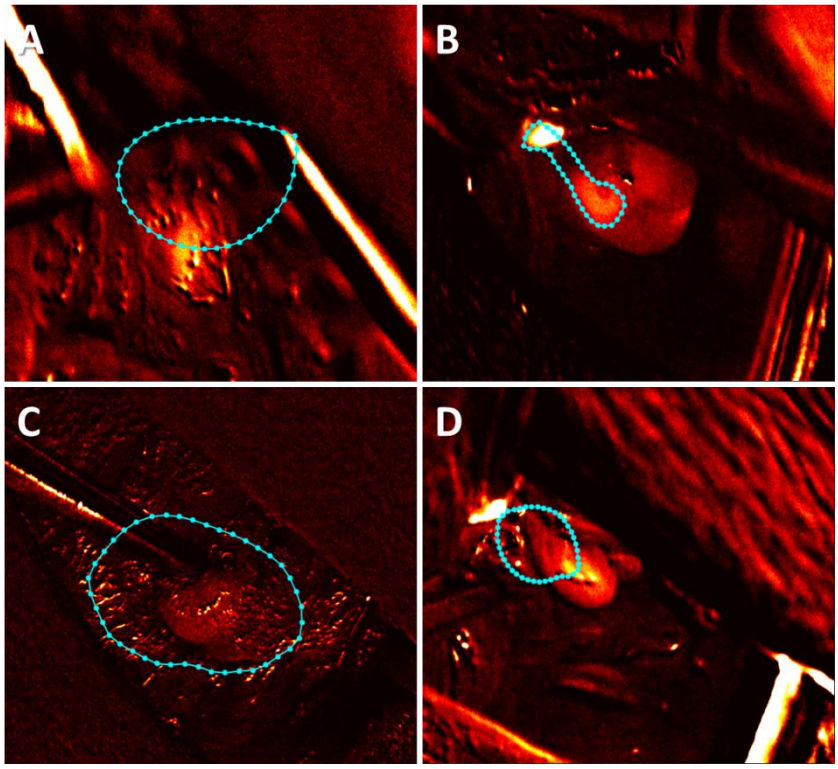

Figure A.1. Intraoperative NIRAF images of parathyroid glands where automated segmentation using the method described in Chapter 5 fails. The presence of specular reflections from metal tools (A), fluorescence from cotton ball sponges (B, D), autofluorescence heterogeneity (B), and weak parathyroid NIRAF (C) result in failure of the algorithm to correctly segment the parathyroid gland. Segmentation results are indicated by dotted cyan contours.

A.3 Convolutional Neural Network for Parathyroid Segmentation

In all four images in Figure A.1, the parathyroid is still visually apparent to the human eye, and a human would be able to demarcate their boundaries. Artificial neural networks are currently used frequently in computer vision tasks, with some implementations outperforming humans in object recognition tasks[2]. U-Net, a fully-convolutional network, was shown to be highly accurate in segmenting neuronal structures in electron microscopy stacks, as well as cell tracking in phase contrast and differential interference contrast microscopy images[3]. Using data augmentation techniques, fewer images were required to train the network.

As an initial attempt at parathyroid segmentation using convolutional neural networks, the following model was created. Similar to the U-Net model, it was fully-convolutional and consisted of a contracting path followed by a symmetric expanding path. However, it contained a lot fewer layers than U-Net to simplify initial training and assess feasibility of the approach. The architecture of the network is displayed in Figure A.2. The input images are of dimensions 1 x 128 x 128 pixels (channels x height x width). These are zero-padded and each convolved with a 16 x 3 x 3 kernel to produce an output that maintains the original spatial dimensions but now has 16 channels (16 x 128 x 128). A rectified linear unit (ReLU) is applied after convolution and the output is batch-normalized. A second zero-padded convolution is performed with another 16 x 3 x 3 kernel to produce an output of the same size as the input. This is again followed by a ReLU and batch-normalization. Next is the first pooling step: a 2 x 2 max pooling is performed to contract the feature map to 16 x 64 x 64. This is followed by a zero-padded convolution with a 32 x 3 x 3 kernel to produce an output of size 32 x 64 x 64. After a ReLU and batch-normalization, a second similar convolution is performed, again followed by ReLU and batch-normalization. Another 2 x 2 max pooling is performed to condense the feature map to 32 x 32 x 32, and this is followed by zero-padded convolution with a 64 x 3 x 3 kernel, ReLU and batch-normalization. At this point, the feature map is of dimensions 64 x 32 x 32. The rest of the network is symmetric to the first half, using max unpooling with corresponding indices from earlier pooling layers to expand the feature map back to the original image size. The final convolutional layer transforms the feature map from a size of 16 x 128 x 128 to 2 x 128 x 128. The first channel contains classification scores for parathyroid, and the second contains scores for background (not parathyroid). Dropout layers were inserted after every pooling and unpooling layer. This introduces stochasticity to the network by randomly dropping channels during training to prevent overfitting and allow for more generalizable results[4].

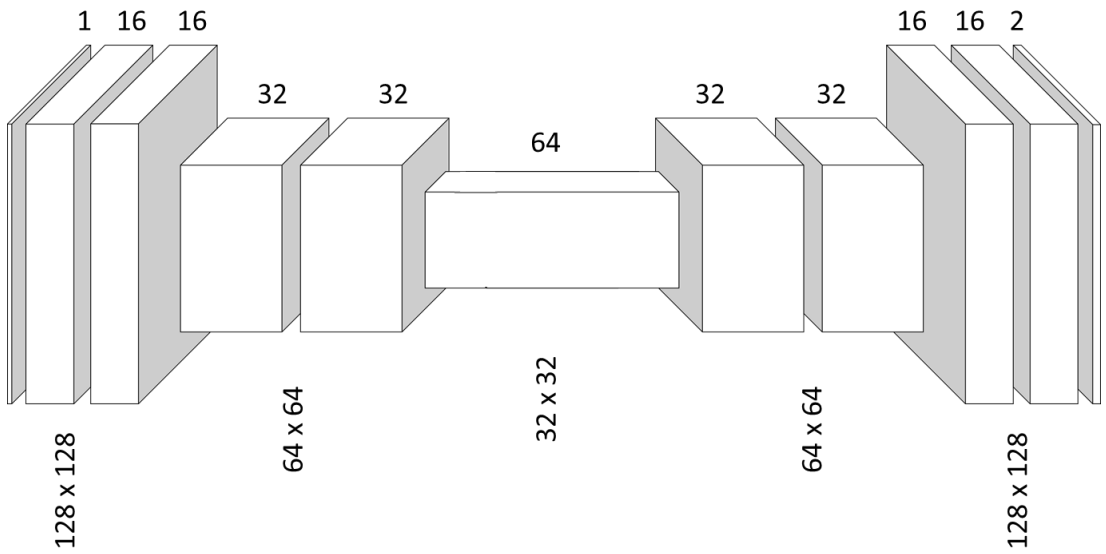

Figure A.2. Architecture of neural network created to evaluate feasibility of the approach for automated parathyroid segmentation. Each box represents a multi-channel feature map with the number of channels indicated above the box and the spatial dimensions of the feature maps indicated below them.

A.4 Model Training

At the time of this work, 67 intraoperative NIRAF images of parathyroid glands had been acquired with the device presented in Chapter 5. These images (originally 1024 x 1280) were resized to 128 x 128 pixels for input to the network. For each image, a segmentation mask was manually drawn and this served as the ground truth parathyroid location. The data was randomly split such that 60 images and their corresponding segmentation masks were used for training. To boost the size of the training dataset, data augmentations were performed to generate 9 new samples for each image and mask, providing a ten-fold increase in the number of training samples. Augmentations included random shifting, scaling, rotation and vertical or horizontal flipping of the images. Images were standardized to have zero mean and unit standard deviation before being input to the network.

The model was constructed and trained using PyTorch. Training was performed for two epochs using a batch size of 32. Thus, for 600 images, 19 iterations of training were performed. The Adam optimizer was chosen for training, and the learning rate was arbitrarily set to 5×10^{-4}.

A.5 Initial Results and Future Outlook

Training the model on a standard GPU took less than 5 minutes and running a single test image through was instantaneous. The segmentation masks generated for 6 test images are displayed in Figure A.3, alongside their respective NIRAF images. The network identifies parathyroid glands in images that were not included in training. It appears to look for high intensity regions of the image with rounded shapes. Even in cases where the high intensity regions are sharp edges, it attempts to make rounded parathyroid-like shapes. It also segments false positives like the cotton ball sponge in Figure A.3F.

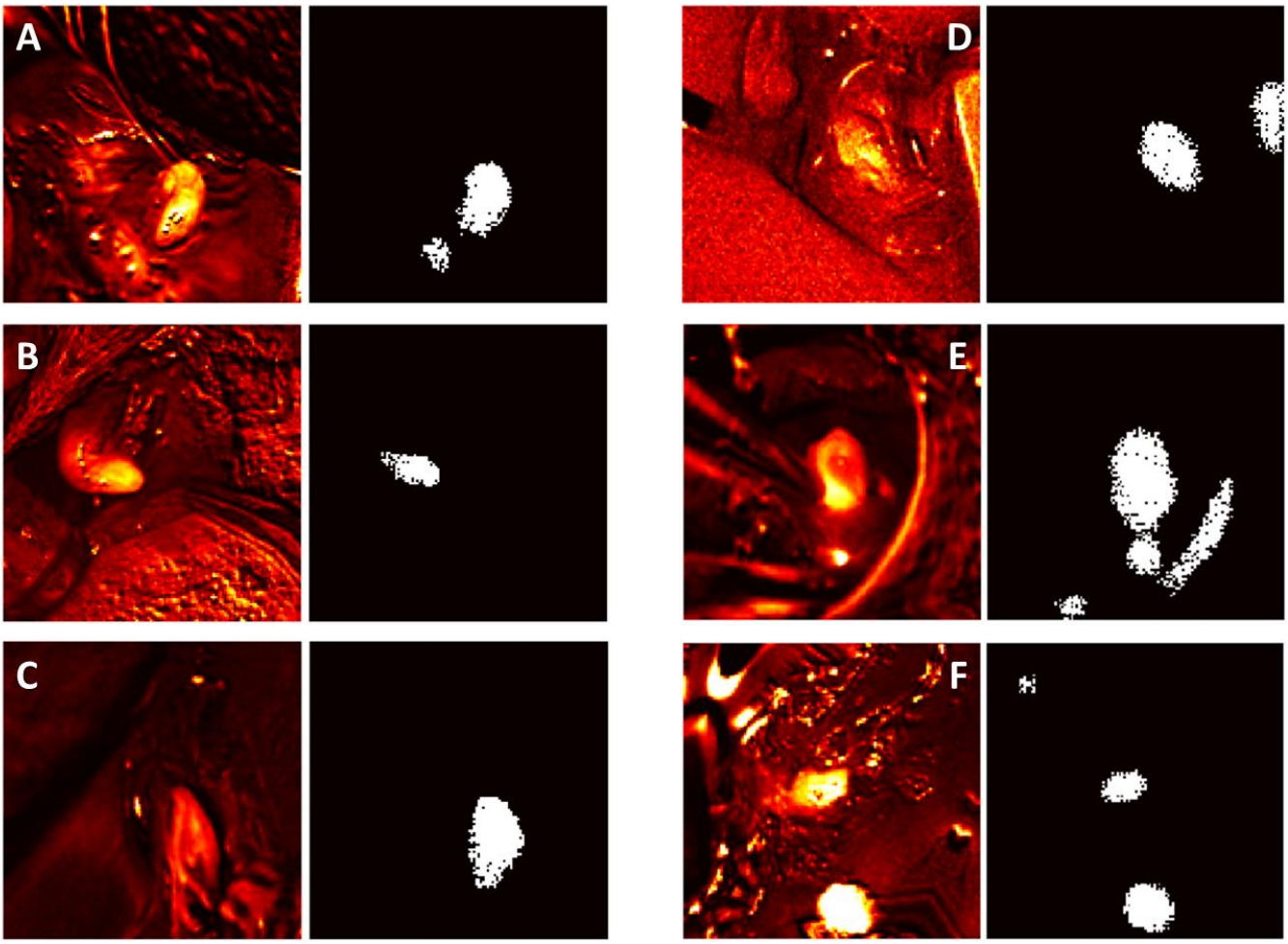

Figure A.3. Test images used to evaluate convolutional neural network. The network identifies high intensity rounded shapes as parathyroid glands. In (D) and (E) where sharp edges create specular reflections, it attempts to create rounded parathyroid-like shapes. Fluorescence from cotton ball sponges (E, F) is also mistaken as parathyroid.

These initial results are highly promising and warrant further investigation to realize an optimal network. The complexity of this network is far below that of U-Net and other state of the art neural networks. There is ample room to scale up the model by adding more layers or potentially just utilizing U-Net. A smaller network was chosen for this feasibility study due to the limited number of training samples, as well as to reduce the amount of time required for training. With more layers to the network and thus more variables to train, it is highly likely that the network can learn to avoid false positives like specular reflections and fluorescence from cotton ball sponges. Both have intensity patterns in the images that are distinct from parathyroid fluorescence. For the most part they have very high and uniform intensity. In addition to expanding the network, more training images need to be acquired, especially images containing specular reflections and cotton ball sponges. Training with more of these images will help the network learn to avoid false positives.

A.6 References

1. Volkov, M., Hashimoto, D. A., Rosman, G., Meireles, O. R. & Rus, D. Machine learning and coresets for automated real-time video segmentation of laparoscopic and robot-assisted surgery. in *Proceedings - IEEE International Conference on Robotics and Automation* 754–759 (Institute of Electrical and Electronics Engineers Inc., 2017). doi:10.1109/ICRA.2017.7989093.
2. Ho-Phuoc, T. CIFAR10 to Compare Visual Recognition Performance between Deep Neural Networks and Humans. *arXiv* (2018).
3. Ronneberger, O., Fischer, P. & Brox, T. U-Net: Convolutional Networks for Biomedical Image Segmentation. in *International Conference on Medical image computing and computer-assisted intervention* 234–241 (Springer, 2015).
4. Li, Z., Gong, B. & Yang, T. Improved dropout for shallow and deep learning. in *Advances in Neural Information Processing Systems* 2531–2539 (Neural information processing systems foundation, 2016).